TM-72-4014-1

CAT-30

AN EMPIRICAL METHOD FOR DETERMINING THE LUNAR GRAVITY FIELD

By

ALFRED JOHN FERRARI

B.E.E. Manhattan College 1963

M.S. The George Washington University 1967

A Dissertation Submitted To

The Faculty Of

The School of Engineering and Applied Science

Of

The George Washington University

In partial satisfaction of the requirements for the degree of Doctor of Science.

September 1971

BIOGRAPHY

ALFRED JOHN FERRARI

Alfred J. Ferrari was born in [redacted], the son of Margaret Ferrari and John C. Ferrari. He attended Loyola High School in New York City and, upon graduation in 1959, he enrolled in Manhattan College, Riverdale, New York. In June of 1963 he received a Bachelor of Electrical Engineering degree. After graduation he entered the United States Air Force and was assigned to the National Security Agency in Washington, D. C. where his work dealt with electronic systems analysis. In September 1964 he entered the George Washington University, Washington, D. C. and received a Master of Science degree in June 1967. In June 1967 he began studies at the George Washington University in a Doctor of Science program. In September 1967, upon completion of military duty, he accepted employment at Bellcomm, Inc., Washington, D. C. Through his work in the Guidance and Navigation Department, he was able to complete his dissertation.

In December 1964 he married the former Janet Lee [redacted] of Darien, Connecticut. There is one child, John Paul Ferrari (1970).

ABSTRACT

A new method has been devised to determine the spherical harmonic coefficients of the lunar gravity field. This method consists of a two-step data reduction and estimation process. In the first step, a weighted least-squares empirical orbit determination scheme is applied to Doppler tracking data from lunar orbits to estimate long-period Kepler elements and rates. Each of the Kepler elements is represented by an independent function of time. The long-period perturbing effects of the earth, sun, and solar radiation are explicitly modeled in this scheme. Kepler element variations estimated by this empirical processor are ascribed to the non-central lunar gravitation features. Doppler data are reduced in this manner for as many orbits as are available. In the second step, the Kepler element rates are used as input to a second least-squares processor that estimates lunar gravity coefficients using the long-period Lagrange perturbation equations.

Pseudo Doppler data have been generated simulating two different lunar orbits. This analysis included the perturbing effects of triaxial lunar harmonics, the earth, sun, and solar radiation pressure. Orbit determinations were performed on these data and long-period orbital elements obtained. The Kepler element rates from these solutions were used to recover triaxial

lunar gravity coefficients. Overall results of this controlled experiment show that lunar gravity coefficients can be accurately determined and that the method is dynamically compatible with long-period perturbation theory.

This selenodesy method has been applied to Doppler data from the Lunar Orbiter I, II, III, and V missions. One hundred ninety-nine sets of Kepler element rates are obtained for gravity field determination. A lunar field of degree and order four is derived from these rates. Equipotential surfaces from this gravity field show the lunar mass distribution to be that of a triaxial ellipsoid with three large areas of mass concentration. The greatest and by far the most dominant of these areas is centered very near the Mare Serenitatis region and covers a large portion of the front side of the moon. The other two regions of mass concentration are located on the far side of the moon but do not correspond to a specific maria region.

This gravity field has been investigated using data from several Apollo missions. Orbit determinations from these data show this field results in improved orbit predictions when compared to those using two other gravity fields. All solutions indicate the lunar gravity field models are still incomplete.

PREFACE

This dissertation has been developed as part of the author's work at Bellcomm, Inc., under contract NASW-417 with the National Aeronautics and Space Administration. The author expresses his appreciation to that Company for the assistance rendered to him in its preparation. The author alone is responsible for its contents. Appreciation is expressed to the National Aeronautics and Space Administration for the use of the Doppler tracking data used in this investigation.

Miss Margaret V. Bullock and Mrs. Sheryl B. Watson of Bellcomm developed the digital computer programs used to embody this method and to obtain numerical results. Appreciation for their work is expressed. Dr. W. G. Heffron also of Bellcomm has also assisted the author by offering suggestions and discussing the various techniques used in the study.

Two members of the faculty of the School of Engineering and Applied Science of the George Washington University have also been of assistance. Appreciation is expressed to Professor G. M. Arkilic for his role in formulating a program of studies for the author and to Professor G. Hintze for acting as the author's Director of Research.

Finally, the author wishes to express his appreciation to his wife, whose support, patience, and encouragement have been so important during the course of this academic program.

TABLE OF CONTENTS

LIST OF TABLES

LIST OF ILLUSTRATIONS

LIST OF SYMBOLS

SYMBOL	DEFINITION
a	Semi-Major Axis of Orbit
a_o	Geometric Average of Osculating Semi-Major Axis
$\bar{a}$	Mean Value of Semi-Major Axis
$\bar{a}_d$	Disturbing Acceleration
$C_{\ell m'}$ $S_{\ell m}$	Gravity Parameters
c	Speed of Light in a Vacuum
D	Mass Density
e	Eccentricity of Orbit
E	Eccentric Anomaly of Orbit
F	Matrix of Partial Derivatives of Kepler Element Rates with Respect to $C_{\ell m'}$ $S_{\ell m}$
f	True Anomaly of Orbit
$F_{\ell mp(I)}$	Inclination Function
$G_{\ell pq(e)}$	Eccentricity Function
H	Matrix of Partial Derivatives of Doppler with Respect to Keplerian Parameters
I	Inclination of Orbit
$\hat{I}$	Unity Matrix
$\bar{k}$	Six Vector of Kepler Elements
$\bar{K}$	Keplerian Parameters
M	Mean Anomaly of Orbit
n	Mean Motion of Satellite

$\bar{p}$	Complete Set of $\{C_{\ell m}, S_{\ell m}\}$
P_ℓ^m	Associated Legendre Polynominal of Degree ℓ and Order m
$R_\oplus$	Earth Perturbation Potential
$R_\odot$	Sun Perturbation Potential
R_{SR}	Solar Radiation Perturbation Potential
$\bar{r}$	Moon Centered Inertial Position
A	Weighting Matrix for Kepler Element Rates
U	Gravitational Potential Function
$\bar{v}$	Moon Centered Inertial Velocity
W	Weighting Matrix for Doppler
$\bar{x}$	Six Vector of Rectangular State
γ	Rotation Rate of the Moon
$\dot{\rho}$	Doppler Measurement
ϕ	Selenographic Latitude
λ	Selenographic Longitude
$\bar{n}$	Noise Vector on Doppler
θ	Angular Displacement Between Rotating and Inertial Axes
Ω	Ascending Node of Orbit
ω	Perifocus of Orbit
$\mu_{\text{(}}$	Gravity Constant of the Moon

CHAPTER I

INTRODUCTION

GENERAL

Observational measurements obtained from earth based tracking of satellites in close lunar orbits provide a unique data source for the identification of lunar gravity parameters. An accurate knowledge of the lunar gravity field is essential for mission planning and for real-time navigation, guidance, and control of the spacecraft for lunar missions. It is also of scientific interest since knowledge of the gravity can be correlated to physical mass concentrations. A number of gravity fields have been obtained from these data. However all have fairly poor prediction qualities. The object of this investigation is to develop a method which can be used for more accurate determination of lunar gravity parameters.

DATA SOURCE

Since 1966 the United States has successfully injected eleven satellites in close lunar orbits. The length of each of these parking orbits is given in Table I. Data was obtained using the three stations of the Deep Space Network (DSN) during the Lunar Orbiter flights, and by seventeen stations of the Manned Space Flight Network (MSFN) during the Apollo missions. The basic data types gathered by each

TABLE I

SATELLITE	PARKING ORBIT TIME
LUNAR ORBITER I	76 DAYS
LUNAR ORBITER II	335 DAYS
LUNAR ORBITER III	243 DAYS
LUNAR ORBITER IV	70 DAYS
LUNAR ORBITER V	179 DAYS
APOLLO 8	20 HOURS
APOLLO 10	62 HOURS
APOLLO 11	62 HOURS
APOLLO 12	86 HOURS
APOLLO 14	68 HOURS
APOLLO 15	144 HOURS

tracking station consist of Doppler frequency shift and range data. Since using the range data requires an extremely accurate knowledge of the lunar ephemeris, this data type is not used for lunar orbit determination or selenodesy. The Doppler data is relatively insensitive to lunar ephemeris errors; hence it is the only data used.

Two types of Doppler data are used: two-way and three-way data. For the case of two-way data a signal is transmitted by a station, frequency shifted by the satellite, and retransmitted to that same station. In the case of three-way data the signal is transmitted by one station (master station), received and frequency shifted by the satellite, and retransmitted to the master staions and to any other stations

(slave stations) which are in the line-of-sight of the satellite. Essentially, the Doppler data type measures the relative velocity between the station and the satellite. No data are acquired when the satellite is occulted by the moon. The tracking stations use very sensitive double-conversion superheterodyne automatic-phase-tracking receivers. The transmitter, receiver, and station timing are driven by very stable atomic frequency standards. The stability of the Doppler frequency-shift data is a direct function of the frequency standard and is on the order of one part in 10^{12}.

All the tracking data gathered to date covers a restricted region of the lunar surface. The inclinations of the Lunar Orbiters were limited to two regions, low inclinations between 10° and 21°, and a high inclination of about 85° (see Figure 1). The inclinations of the Apollo missions ranged from about 178° to 154° (retrograde orbits). (See Figure 2). Hence there exists a large gap in the tracking coverage in the region between 26° and 85°. Any anomalous areas in the lunar mass distribution existing in the untracked region produce only secondary variations in the orbits that have been tracked and consequently are very difficult to determine accurately.

Attitude control maneuvers performed by the satellite have damaging effects on the overall usefulness of these data for selenodesy purposes. In the case of Lunar Orbiter the

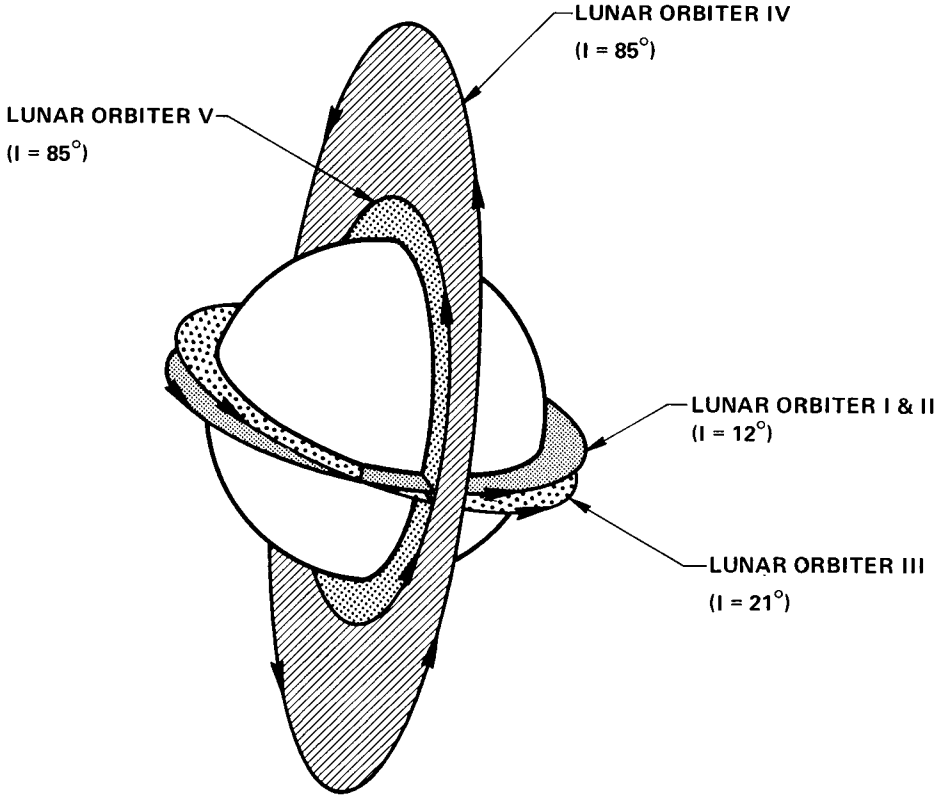

LUNAR ORBITER	PERILUNE ALT. (km)	APOLUNE ALT. (km)
I	50	1850
II	50	1850
III	50 (140)*	1850 (320)*
IV	2700	6100
V	100	1500

*POST MANEUVER

FIGURE 1 - LUNAR ORBITER ORBITAL GEOMETRY

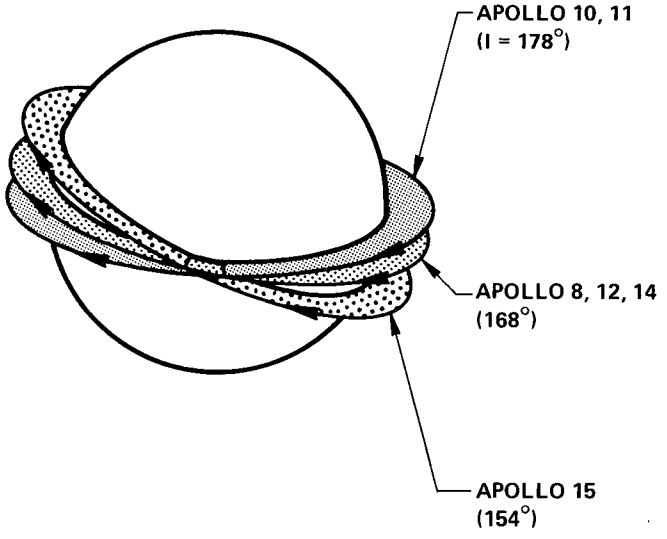

APOLLO	PERILUNE ALT. (km)	APOLUNE ALT. (km)
8	95	95
10	95	95
11	95	95
12	95	95
14	13 (95)*	95 (95)*
15	13 (95)*	95 (95)*

*POST MANEUVER

FIGURE 2 - APOLLO ORBITAL GEOMETRY

attitude control system was not coupled in either the pitch or yaw direction. During all of the early Apollo missions (8, 10, and 11) a large number of attitude control maneuvers were performed using only one thruster quad. In each case the effect of these maneuvers was to produce not only the desired rotation but also a translational velocity for the satellite. The trajectory of the satellite is noticeably disturbed by these propulsive maneuvers. As pointed out by Lorell[1], in theory these effects can be modeled; but in practice it is a very difficult and costly operation. Further, because of engineering uncertainties and incompleteness of telemetry records, the reliability of results would be questionable. Every precaution possible is taken during the course of this analysis to use tracking data which is of free-flight quality (thrust free).

REVIEW OF PREVIOUS METHODS

Two general methods have been used to obtain lunar gravity fields; the direct method and the indirect method or long-term selenodesy method.

The direct method, principally used by Langley Research Center, attempts to estimate the gravity field from the Doppler tracking data. In this method the solution parameter set is augmented to include both dynamical state variables and lunar harmonic parameters. Large batches of tracking data covering long time periods from many satellites

are used. Results obtained by Michael[2], Tolson and Gapcynski[3], and Gapcynski, Blackshear, and Compton[4], are representative of this method.

In the indirect method solutions are obtained using a two-step process. The first step is to regress Doppler observations spanning about one day using an assumed gravity field to determine the satellite state at some particular time. The osculating states generated are averaged for each satellite period to obtain a mean value of the Kepler elements for that particular orbit. This process is repeated for each available day of tracking data. The second step in this method involves fitting the long-period perturbation equations to the Kepler element variations. The lunar gravity determination is accomplished by numerically integrating the perturbation equations and differentially correcting a set of gravity parameters so as to give a best fit to the Kepler element variations. The results obtained by Blackshear, Compton, and Schiess[5], Lorell[6], and Risdal[7], demonstrate this method.

OUTLINE OF THIS INVESTIGATION

A new method for determining the lunar gravity field is developed which uses an empirical orbit determination (OD) and the long-period perturbation equations. The gravity determintion is a two step process as in the indirect method.

The empirical OD represents the Kepler orbital elements of the satellite as a six-dimensional time series.

The functional form chosen for each orbital element is that which best represents the long-period and secular variations in the orbital elements. In the first step of the process, tracking data is reduced to obtain simultaneous estimates for the orbital elements and the orbital element rates. This process is repeated for as many different spans of data and different satellites as are available (see Figure 3). In the second step, the perturbation equations, linear in the gravity parameters, are solved using the orbital elements and element rates to obtain a field (see Figure 4).

This method differs significantly from the long-period approach that has been previously used in that the Doppler data reduction uses no assumed model and directly estimates a mean orbital element state. Further and perhaps most importantly, the simultaneous estimation of Kepler states and rates makes each solution independent of the next with respect to the gravity parameter estimator.

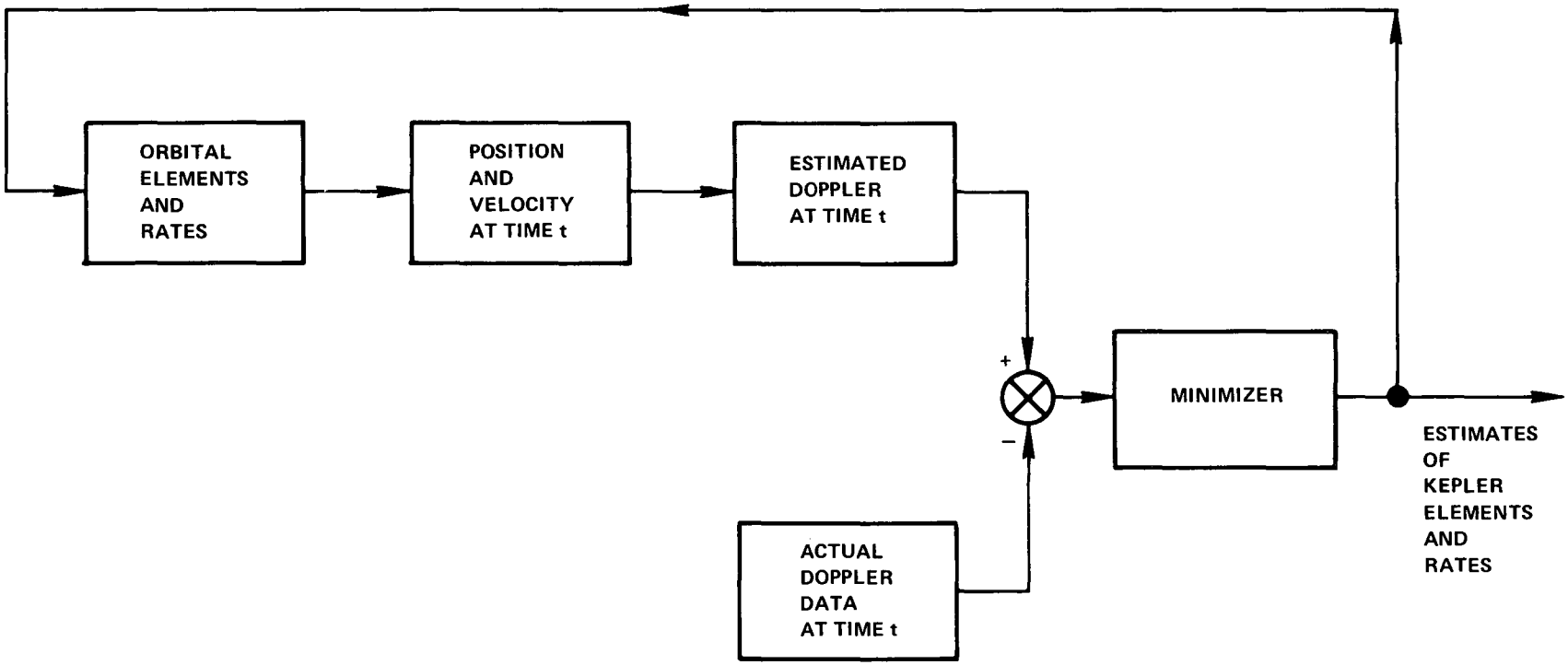

FIGURE 3 - EMPIRICAL ORBIT DETERMINATION

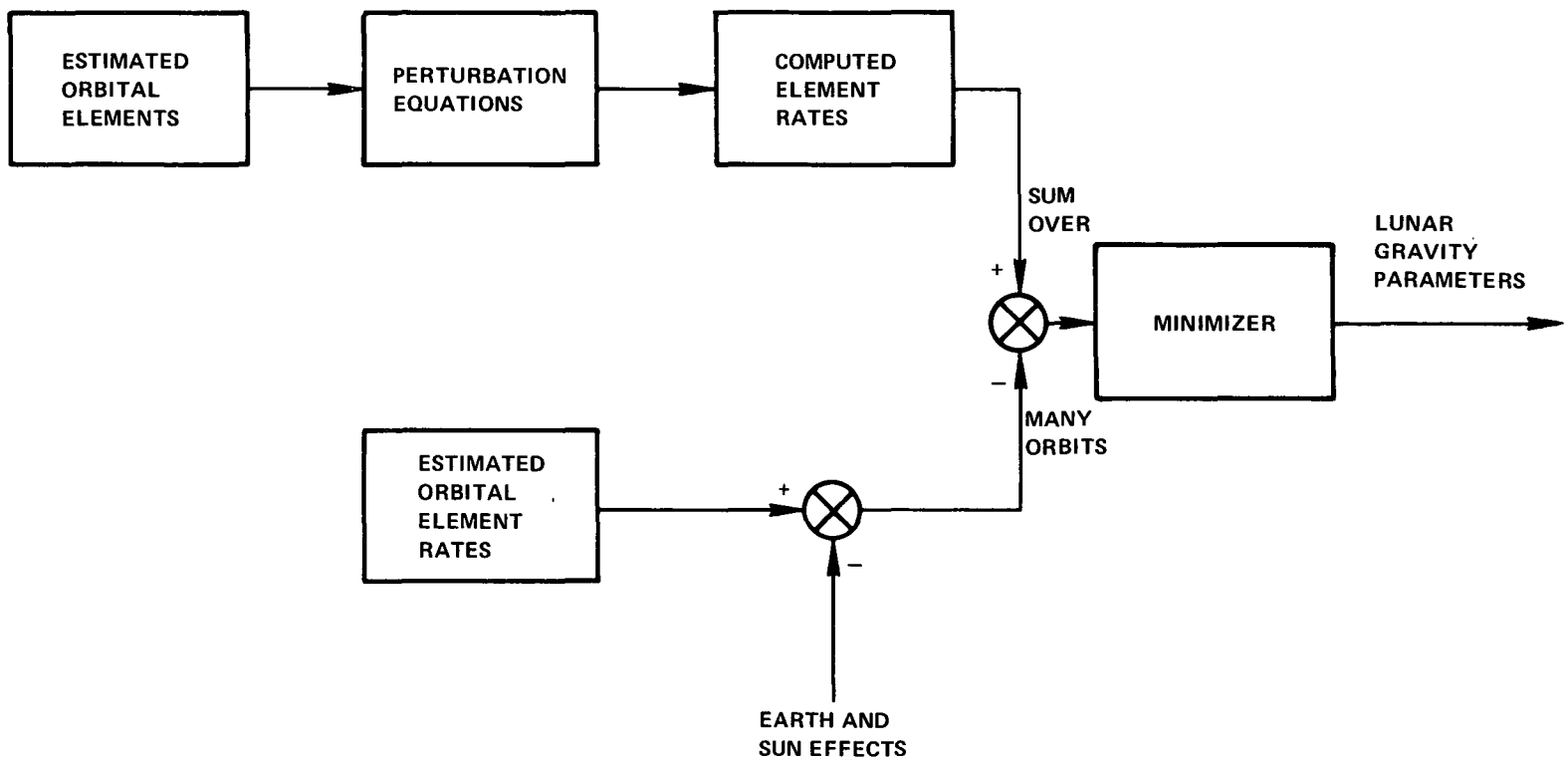

FIGURE 4 - DETERMINATION OF GRAVITY PARAMETERS

CHAPTER II

DYNAMICAL FORMULATION

The motion of a close lunar satellite is governed by a perturbed Newtonian gravitational law of attraction. The perturbations arise from the non-central properties of the lunar mass distribution and from the disturbing effects of the gravity fields of the earth, the sun, and other planets. These perturbing attractions are small; their effects are at least one thousand times less than the inverse square attraction of the moon.

The general equations of motion for a satellite referenced to an inertial moon centered coordinate system is:

$$\frac{d^2\bar{r}}{dt^2} = -\mu_{\text{☾}} \frac{\bar{r}}{r^3} + \bar{a}_d \qquad (2.1)$$

where $\bar{r}$ is the position vector, $\mu_{\text{☾}}$ is the product of the lunar mass and the universal gravitational constant, and $\bar{a}_d$ is the sum of all the perturbations. Although the perturbations are small numerically, their integrated effects are non-negligible and produce changes in the satellite's orbit.

The purpose of this chapter is to present the basic equations of Newtonian or Keplerian motion. These equations will be extended to account for a primary gravity field of arbitrary mass distribution and to account for the perturbing effects of third bodies (e.g., the earth and sun).

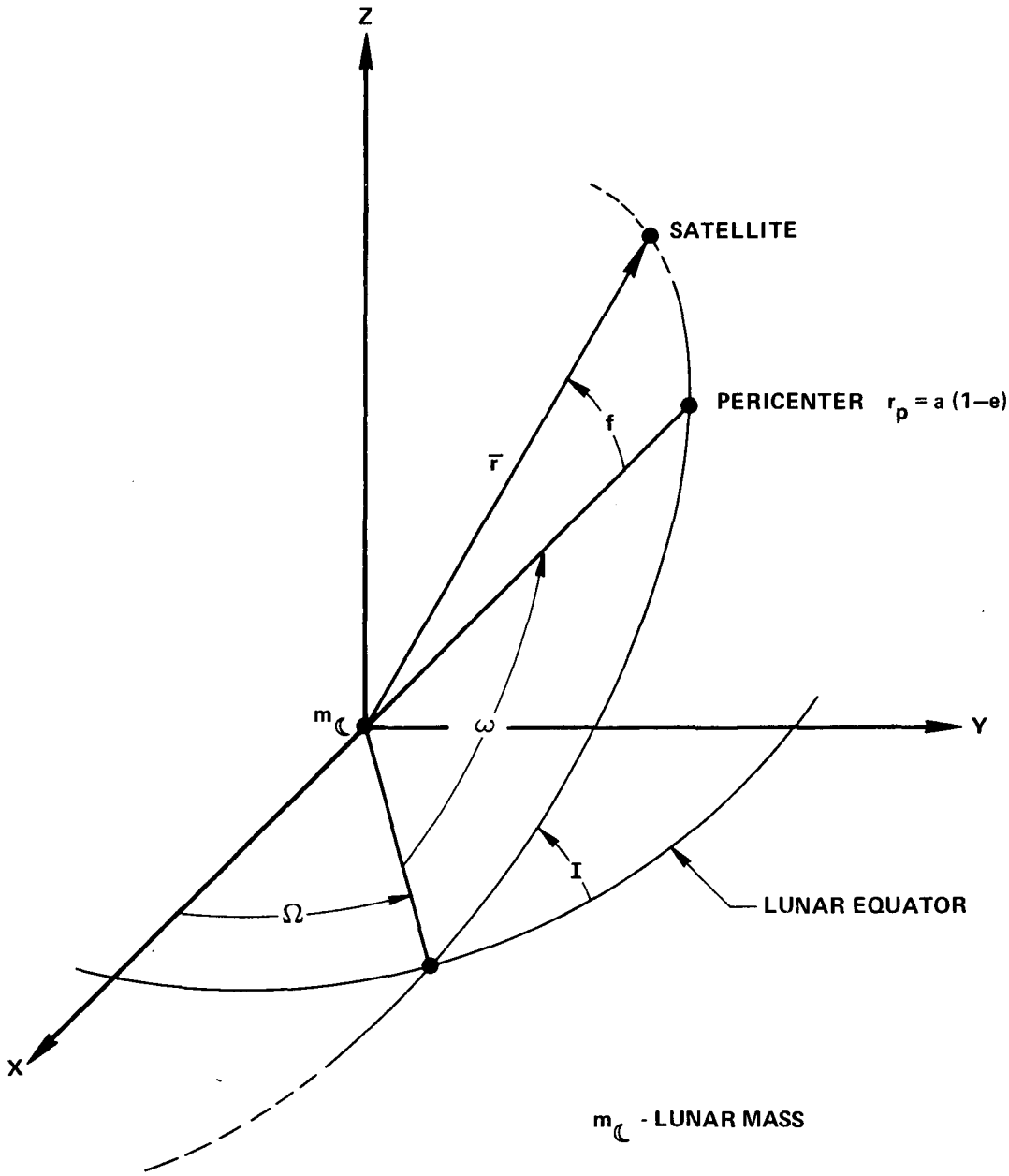

FIGURE 5 - GEOMETRY OF ORBITAL ELEMENTS

NEWTONIAN MOTION

The equations of motion for a satellite located at position $\bar{r}$ in a moon centered inertial system under the influence of an inverse square (Newtonian) gravity field are:

$$\ddot{\bar{r}} = -\mu \frac{\bar{r}}{r^3} \qquad (2.2)$$

These equations possess closed form solutions which characterize particle motion as follows:

1. The particle moves in a plane passing through the center of mass and has a constant angular momentum $\bar{h} = \bar{r} \times \bar{v}$ which is perpendicular to this plane.
2. The path of the motion is a conic section.

Since the equations of motion (2.2) are a set of three second order differential equations, a complete solution is uniquely specified by six integration constants. Geometrically, these constants are usually interpreted as the classical Kepler elements given below (see Figure 5).

a - semi-major axis of the orbit

e - eccentricity of the orbit

I - inclination of the orbital plane

Ω - longitude of the ascending node

ω - argument of pericenter

T_o - time of pericenter passage.

The variables a and e define the shape of the conic, I, Ω and ω are the Euler angles which specify the orientation of the orbit plane and axes, and T_o locates the position of the satellite in the orbit relative to pericenter. The time of pericenter passage is relatable to the mean (M), true (f), and eccentric (E) anomalies using the following conic relationships:

$$M(t) = \sqrt{\frac{\mu_\oplus}{a^3}}\,(t-T_o) \qquad (2.3)$$

$$M(t) = E - e \sin E \text{ (elliptical orbit)} \qquad (2.4)$$

$$f = 2 \tan^{-1}\left[\sqrt{\frac{1+e}{1-e}} \tan \frac{E}{2}\right] \qquad (2.5)$$

The satellite state is defined as a six vector of position and velocity;

$$\bar{x} = \begin{bmatrix} \bar{r} \\ \bar{v} \end{bmatrix} \qquad (\dot{\bar{r}} = \bar{v}) \qquad (2.6)$$

Correspondingly the satellite Kepler element vector is a six vector of orbital elements

$$\bar{k} = \begin{bmatrix} a \\ e \\ I \\ \Omega \\ \omega \\ M \end{bmatrix} \qquad (2.7)$$

The Kepler elements at any instant of time are non-linear functions of the satellite state and vice versa (see Appendix A):

$$\begin{aligned} \bar{x} &= \bar{x}(\bar{k}) \\ \bar{k} &= \bar{k}(\bar{x}) \end{aligned} \tag{2.8}$$

It is important to note here that the entire Newtonian development is based on an inverse square force law which assumes a spherically symmetric gravitational potential of the form:

$$U(\bar{r}) = \frac{\mu}{r} \tag{2.9}$$

Potential used here has the opposite sign to that used for potential energy in physics.

PERTURBED MOTION

If the satellite is now assumed to be under the gravitational influence of a primary planet (moon) of arbitrary non-homogeneous mass distribution, and of other planets, the gravitational potential of the satellite has the form:

$$U(\bar{r}) = \frac{\mu}{r} + R(\bar{r}) \tag{2.10}$$

where R is the disturbing function arising from the non-central effects. The equations of motion for the satellite now become:

$$\ddot{\bar{r}} = \nabla U = -\mu \left(\frac{\bar{r}}{r^3} + \frac{\partial}{\partial \bar{r}} R \right) \qquad (2.11)$$

where $\bar{a}_d \equiv \frac{\partial}{\partial \bar{r}} R$ and ∇ is the gradient operator. With $R \neq 0$ the Kepler orbital elements in general become functions of time. Since the non-central portion of the gravity field is small in comparison to the central part, the magnitude of variation in the Kepler elements is also small. The three second order differential equations (2.11) describing the perturbed satellite motion can be transformed into the orbital coordinate system using the method of variation of arbitrary constants[8] to obtain the time rate of change of the Keplerian elements (perturbation equations). The result is that the satellite state is now specified by six first order non-linear perturbation equations[9]:

$$\frac{da}{dt} = \frac{2}{na} \frac{\partial R}{\partial M} \qquad (2.12)$$

$$\frac{de}{dt} = \frac{\sqrt{1-e^2}}{na^2 e} \left[\sqrt{1-e^2} \frac{\partial R}{\partial M} - \frac{\partial R}{\partial \omega} \right] \qquad (2.13)$$

$$\frac{d\omega}{dt} = \frac{\sqrt{1-e^2}}{na^2} \left[\frac{1}{e} \frac{\partial R}{\partial e} - \frac{\cot I}{1-e^2} \frac{\partial R}{\partial I} \right] \qquad (2.14)$$

$$\frac{d\Omega}{dt} = \frac{\csc I}{na^2\sqrt{1-e^2}} \frac{\partial R}{\partial I} \qquad (2.15)$$

$$\frac{dI}{dt} = \frac{\csc I}{na^2\sqrt{1-e^2}} \left[\cos I \frac{\partial R}{\partial \omega} - \frac{\partial R}{\partial \Omega}\right] \tag{2.16}$$

$$\frac{dM}{dt} = n - \frac{1}{na}\left[\frac{1-e^2}{ae}\frac{\partial R}{\partial e} + 2\frac{\partial R}{\partial a}\right] \tag{2.17}$$

where the mean motion $n = \sqrt{\frac{\mu_{\leftmoon}}{a^3}}$. In vector notation these equations have the following general form:

$$\frac{d\bar{k}}{dt} = \bar{f}(\bar{k},t) \tag{2.18}$$

In order to carry out a solution for the equations, the disturbing function R must be specified and expressed in orbital plane coordinates. The disturbing function assumed in this investigation will have components arising from the non-central part of lunar gravity, $R_{\leftmoon}$, earth and sun perturbations, $R_{\oplus}$ and $R_{\odot}$, and solar radiation pressure, R_{SR}. Hence,

$$R = R_{\leftmoon} + R_{\oplus} + R_{\odot} + R_{SR} \tag{2.19}$$

LUNAR POTENTIAL FUNCTION

The general form accepted by the International Astronomical Union[10] in 1962 for the representation of the lunar gravity field is the spherical harmonic expansion expressed in selenographic coordinates. The selenographic coordinate system is moon fixed and oriented such that the

x-y plane is the lunar equatorial plane, the x-axis coincides with the mean earth-moon line through Sinus Medii, and the z-axis is directed along the moon's mean spin axis. The selenographic axis system rotates about the z-axis of the inertial system with a sidereal period of 27.32 days.

The lunar gravitational potential is the solution to the Laplace equation ($\nabla^2 U=0$) in spherical coordinates and is expressed as follows:

$$U(r,\phi,\lambda) = \frac{\mu_{\mathbb{C}}}{r}\left[1 + \sum_{\ell=2}^{\infty}\sum_{m=0}^{\ell}\left(\frac{R_e}{r}\right)^{\ell} P_\ell^{\,m}(\sin\phi)\left\{C_{\ell m}\cos m\lambda + S_{\ell m}\sin m\lambda\right\}\right] \tag{2.20}$$

In this equation R_e is the mean radius of the moon, $P_\ell^{\,m}$ is the associated Legendre polynominal, (r,ϕ,λ) are the selenographic radius, latitude, and longitude, and $C_{\ell m}$, $S_{\ell m}$ are the gravitational parameters which describe the non-central features of the lunar field. The objective of this investigation is to determine a finite set of $\{C_{\ell m}, S_{\ell m}\}$ which accurately describes the lunar field. It is assumed that the origin of coordinates is located at the center of mass of the moon. Using this assumption, the terms of first degree ($\ell=1$) are omitted from the expansion since they represent center of mass displacements in each dimension. The terms of degree ℓ and order $m=0$ are known as zonals and are symmetric about the z-axis. Terms of degree ℓ and order m are called

tesserals (ℓ=m are sectorials) and are functions of all three dimensions. The potential of the moon is related to its density distribution D as follows:

$$U(\bar{r}) = G\iiint \frac{D(\bar{r})}{|\bar{r} - \bar{r}'|} d\bar{r} \qquad (2.21)$$

where G is the gravitational constant and $\bar{r}'$ is the distance to the mass element.

Two examples of the perturbations in the potential, one for an even degree zonal, C_{20}, and one for an odd zonal, C_{30}, are shown in Figure 6.

The disturbing function for the lunar potential is:

$$R_{\leftmoon} = U(r,\phi,\lambda) - \frac{\mu_{\leftmoon}}{r} \qquad (2.22)$$

where U here is given by equation (2.20). The disturbing function can also be represented as the sum of zonal and tesseral terms.

$$R_{\leftmoon} = \sum_{\ell=2}^{\infty} \sum_{m=0}^{n} U_{\ell m} \qquad (2.23)$$

where each particular term, $U_{\ell m}$, is

$$U_{\ell m} = \mu_{\leftmoon} \frac{R_e^{\ell}}{r^{\ell+1}} P_{\ell}^{m}(\sin\phi)(C_{\ell m} \cos m\lambda + S_{\ell m} \sin m\lambda) \qquad (2.24)$$

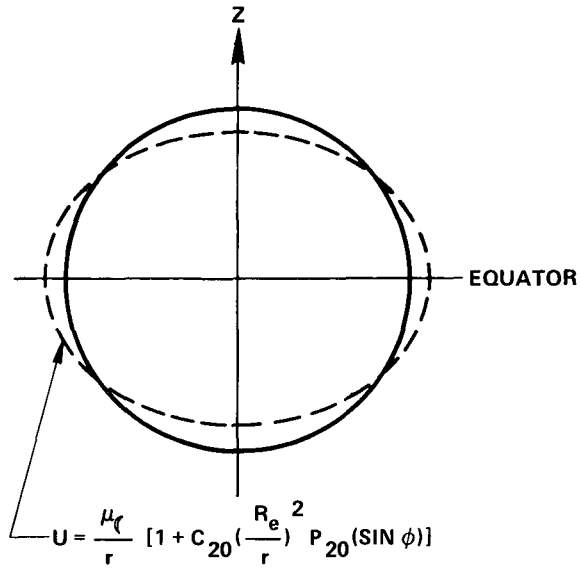

OBLATE $C_{20} < 0$

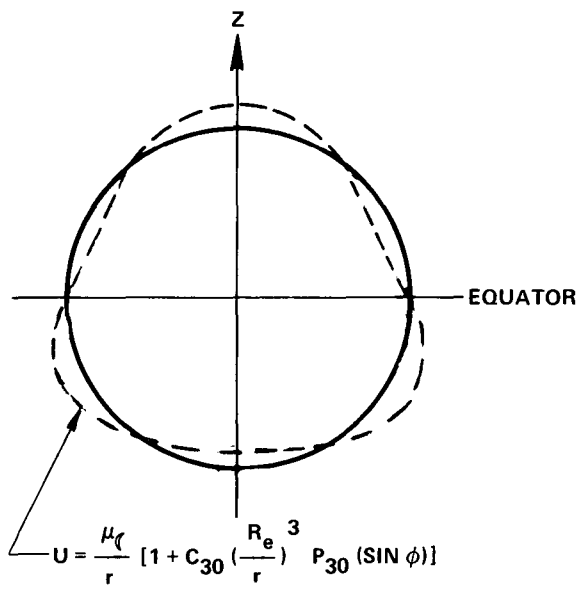

PEAR SHAPE $C_{30} > 0$

FIGURE 6 - PERTURBED POTENTIALS

A general formulation for transforming each term in the disturbing function of a primary body has been developed by Kaula[11]. During the course of this derivation the spherical harmonic potential is converted from the selenographic spherical coordinate system (see Eq. 2.20) to the Kepler elements referenced to the inertial system. The basic assumption in this derivation is that the inertial and selenographic systems share a common equatorial plane and that the selenographic system rotates about the polar (z) axis of the inertial system (see Figure 7).

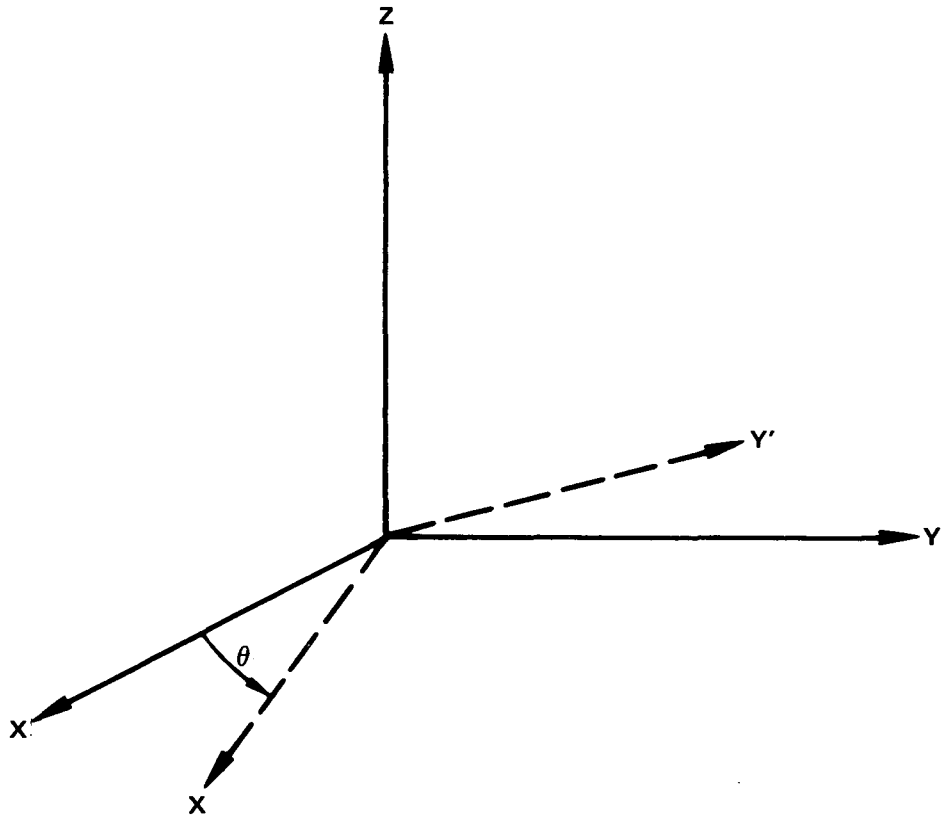

FIGURE 7 - ROTATING COORDINATES

The disturbing potential expressed in orbit plane coordinates is:

$$R_{\ell}(\bar{k}) = \sum_{\ell=2}^{\infty} \sum_{m=0}^{\ell} \mu_{\ell} \frac{R_e^{\ell}}{a^{\ell+1}} P(I,e) S_{\ell mpq}(\omega, M, \Omega, \theta) \qquad (2.25)$$

where

$$P(I,e) = \sum_{p=0}^{\ell} \sum_{q=-\infty}^{+\infty} F_{\ell mp}(I) G_{\ell pq}(e) \qquad (2.26)$$

and

$$F_{\ell mp}(I) = \sum_{t} \frac{(2\ell-2t)!}{t!(\ell-t)!(\ell-m-2t)!\, 2^{(2\ell-2t)}} \sin^{\ell-m-2t} I \cdot$$

$$\sum_{s=0}^{m} \binom{m}{s} \cos^{s} I \sum_{c} \binom{\ell-m-2t+s}{c} \binom{m-s}{p-t-c} (-1)^{c-k} \qquad (2.27)$$

(p, q, t, s, c, and k are dummy indices)

where k is the integer part of $\frac{(\ell-m)}{2}$, t is summed to the lesser of p or k, and c is summed over all values which make the binomial coefficient nonzero.

The function $G_{\ell pq}(e)$ in equation (2.26) is defined as follows:

$$G_{\ell pq}(e) = (-1)^{|q|} (1+\beta^2)^{\ell} \beta^{|q|} \sum_{k=0}^{\infty} T_{\ell pqk} Q_{\ell pqk} \beta^{2k} \qquad (2.27)$$

where

$$\beta = \frac{e}{1+\sqrt{1-e^2}} \qquad (2.28)$$

$$T_{\ell pqk} = \sum_{r=o}^{h} \binom{2p'-2\ell}{h-r} \frac{(-1)^r}{r!} \left[\frac{(\ell-2p'+q')e}{2\beta}\right]^r \qquad (2.29)$$

$$h = k+q', \quad q'>0; \quad h=k, \quad q'<0$$

and

$$Q_{\ell pqk} = \sum_{r=o}^{h} \binom{-2p'}{h-r} \frac{1}{r!} \left[\frac{(\ell-2p'+q')e}{2\beta}\right]^r \qquad (2.30)$$

$$h=k, \quad q'>0; \quad h=k-q', \quad q'<0$$

$$p'=p, \quad q'=q \quad \text{for} \quad p\leq \ell/2$$

$$p'=\ell-p, \quad q'=-q \quad \text{for} \quad p>\ell/2$$

Also in equation (2.25)

$$S_{\ell mpq} = \begin{bmatrix} C_{\ell m} \\ -S_{\ell m} \end{bmatrix}_{\substack{\ell-m \text{ odd}}}^{\ell-m \text{ even}} \cos[(\ell-2p)\omega+(\ell-2p+q)M + m(\Omega-\theta)] + \qquad (2.31)$$

$$\begin{bmatrix} S_{\ell m} \\ C_{\ell m} \end{bmatrix}_{\substack{\ell-m \text{ odd}}}^{\ell-m \text{ even}} \sin[(\ell-2p)\omega + (\ell-2p+q)M + m(\Omega-\theta)]$$

and θ is the angular displacement between the inertial and the graphic axis systems.

The effects of the $U_{\ell m}$ disturbing term can be approximated by using standard perturbation theory concepts[12]. Essentially each term gives rise to short-period and either long-period (and very long-period) or secular variations in the orbital elements. As applied to this dynamical system, short-period variations are those which are periodic with a period of an integer multiple less than the satellite orbit period. Long-period variations are again periodic with a period which is an integer multiple less than the period of the moon (28 days). Very long-period variations have a period less than the period of the perifocus rotation. Secular variations are nearly linear in time. Examining equation (2.31), these different types of variations are associated with the following factors:

1. Short-Period: $(\ell-2p+q)M$
2. Long Period: $m(\Omega-\theta)$
3. Very Long-Period: $(\ell-2p)\omega$
4. Secular: $(\ell-2p) = (\ell-2p+q) = m = 0$

Analysis[13] has shown that the long-period satellite dynamics can be accurately determined from Doppler tracking data. This form of the perturbation equations, the long-period equations, can be obtained by averaging the lunar disturbing function, R , with respect to the mean anomaly.

$$\bar{R}_{\ell} = \frac{1}{2\pi}\int_{o}^{2\pi} R_{\ell}\, dM \qquad (2.32)$$

This calculation was also carried out by Kaula and the result simplifies (2.25) to the following:

$$\bar{R}_{\ell} = \sum_{\ell=2}^{\infty} \sum_{m=0}^{\ell} \mu_{\ell} \frac{R_e^{\ell}}{a^{\ell+1}} P'(I,e)\, S_{\ell mpq(\omega,\Omega,\theta)} \qquad (2.33)$$

where $q = 2p-\ell$ only and

$$P'(I,e) = \sum_{p=0}^{k} F_{\ell mp}(I) G_{\ell pq}(e) \qquad (2.34)$$

$F_{\ell mp}(I)$ is given by (2.27) and $G_{\ell pq}(e)$ is:

$$G_{\ell pq}(e) = \frac{1}{(1-e^2)^{\ell-1/2}} \sum_{d=o}^{p'-1} \binom{\ell-1}{2d+\ell-2p'} \binom{2d+\ell-2p'}{d} \left(\frac{e}{2}\right)^{2d+\ell-2p'} \qquad (2.35)$$

in which

$$p' = p \qquad \text{for} \qquad p \leq \ell/2$$

$$p' = \ell-p \qquad \text{for} \qquad p \geq \ell/2$$

and $S'_{\ell mpq}(\omega,\Omega,\theta)$ is

$$S'_{\ell mpq} = \begin{bmatrix} C_{\ell m} \\ -S_{\ell m} \end{bmatrix} \begin{matrix} \ell-m \text{ even} \\ \ell-m \text{ odd} \end{matrix} \cos\left[(\ell-2p)\omega + m(\Omega-\theta)\right] \quad +$$

$$\begin{bmatrix} S_{\ell m} \\ C_{\ell m} \end{bmatrix}_{\ell-m \text{ odd}}^{\ell-m \text{ even}} \sin\left[(\ell-2p)\omega + m(\Omega-\theta)\right] \tag{2.36}$$

It should be noted here that this entire long-period averaging procedure is accurate to the first order[14]. (Terms of order ε^2 and above are neglected.) The long periodic variations experienced by $\bar{R}_\ell$ can be either long-periodic in the ascending node ($m \neq 0$), very long-periodic in the perifocus ($\ell - 2p \neq 0$), both, or secular ($m = 0$, $\ell = 2p$). The secular variations are associated only with zonal perturbations of even degree[15]. (Very long-periodic variations are also experienced by these terms.) Zonal terms of odd degree have only very long-periodic variations. Tesseral and sectorial terms have both periodic and long-periodic variations.

Since the disturbing function, $\bar{R}_\ell$, is independent of the mean anomaly, two of the perturbation equations (2.12 and 2.13) simplify to:

$$\frac{da}{dt} = 0 \tag{2.37}$$

$$\frac{de}{dt} = -\frac{\sqrt{1-e^2}}{na^2e} \frac{\partial \bar{R}}{\partial \omega} \tag{2.38}$$

Therefore, to first order exactness, the semi-major axis of the orbit is a constant of the motion.

The complete analytical equations specifying the long-period dynamics of a satellite under the influence of

a moon of arbitrary mass distribution are given by (2.37), (2.38), (2.14), (2.15), (2.16), (2.17), (2.33), (2.34), (2.27), (2.35), and (2.36). As an example of the form of long-period equations, the perturbation equations for the C_{20} zonal term and the C_{22} sectorial are presented:

For C_{20}:

$$\frac{da}{dt} = \frac{de}{dt} = \frac{dI}{dt} = 0 \tag{2.39}$$

$$\frac{d\Omega}{dt} = \frac{3}{2} \frac{n\, C_{20}}{(1-e^2)^2} \left(\frac{R_e}{a}\right)^2 \cos I \tag{2.40}$$

$$\frac{d\omega}{dt} = \frac{3}{4} \frac{n\, C_{20}}{(1-e^2)^2} \left(\frac{R_e}{a}\right)^2 (1-5\cos^2 I) \tag{2.41}$$

$$\frac{dM}{dt} = n \left[1 - \frac{3}{4} \frac{C_{20}}{(1-e^2)^{3/2}} \left(\frac{R_e}{a}\right)^2 (3\cos^2 I - 1)\right] \tag{2.42}$$

For C_{22}:

$$\frac{da}{dt} = \frac{de}{dt} = 0 \tag{2.43}$$

$$\frac{dI}{dt} = \frac{3n\, C_{22}}{(1-e^2)^2} \left(\frac{R_e}{a}\right)^2 \sin I \sin 2(\Omega-\theta) \tag{2.44}$$

$$\frac{d\Omega}{dt} = \frac{3n\, C_{22}}{(1-e^2)^2} \left(\frac{R_e}{a}\right)^2 \cos I \cos 2(\Omega-\theta) \tag{2.45}$$

$$\frac{d\omega}{dt} = \frac{3}{2} n \frac{C_{22}}{(1-e^2)^2} \left(\frac{R_e}{a}\right)^2 \cos 2(\Omega-\theta)(5\sin^2 I - 2) \qquad (2.46)$$

$$\frac{dM}{dt} = n \left[1 + \frac{9}{2} C_{22} \left(\frac{R_e}{a}\right)^2 \frac{\sin^2 I \cos 2(\Omega-\theta)}{(1-e^2)^{3/2}}\right] \qquad (2.47)$$

For both sets of perturbations the dynamical equations are coupled non-linear equations (linear in the gravity parameters). A principal difference between the zonal term and the sectorial (and this is true in general) is that zonal perturbation equations are autonomous whereas the others are not.

EARTH AND SUN PERTURBATIONS

The disturbing function for a third body (earth or sun in this case) located at $\bar{r}_3$ on a satellite located at $\bar{r}$ has been computed by Brouwer and Clemence[16].

$$R_3 = \frac{\mu_3}{r_3}\left[\left(\frac{r}{r_3}\right)^2 \left(-\frac{1}{2} + \frac{3}{2}\cos^2\psi\right) + \left(\frac{r}{r_3}\right)^3 \left(-\frac{3}{2}\cos\psi + \frac{5}{2}\cos^3\psi\right) + \ldots\right] \qquad (2.48)$$

where μ_3 represents the third body mass and ψ is the angle between $\bar{r}$ and $\bar{r}_3$ (see Figure 8) and $\bar{r}_3 >> \bar{r}$. This expansion is accurate to third order. In order to obtain the long-period portion of this disturbing function, it must be averaged over the satellite orbit.

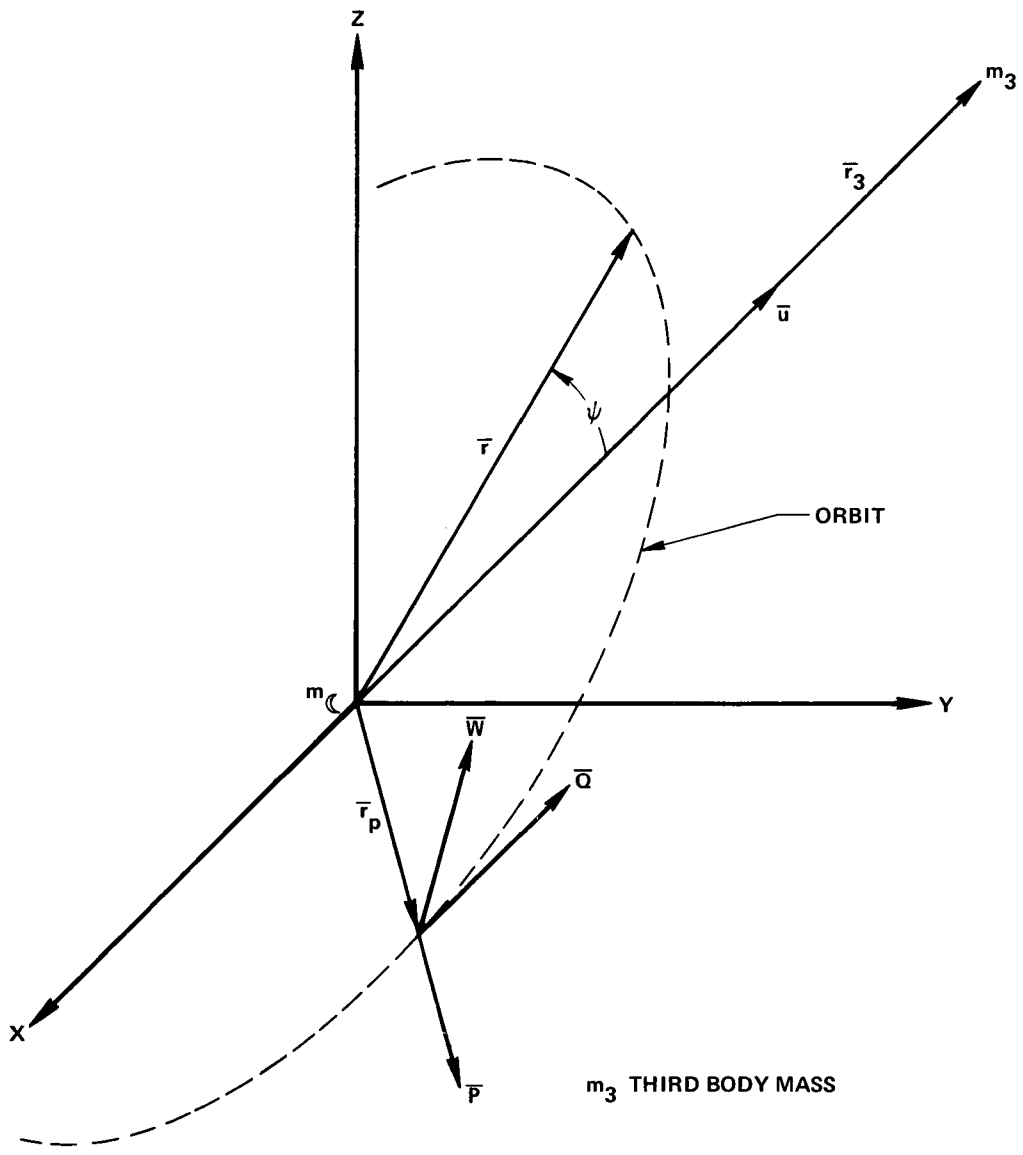

FIGURE 8 - THIRD BODY LOCATION

The averaging with respect to the anomaly of this disturbing function has been performed by Liu and Lorell[17] and has the following form:

$$\bar{R}_3 = \frac{\mu_3}{r_3}\left[\bar{F}_2 + \bar{F}_3\right] \tag{2.49}$$

where

$$\bar{F}_2 = \left(\frac{a}{r_3}\right)^2 \frac{1}{2}\left[-(1+3/2\ e^2) + 3A^2(2e^2+1/2) + \frac{3B^2}{2}(1-e^2)\right] \tag{2.50}$$

$$\bar{F}_3 = \frac{5}{4}\left(\frac{a}{r_3}\right)^3 Ae\left[3(1+3/4\ e^2) - 5A^2(e^2+3/4) - \frac{15}{4}B^2\ (1-e^2)\right] \tag{2.51}$$

and $A = \bar{u} \cdot \bar{P}$, $B = \bar{u} \cdot \bar{Q}$. $\bar{u}$ is the unit vector in the direction of the third body, $\bar{P}$ is a unit vector to the perifocus and $\bar{Q}$ is a unit vector in the orbit plane orthogonal to $\bar{P}$.

Hence, the total dynamical effect on a satellite in lunar orbit due to either the earth or sun is formed by evaluating the perturbation equations using (2.49) as the disturbing function.

PHYSICAL LIBRATIONS OF THE MOON

In the derivation of the lunar disturbing function R_ℓ it is assumed that the selenographic axis system to which the gravity parameters are referenced rotates about the polar axis of the inertial system. In addition to this polar axis rotation, the selenographic system undergoes additional

small rotations about all three axes due to precession and physical librations. Since these rotations are not included in the analytical formulation a correction must be applied to the long-period equations. Analysis[18] shows these effects can be eliminated if the selenographic system fixed at epoch is used.

SOLAR RADIATION PRESSURE

The perturbing effects of solar radiation pressure have been derived by Kozai[19]. The variations in the orbital elements are:

$$\Delta a_{SR} = 0 \tag{2.52}$$

(first order approximation)

$$\Delta e_{SR} = -\frac{F\sqrt{1-e^2}}{a\,n^2}\left|\frac{1}{4}A^*\sqrt{1-e^2}\cos 2E+B^*\left(\frac{1}{4}\sin 2E-2e\sin E+\frac{3}{2}E\right)\right|_{E_1}^{E_2} \tag{2.53}$$

$$\Delta I_{SR} = \frac{FC^*}{a\,n\sqrt{1-e^2}}\left|\cos\omega\left[(1+e^2)\sin E-\frac{e}{4}\sin 2E-\frac{3}{2}eE\right]+\sqrt{1-e^2}\sin\omega\left[\cos E-\frac{e}{4}\cos 2E\right]\right|_{E_1}^{E_2} \tag{2.54}$$

$$\Delta\Omega_{SR} = -\frac{FC^*}{an^2\sin I\sqrt{1-e^2}}\left|\sin\omega\left[(1+e^2)\sin E-\frac{e}{4}\sin 2E-\frac{3}{2}eE\right]-\sqrt{1-e^2}\cos\omega\left[\cos E-\frac{e}{4}\cos 2E\right]\right|_{E_1}^{E_2} \tag{2.55}$$

$$\Delta\omega_{SR} = \frac{-F}{a\, r_e^2} \left| A^* \sqrt{1-e^2}\ (e \sin E + \frac{1}{4} \sin 2E - \frac{3}{2} E) + \right.$$

$$\left. B^* (e \cos E - \frac{1}{4} \cos 2E) \right|_{E_1}^{E_2} - \cos I\ \Delta\Omega_{SR} \qquad (2.56)$$

$$\Delta M_{SR} = \frac{2F}{a\, n^2} \left| A^* [(1+e^2) \sin E - \frac{e}{4} \sin 2E - \frac{3}{2} eE] - \right.$$

$$\left. B^* \sqrt{1-e^2} [\cos E - \frac{e}{4} \cos 2E] \right|_{E_1}^{E_2} - \sqrt{1-e^2} (\Delta\Omega_{SR} + \cos I\ \Delta\Omega_{SR}) \qquad (2.57)$$

where F is the magnitude of solar acceleration and $A^* = \bar{P} \cdot \bar{u}_\odot$, $B^* = \bar{Q} \cdot \bar{u}_\odot$, $C^* = \bar{W} \cdot \bar{u}_\odot$. $\bar{u}_\odot$ is a unit vector in the direction of the sun, $\bar{P}$, $\bar{Q}$, $\bar{W}$ are vectors to perifocus, in the orbit plane orthogonal to $\bar{P}$, and normal to the orbit plane orthogonal to $\bar{P}$ and $\bar{Q}$, respectively.

$$F = \left(\frac{\tilde{A}}{m}\right)\left(\frac{S_\odot}{c}\right)\left(\frac{r_\odot}{r}\right)^2 (1+\upsilon) \qquad (2.58)$$

where $\tilde{A}$ is the satellite effective cross-sectional area, m is the mass, $S_\odot$ is the solar constant, $r_\odot$ the distance to the sun, υ is the reflection coefficient, and c is the speed of light.

These perturbations are only acting on the satellite when it is in sunlight. A test used to determine the sun's visibility is (see Figure 9):

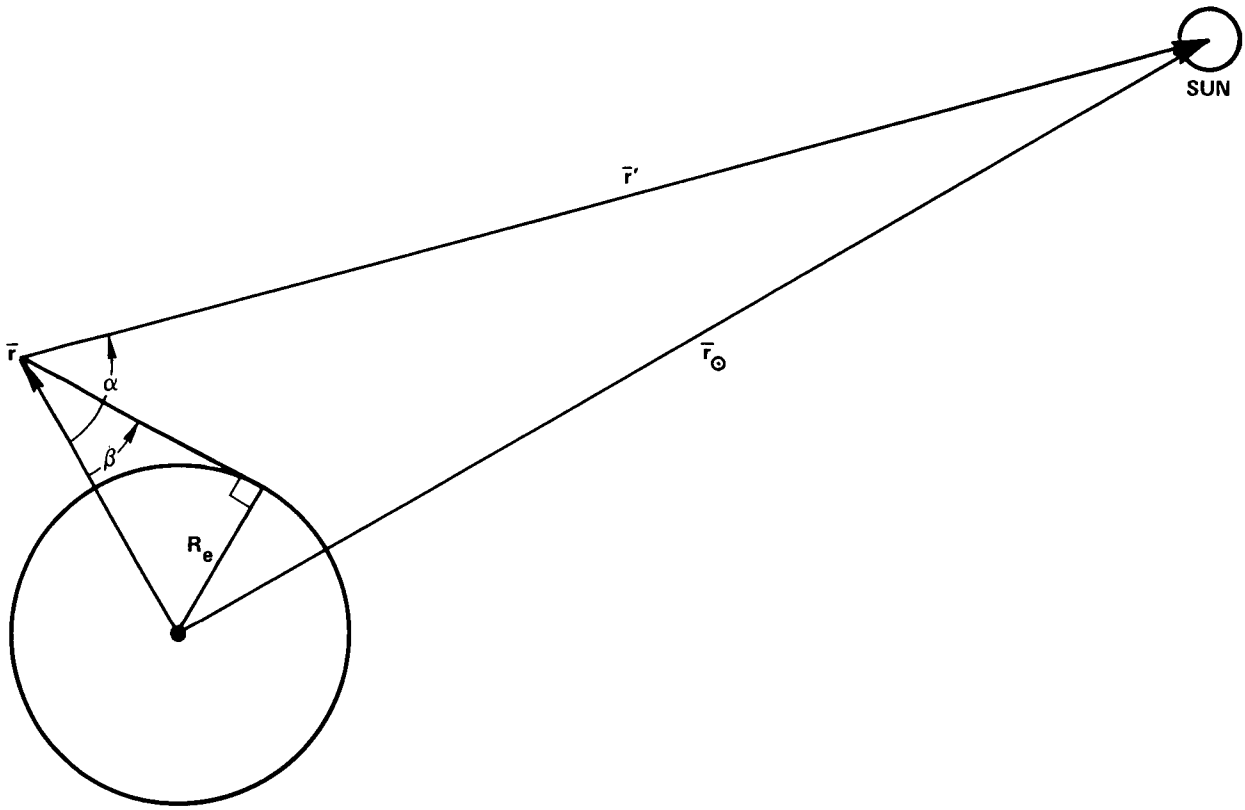

FIGURE 9 - SATELLITE SUN GEOMETRY

$|\alpha| \leq |\beta|$ perturbations are zero

$|\alpha| > |\beta|$ perturbations are present

where .

$$|\beta| = \left|\tan^{-1} \frac{R_e}{r}\right| \tag{2.59}$$

$$|\alpha| = \left|\cos^{-1} \frac{-\bar{r}\cdot\bar{r}'}{rr'}\right| \tag{2.60}$$

and

$$\bar{r}' = \bar{r}_\odot - \bar{r} \tag{2.61}$$

SUMMARY

The perturbation equations for the long-period motion of a lunar satellite under the gravitational influence of a primary of arbitrary mass distribution and the earth, sun, and solar radiation are presented. The general form of these dynamical equations is as follows:

$$\frac{da}{dt} = 0 \tag{2.62}$$

$$\frac{de}{dt} = \sum_{\ell,m} \frac{de_{\ell,m}}{dt} + \frac{de_\oplus}{dt} + \frac{de_\odot}{dt} + \frac{de_{SR}}{dt} \tag{2.63}$$

$$\frac{dI}{dt} = \sum_{\ell,m} \frac{dI_{\ell,m}}{dt} + \frac{dI_\oplus}{dt} + \frac{dI_\odot}{dt} + \frac{dI_{SR}}{dt} \tag{2.64}$$

$$\frac{d\Omega}{dt} = \sum_{\ell,m} \frac{d\Omega_{\ell,m}}{dt} + \frac{d\Omega_\oplus}{dt} + \frac{d\Omega_\odot}{dt} + \frac{d\Omega_{SR}}{dt} \tag{2.65}$$

$$\frac{d\omega}{dt} = \sum_{\ell,m} \frac{d\omega_{\ell,m}}{dt} + \frac{d\omega_{\oplus}}{dt} + \frac{d\omega_{\odot}}{dt} + \frac{d\omega_{SR}}{dt} \qquad (2.66)$$

$$\frac{dM}{dt} = \sum_{\ell,m} \frac{dM_{\ell,m}}{dt} + \frac{dM_{\oplus}}{dt} + \frac{dM_{\odot}}{dt} + \frac{dM_{SR}}{dt} \qquad (2.67)$$

These long-period perturbation equations form an analytical basis for the development of the empirical OD.

CHAPTER III

EMPIRICAL ORBIT DETERMINATION

One method of modeling the perturbed motion of a lunar satellite is to represent each of the Kepler elements of the orbit as an independent time function[20]. This representation forms the basis of the empirical orbit determination method. Using Doppler tracking data and a minimizing process, estimates are obtained for the parameters which characterize these time functions.

The purpose of this chapter is to present the theory and equations used to represent the long-period motion of the lunar satellite.

MATHEMATICAL THEORY

The long-period time dependence induced in each of the Kepler elements by non-central gravity perturbations is given by the perturbation equations (2.62-2.67).

$$\frac{d\bar{k}}{dt} = \bar{f}(\bar{k},t)$$

Since these equations are non-linear, general closed form solutions are not obtainable. The non-central effects are extremely small compared to the central body term; consequently solutions can be approximated.

If an analytic quadrature is performed on each perturbation equation, a set of integral equations results:

$$\bar{k}(t) = \bar{k}(t_o) + \int_{t_o}^{t} \bar{f}(\bar{k},t)dt \qquad (3.1)$$

The kernels, or forcing functions, appearing above are non-separable, non-linear functions. If only the perturbations arising from the lunar disturbing function are considered, these kernels can be categorized into two types:

1. $\bar{f}(\bar{k},t) = \bar{f}(\bar{k})$ (autonomous) (3.2)

2. $\bar{f}(\bar{k},t) = g(\bar{k})\sin m\gamma t + \bar{h}(\bar{k})\cos m\gamma t$ (3.3)

$m = 1,2,3,...$ (perturbation order index)

where γ (1/27.32 rev/day) is the rotational rate of the moon ($\theta \equiv \gamma t$). (This categorization does not apply when the standard Kepler elements become singular, for nearly circular, nearly equatorial orbits. However, a similar approximation can then be used with a modified orbital element set.) The first or autonomous kernel corresponds to zonal perturbations, and the second to tesseral and sectorial perturbations. If it is assumed that for periods of time of 24 hours or less the magnitude of variation in the Kepler elements is small, then $\bar{f}(\bar{k})$, $\bar{g}(\bar{k})$, and $\bar{h}(\bar{k})$ can be considered constant.

Solutions to equations possessing autonomous kernels have the following simple form:

$$\bar{k}(t) = \bar{k}(t_o) + \bar{f}(t_o)(t-t_o) \qquad (3.4)$$

These solutions have the linear properties of secular variations. Using the same time approximation made previously (as for 3.4), solutions for the non-autonomous kernels can be given as follows:

$$\bar{k}(t) = \bar{c}_1(t_o) + \bar{c}_2(t_o)\sin m\,\gamma(t-t_o) + \bar{c}_3(t_o)\cos m\,\gamma(t-t_o) \qquad (3.5)$$

where $\bar{c}_1$, $\bar{c}_2$, and $\bar{c}_3$ are constants and $\bar{c}_1(t_o) = \bar{k}(t_o) - \bar{c}_3(t_o)$.

If the time period of the data span $(t-t_o)$ is smaller than the period of a spherical harmonic perturbing term, this solution can be expanded in a truncated Taylor series:

$$\bar{k}(t) = \bar{c}_1(t_o) + \bar{c}_2(t_o)\left[m\,\gamma(t-t_o) + \ldots.\right] + \bar{c}_3(t_o)\left[1 - \frac{m^2\gamma^2}{2}(t-t_o)^2 + \ldots..\right] \qquad (3.6)$$

or

$$\bar{k}(t) = \bar{\Delta}_o + \bar{\Delta}_1 t + \bar{\Delta}_2 t^2 + \ldots. \qquad (3.7)$$

where the $\bar{\Delta}_j$ represent vector constants.

Hence the functional form for the Kepler elements which best represents the long period and secular effects is that given by (3.7). Two typical Kepler elements (for example $\Omega(t)$ and $e(t)$) are represented as follows:

$$\Omega(t) = \Omega_o + \Omega_1 t \qquad \text{(secular variation)}$$

$$e(t) = e_o + e_1 t + e_2 t^2 \qquad \text{(secular and long-period variation)}$$

The terms Ω_o, Ω_1, e_o, e_1, and e_2 are examples of Keplerian parameters determined by the empirical OD method.

Since the third body and solar radiation perturbations affect the satellite state in orbit, these effects must be included in the Kepler element equations. The actual six-dimensional time series used to represent the Keplerian motion of the satellite is:

$$a(t) = \bar{a} \qquad \text{constant} \qquad (3.8)$$

$$e(t) = e_o + e_1 t + e_2 t^2 + \delta e_{\oplus} + \delta e_{\odot} + \delta e_{SR} \qquad (3.9)$$

$$I(t) = I_o + I_1 t + I_2 t^2 + \delta I_{\oplus} + \delta I_{\odot} + \delta I_{SR} \qquad (3.10)$$

$$\Omega(t) = \Omega_o + \Omega_1 t + \Omega_2 t^2 + \delta\Omega_{\oplus} + \delta\Omega_{\odot} + \delta\Omega_{SR} \qquad (3.11)$$

$$\omega(t) = \omega_o + \omega_1 t + \omega_2 t^2 + \delta\omega_{\oplus} + \delta\omega_{\odot} + \delta\omega_{SR} \qquad (3.12)$$

$$M(t) = M_o + M_1 t + M_2 t^2 \qquad (3.13)$$

where the orbital element variations $\delta\bar{k}$ are found by numerical integration. The third body and solar radiation perturbations are those developed in the previous chapter. No explicit third body and radiation pressure perturbations are modeled for the mean anomaly. Hence the time-series for M(t) includes the perturbations of the moon, earth, sun, and solar radiation. The reasons for this representation are associated with the semi-major axis estimation and are discussed later in this chapter.

Terms of quadratic order are used in the time-series since for the time periods (24 hours or less) over which solutions are obtained, these will adequately (by conservative standards) represent long-period perturbations of up to order seven (m=7). (A harmonic perturbation of order seven has a period of four days. Any one day segment of this harmonic can be well represented by a quadratic function.)

DATA REDUCTION

The Doppler observation ($\dot{\rho}$) is a scalar quantity that is a non-linear function of the satellite state, $\bar{k}$, the relative earth/moon configuration and the earth-based tracking station position and rotational velocity. During the orbit determination only the estimates of the satellite state are refined. The tracking data $\dot{\rho}_{obs}$ is related to the satellite state as follows[21] (see Appendix B)

$$\dot{\rho}_{obs}\ (t) = \dot{\rho}[\bar{k}(t)] + \eta \qquad (3.14)$$

where η is the random noise associated with the physical measurements. The measurement errors are assumed to have the following properties:

$$Exp[\eta] = 0 \qquad (3.15)$$

$$Exp[\eta^2] = \sigma^2 \qquad (3.16)$$

where Exp is the expectation operator and σ^2 is the variance of the Doppler noise. Since the Doppler is a non-linear function of the Kepler state, the output equation (3.14) must be linearized about a reference trajectory.

If $\bar{k}(t)$ is the true Kepler state, $\bar{k}^*(t)$ is the reference state, and $\Delta\bar{k}$ the deviation, then

$$\bar{k}(t) = \bar{k}^*(t) + \Delta\bar{k}(t) \qquad (3.17)$$

Using (3.14)

$$\dot{\rho}_{obs} = \dot{\rho}[\bar{k}^*(t)] + \left(\frac{\partial\dot{\rho}}{\partial\bar{k}}\right)^* \Delta\bar{k} + ... + \eta \qquad (3.18)$$

Defining $\Delta\dot{\rho}(t) = \dot{\rho}_{obs} - \dot{\rho}[\bar{k}^*(t)]$

and $J(t) = \left(\frac{\partial\dot{\rho}}{\partial\bar{k}}\right)^*$

the linearized relationship between the deviation in the Kepler state and the deviation in the Doppler is:

$$\Delta\dot{\rho}(t) = J\,\Delta\bar{k}(t) + n \tag{3.19}$$

Using a similar procedure, a linear relationship relating the Kepler state $\bar{k}$ and the parameter vector $\bar{K}$ can be obtained. $\bar{K}$ is an (n×1) vector consisting of the solution parameters

$$\bar{K} = \begin{bmatrix} \bar{a} \\ e_o \\ e_1 \\ e_2 \\ I_o \\ \cdot \\ \cdot \\ \cdot \\ M_2 \end{bmatrix} \tag{3.20}$$

Since these Keplerian parameters are constant over the trajectory, an expansion of $\bar{K}$ can be performed about a reference set $\bar{K}^*$ at some time t_o.

$$\bar{K}(t_o) = \bar{K}^*(t_o) + \Delta\bar{K}(t_o) \tag{3.21}$$

Since

$$\bar{k} = \bar{k}[\bar{K}(t_o), t] \tag{3.22}$$

then

$$\bar{k}(t) = \bar{k}[\bar{K}^*(t_o), t] + \left(\frac{\partial\bar{k}}{\partial\bar{K}}\right)^* \Delta\bar{K}(t_o) + \ldots.$$

or
$$\Delta\bar{k} = \left(\frac{\partial\bar{k}}{\partial\bar{K}}\right)^{*} \Delta\bar{K}(t_o) \tag{3.23}$$

Deviations in the parameter set $\Delta\bar{K}(t_o)$ are then linearly related to deviations in the Kepler elements. The output Doppler equation (3.19) can now be expressed in terms of the solution parameters.

$$\Delta\dot{\rho}(t_k) = H(t_k)\ \Delta\bar{K}(t_o) + \eta \tag{3.24}$$

where
$$H \equiv \left(\frac{\partial\dot{\rho}}{\partial\bar{k}}\right)^{*}\left(\frac{\partial\bar{k}}{\partial\bar{K}}\right)^{*}$$

The primary objective in orbit determination can be simply stated as follows: Given a batch of Doppler measurements valid at many times $t_1, t_2, \ldots, t_r$, find the set of Keplerian parameters which best fits these data. The linear relationship between the Keplerian parameters and the Doppler can be generalized as follows:

$$\overline{\Delta\dot{\rho}} = [H]\Delta\bar{K} + \bar{\eta} + \bar{s} \tag{3.25}$$

where

$\overline{\Delta\dot{\rho}}$ is the (r × 1) observation vector

H is the linearized set of functions relating the observation and state (r × n) matrix

$\Delta\bar{K}$ is the column vector of Keplerian parameters (n × 1)

$\bar{\eta}$ is an (r × 1) vector of observation noise

$\bar{s}$ is an (r × 1) vector of systematic modeling errors.

Since the Keplerian parameters $\bar{K}$ only attempt to represent the long-period dynamics of the orbit, then at any point in time there will always be a systematic residual ($\bar{s}$) associated with the unmodeled short-period satellite variations. Various data smoothing techniques were used on the Doppler data in an attempt to eliminate these short-period variations. None of these approaches has succeeded. Attempts to model the short-period variations directly in the empirical OD also have not been successful.

Given the linear system of equations (3.24) the next step in the OD process is to formulate an estimation scheme which minimizes the estimation error and yields a best estimate of the Keplerian parameters. If the random quantities in the dynamical system are assumed to be normally distributed, there are three linear estimators[22] (least squares, minimum variance, and maximum likelihood) which all would yield the same results and could be used for this function. However, since the errors in the dynamical system are not random, and since the data to be processed is in batches, the weighted least squares estimator was chosen to perform the data reduction.

An error function, ε, for r observations is given as follows:

$$\varepsilon = [\bar{v}^T W \bar{v}] \qquad (\bar{v} = \bar{\eta} + \bar{s}) \tag{3.26}$$

or

$$\varepsilon = (\overline{\Delta\dot{\rho}} - H\Delta\bar{K})^T W(\overline{\Delta\dot{\rho}} - H\Delta\bar{K}) \tag{3.27}$$

where for one data type W is an (r × r) diagonal weighting matrix. For a minimum, the first variation of ε must vanish;

$$\delta\varepsilon = 0 = -(\overline{\Delta\dot{\rho}} - H\Delta\hat{\bar{K}})^T W\, H\delta\bar{K} - (H\delta\bar{K})^T W(\overline{\Delta\dot{\rho}} - H\Delta\hat{\bar{K}}) \tag{3.28}$$

where $\hat{\overline{\Delta K}}$ is the value of $\bar{K}$ that extremizes ε and $\delta\bar{K}$ is the variation in $\bar{K}$. Since this is a scalar equation,

$$0 = -(\overline{\Delta\dot{\rho}} - H\hat{\overline{\Delta K}})^T W\, H\, \delta\bar{K} \tag{3.29}$$

But $\delta\bar{K}$ is arbitrary, hence

$$(\overline{\Delta\dot{\rho}} - H\hat{\overline{\Delta K}})^T W\, H = 0 \tag{3.30}$$

Transposing and solving ($W = W^T$):

$$\underbrace{\hat{\overline{\Delta K}}}_{(n \times 1)} = \underbrace{[H^T W\, H]^{-1}}_{(n \times n)} \quad \underbrace{H^T W\, \overline{\Delta\dot{\rho}}}_{(n \times 1)} \tag{3.31}$$

(for minimum $\delta^2\varepsilon = 2\delta\bar{K}^T[H^T W H]^{-1}\,\delta\bar{K} > 0$ for arbitrary $\delta\bar{K}$).

Since this minimization process was obtained by linearizing a non-linear set of equations, the least squares

estimation must be performed iteratively. The processing of r Doppler measurements and the resulting set of differential corrections $\hat{\overline{\Delta K}}$ constitutes one computing iteration. The convergence criterion for two successive iterations is as follows:

$$\frac{\sum_{i=1}^{r} \Delta\dot{\rho}(t_i)^2 \Big|_{(K-1)}}{\sum_{i=1}^{r} \Delta\dot{\rho}(t_i)^2 \Big|_{(K)}} - 1 < \delta \qquad (3.32)$$

where $\delta = 10^{-4}$ and (K-1) and K designate computing iterations.

The entries in the H matrix are the partial derivatives of the Doppler with respect to the Keplerian parameters. These terms are found by using the chain rule for differentiable functions:

$$\frac{\partial\dot{\rho}}{\partial\overline{K}} = \frac{\partial\dot{\rho}}{\partial\overline{x}} \cdot \frac{\partial\overline{x}}{\partial\overline{k}} \cdot \frac{\partial\overline{k}}{\partial\overline{K}} \qquad (3.33)$$

Each of the derivatives used in the above equation is given in Appendix C.

SEMI-MAJOR AXIS DETERMINATION

Studies using both pseudo and real Doppler data have shown that the least squares process does not converge when the semi-major axis is included as an independent parameter. This condition was also observed by the Smithsonian Astrophysical Observatory in earth satellite work[23].

Since the mean motion of the orbit, even in the presence of perturbations, is nearly inversely proportional to the semi-major axis to the three halves power, then the estimated mean motion can be used to imply a semi-major axis. The constraint equation between the mean motion and semi-major axis must include the long-period effects of the earth, sun, and solar radiation and some representation for the lunar field. The third body perturbations on the mean anomaly have been given in the previous chapter. The L1 lunar gravity model[24] (see Table II) developed by Langley Research Center is used.

TABLE II. L1 GRAVITY FIELD

$$C_{20} = -2.07108 \times 10^{-4}$$

$$C_{22} = 0.20716 \times 10^{-4}$$

$$C_{30} = 0.21 \times 10^{-4}$$

$$C_{31} = 0.34 \times 10^{-4}$$

$$C_{33} = 0.02583 \times 10^{-4}$$

The second degree terms in this model were determined on the basis of astronomical observations of the moon's physical librations and hence can be assumed known to at least one signigicant digit. The third degree terms were obtained from previous analyses of Lunar Orbiter and Apollo data.

The average value of the semi-major axis (a_o) with respect to mean anomaly is found by setting the mean anomaly perturbation equation equal to the empirically determined mean motion. Using equations (2.62) and (3.13), the following relationship is made:

$$\hat{\dot{M}} = \hat{M}_1 + 2\hat{M}_2 t \tag{3.34}$$

$$\hat{\dot{M}} = \sqrt{\frac{\mu}{a_o^3}} + \dot{M}_{C_{20}} + \dot{M}_{C_{22}} + \dot{M}_{C_{30}} + \dot{M}_{C_{31}} + \dot{M}_{C_{33}} + \dot{M}_{\oplus} + \dot{M}_{\odot} + \dot{M}_{SR}$$

where $\hat{M}_1$ and $\hat{M}_2$ are the estimated Keplerian parameters. Since this is a non-linear equation in a_o, it is solved using Newton's Method. The value a_o is the geometric average of the semi-major axis under the perturbing influences of the L1 lunar gravity field, the earth and sun, and solar radiation.

For the case of secular perturbations on an earth satellite, Kozai[25] has shown that a mean value of the semi-major axis $\bar{a}$ yields the average satellite position in the orbit. This value is derived such that the deviations in the position of the orbit due to perturbations averaged over the orbit yield only short-period variations.

$$\frac{1}{2\pi}\int_o^{2\pi} \delta r \, dM = \sum_{\zeta=1}^{\infty} b_\zeta \cos(\zeta M + d_\zeta) \tag{3.35}$$

where $\delta r = r_{TRUE} - r_{LONG\ PERIOD}$ and b_ζ and d_ζ are constants.

Hence the value $\bar{a}$ yields the proper mean position over the orbit. Kozai has derived the relationship between the average value, a_o, and the mean value, $\bar{a}$, for the C_{20} perturbation:

$$\bar{a} = a_o \left[1 + \frac{3}{2} C_{20} \left(\frac{R_e}{a}\right)^2 \frac{(1-3/2 \sin^2 I)}{(1-e^2)^{3/2}}\right] \tag{3.36}$$

also since:

$$\dot{M}_{20} = \sqrt{\frac{\mu_\oplus}{a_o^3}} \left[1 - \frac{3}{2} \left(\frac{R_e}{a}\right)^2 \frac{C_{20}(1-3/2 \sin^2 I)}{(1-e^2)^{3/2}}\right] \tag{3.37}$$

then the following modified Kepler law is valid:

$$\dot{M}_{20}^2 \bar{a}^3 = \tilde{\mu} \tag{3.38}$$

where:

$$\tilde{\mu} = \mu_\oplus \left[1 + \frac{3}{2} C_{20} \left(\frac{R_e}{a}\right)^2 \frac{(1-3/2 \sin^2 I)}{(1-e^2)^{3/2}}\right] \tag{3.39}$$

Hence the presence of the C_{20} term essentially changes the effective mass of the moon.

Odd degree zonal, tesseral, and sectorial terms in the semi-major axis constraint equation do not require mean value corrections[26]. Analysis has shown that the correction for the sun and solar radiation are on the order of a foot or less; hence no factor is included for these perturbations. The mean value correction arising from the earth perturbations is included.

An analytical procedure was used to derive the relationship between the mean and average values of the semi-major axis for earth effects. The basic formulation for the disturbing effects of the sun on the moon's orbit was used as a model. The secular effects on the mean motion generated by earth perturbations is as follows[27]:

$$\dot{M}_{\oplus} = \sqrt{\frac{\mu_{\mathbb{C}}}{a_o^3}} \left[1 - \frac{7}{4} \frac{n_{\oplus}^2}{n^2} (1-3/2 \sin^2 I)\right] \qquad (3.40)$$

where terms of order e^2 are neglected and $n_{\oplus}$ is the mean motion of the earth. Extending the mean value solution given by Brouwer and Clemence to allow for varying inclinations, (see Appendix D),

$$\bar{a} = a_o \left[1 + \frac{n_{\oplus}^2}{n^2} (1-3/2 \sin^2 I)\right] \qquad (3.41)$$

where again terms of order e^2 are neglected. Both of these formulas agree well with those given for the sun's perturbations on the moon (case in which I = 23°).

The general procedure for implying a mean value semi-major axis has two steps. First, the average value of the semi-major axis, a_o, is determined once per iteration using equation (3.34). Then, the mean value, $\bar{a}$, is calculated using equations (3.36) and (3.41);

$$\bar{a} = a_o[1 + \varepsilon_{20} + \varepsilon_{\oplus}] \qquad (3.42)$$

where the ε terms are the mean value corrections.

The quantity a_o is the average value of the osculating semi-major axis. The quantity $\bar{a}$ is introduced to make long-period perturbation theory represent the average satellite orbit. Since this variable is introduced to insure compatibility between the long-period and associated rectangular equations of motion, it is only used for data reduction.

After convergence has been reached, the mean anomaly rate, $\dot{M}$, is adjusted to remove the earth, sun, and solar radiation effects.

$$\dot{M}_{\text{☾}} = \hat{\dot{M}}_1 + 2\hat{\dot{M}}_2 t - \dot{M}_{\oplus} - \dot{M}_{\odot} - \dot{M}_{SR} \qquad (3.43)$$

Here $\dot{M}_{\text{☾}}$ is the anomaly rate arising only from lunar gravity. The average semi-major axis value, $a_{\text{☾}}$, for the lunar gravity is found by solving the following equation:

$$\dot{M}_{\text{☾}} = \sqrt{\frac{\mu_{\text{☾}}}{a_{\text{☾}}^3}} + \dot{M}_{20} + \dot{M}_{22} + \dot{M}_{30} + \dot{M}_{31} + \dot{M}_{33} \qquad (3.44)$$

It is this value of the semi-major axis that completes the $\bar{K}$ parameter set and is used for gravity field determination. One such value of $a_{\text{☾}}$ is found for each solution.

SOLUTION PARAMETERS

The output from processing a batch of Doppler measurements is a best estimate for a set of Keplerian parameters, $\hat{\bar{K}}$. Since the third body perturbations are modeled separately in the OD process, and the mean anomaly parameter is adjusted

for third body effects, these Keplerian parameters represent the variation in the Kepler orbital elements arising from the non-central part of lunar gravity. These solution parameters give a simultaneous time history of the Kepler elements and element rates valid over the data span. A detailed block diagram of the empirical processor is shown in Figure 10.

The time histories of the Kepler elements and element rates are used as input data to a second processor which fits lunar gravity harmonics to the Kepler element rates. Since the solution parameters provide continuous time functions for the orbital elements and rates they can be sampled at any desired frequency. The long-period lunar gravity effects have periods which are much greater than a typical lunar orbiter period (lunar effects have periods of days whereas a typical satellite period is three hours), hence there will be no aliasing of gravity information if the element states and rates are evaluated once per satellite period. For example, if a typical data span contains five satellite periods, then five sets of Kepler elements and element rates are obtained.

The Kepler element rates, which form the actual data for the gravity estimation, consist of the following five rates

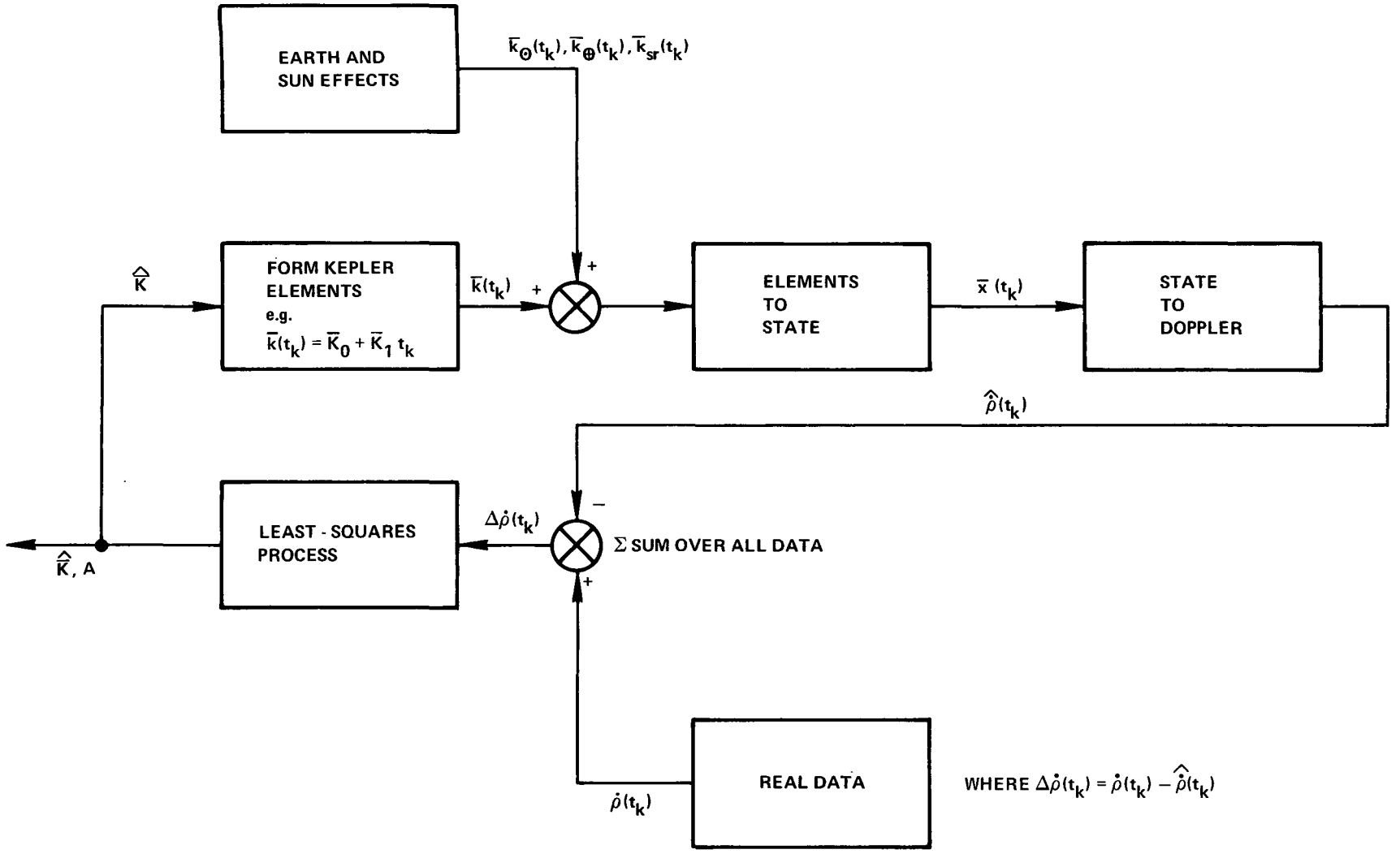

FIGURE 10 - ORBIT DETERMINATION BLOCK DIAGRAM

$$\dot{\bar{K}} = \begin{bmatrix} \dot{e} \\ \dot{I} \\ \dot{\Omega} \\ \dot{\omega} \\ \dot{M} \end{bmatrix} \qquad (3.45)$$

The semi-major axis rate is zero in long-period theory, so it is not used.

The five orbital element rates are simultaneously processed to obtain gravity coefficients. Since the input data consists of five different quantities ($\dot{e}$, $\dot{I}$, $\dot{\omega}$, $\dot{\Omega}$, $\dot{M}$), a weighting matrix is required to define the relative accuracies of each of the rates.

If the empirical OD method could model the Doppler such that the residuals remaining after convergence were normally distributed random errors, the $[H^T W H]^{-1}$ matrix given by equation (3.31) would be the covariance matrix associated with the $\hat{\bar{K}}$ solution set. Since only the long-period satellite dynamics are represented in the empirical process, then the $[H^T W H]^{-1}$ matrix is not the covariance matrix of the process[28]. However since the terms in the $[H^T W H]^{-1}$ matrix do reveal the relative sensitivity and correlations among the solution parameters, it is assumed for weighting purposes that these terms can be regarded as variances and covariances in the conventional manner.

The weighting matrix for the orbital element rates, A, is a (5×5) matrix having the following form[29]:

$$A^{-1} = \begin{bmatrix} \sigma_{\dot{e}}^2 & \tau_{12} & \tau_{13} & \tau_{14} & \tau_{15} \\ \tau_{21} & \sigma_{\dot{I}}^2 & \cdots & \cdots & \cdots \\ \vdots & & \sigma_{\dot{\Omega}}^2 & \cdots & \vdots \\ \vdots & & & \sigma_{\dot{\omega}}^2 & \vdots \\ \tau_{51} & \cdots & \cdots & \cdots & \sigma_{\dot{M}}^2 \end{bmatrix} \tag{3.46}$$

where $\sigma_{\dot{k}}^2$ are the error variances among the rates and τ_{ij} are the covariances. It is assumed that the mean error in the Keplerian parameters is zero. Each of the orbital element rates has the following form,

$$\dot{\hat{\Omega}} = \hat{\Omega}_1 + 2\hat{\Omega}_2 t \tag{3.47}$$

The variance of the error in $\dot{\hat{\Omega}}$ is found as follows:

$$\sigma_{\dot{\Omega}}^2 = \mathrm{Exp}[(\hat{\Omega}_1 - \Omega_1)^2 + 4t(\hat{\Omega}_1 - \Omega_1)(\hat{\Omega}_2 - \Omega_2) + 4t^2(\hat{\Omega}_2 - \Omega_2)^2] \tag{3.48}$$

or

$$\sigma_{\dot{\Omega}}^2 = \sigma_{\Omega_1}^2 + 4t\ \mathrm{cov}(\varepsilon_{\Omega_1}\varepsilon_{\Omega_2}) + 4t^2\ \sigma_{\Omega_2}^2 \tag{3.49}$$

where $\varepsilon_{\Omega_1} = (\hat{\Omega}_1 - \Omega_1)$ and $\varepsilon_{\Omega_2} = (\hat{\Omega}_2 - \Omega_2)$.

The covariance terms among the rates (e.g., cov $(\varepsilon_{\dot{\Omega}}\varepsilon_{\dot{\omega}})$) are formulated in a similar way (see 3.48)

$$\text{cov}(\varepsilon_{\dot{\Omega}}\varepsilon_{\dot{\omega}}) = \text{cov}(\varepsilon_{\Omega_1}\varepsilon_{\omega_1}) + 2t[\text{cov}(\varepsilon_{\Omega_1}\varepsilon_{\omega_2}) + \text{cov}(\varepsilon_{\Omega_2}\varepsilon_{\omega_1})] + 4t^2\,\text{cov}(\varepsilon_{\Omega_2}\varepsilon_{\omega_2}) \qquad (3.50)$$

Then if it is assumed for weighting purposes that the $[H^T W H]^{-1}$ is the covariance matrix, each of the entries in the A matrix can be found from the appropriate slots in the $[H^T W H]^{-1}$ matrix. Hence a weighting matrix is automatically obtained for each set of orbital element rates.

PSEUDO DATA SIMULATIONS

In order to demonstrate the operational capabilities of the empirical orbit determination method, pseudo Doppler data were generated from numerically integrated trajectories and converged solutions were obtained. The estimated Keplerian parameters from two such typical convergences are presented. In both cases a triaxial lunar gravity field is assumed (C_{20} and C_{22} harmonics) and the earth, sun, and solar radiation perturbations are also included. No noise or biases are added to the pseudo data.

The first data simulation was generated for a Lunar Orbiter V (polar) orbit. The data span contains tracking data from three stations (Goldstone, Calf., Madrid, Spain, and Woomera, Australia) and is approximately 21 hours 30 minutes in

duration. The epoch data and initial conditions for this orbit are:

Epoch Date: Aug. 9, 1967 7 hours 20 min.

Initial Conditions: (Selenographic)

a = 8,324,332 ft. e = .27618984

I = 84°.764923 Ω = 70°.2050009

ω = 1°.8616071 M = 244°.73644

The Doppler residuals ($\Delta\dot{\rho}$) associated with this convergence are shown in Figure 11. These residuals are systematic and have the general form of the unmodeled short-period orbital variations. The residuals possess a mean of .0216 feet per second (fps) and a standard deviation of σ = .1 fps.

The Keplerian parameter set used consists of thirteen terms. The best estimates for these parameters are:

e_o = .27600103

e_1 = .46568305 $\times 10^{-9}$

I_o = 84°.765987

I_1 = .89524714 $\times 10^{-6}$ deg/sec.

Ω_o = 70°.202817

Ω_1 = -.61366823 $\times 10^{-6}$ deg/sec.

Ω_2 = .74160675 $\times 10^{-12}$ deg/sec^2

ω_o = 1°.8611893

ω_1 = -.34733259 $\times 10^{-5}$ deg/sec.

ω_2 = -.12242802 $\times 10^{-11}$ deg/sec^2

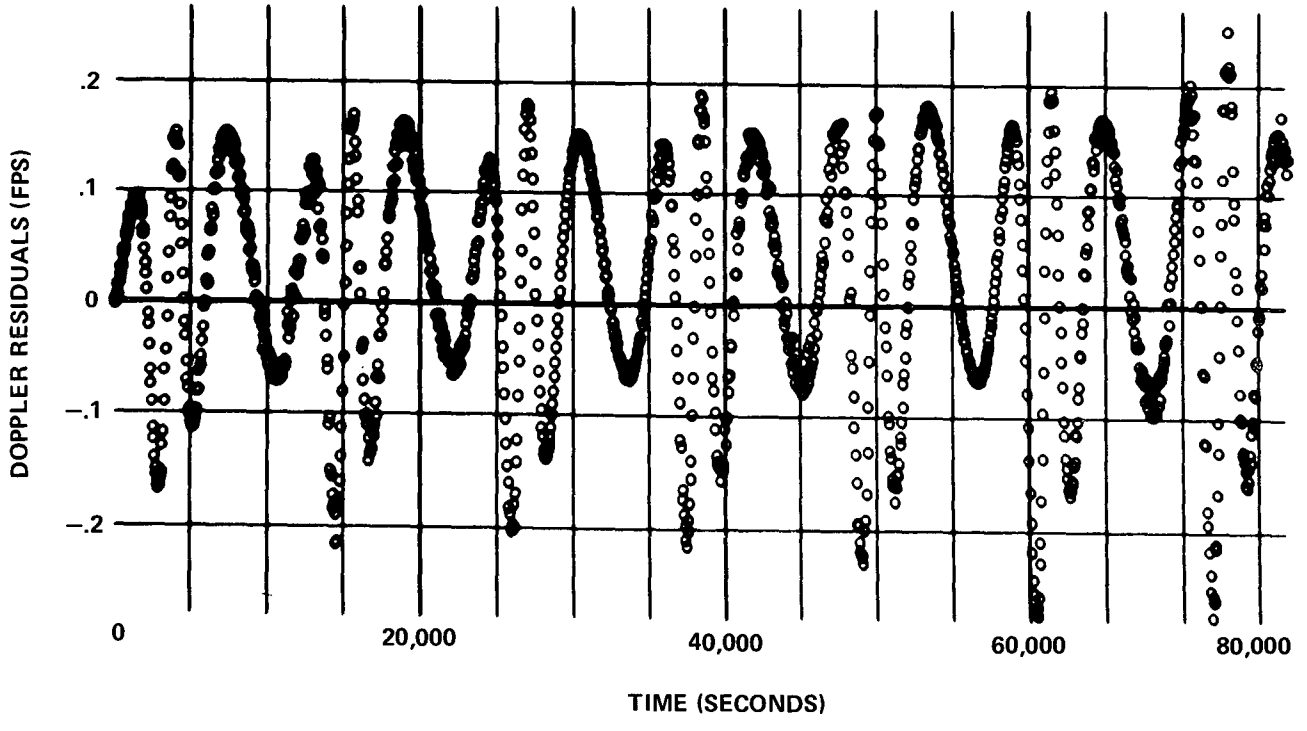

FIGURE 11 - LUNAR ORBITER V PSEUDO DATA DOPPLER RESIDUALS

M_o = 244?73515

M_1 = .031390311 deg/sec.

M_2 = $-.55419592 \times 10^{-11}$ deg/sec^2

The constrained values of the semi-major axis obtained are:

a_o = 8,323,991 ft.

$\bar{a}$ = 8,324,561 ft.

In order to determine the quality of this converged solution, comparisons are made between the numerically integrated source trajectory and the solution obtained. Figures 12-15 show the variations in the six Kepler elements for both the converged solution and the source trajectory. The variations presented for the eccentricity (e) and the three Euler angles (I, Ω, ω) (see Figures 12 and 13) show the actual variations of these elements plotted on common axes. Since the variations in the mean anomaly are very large and the semi-major axis has a large magnitude, the differences in the converged solution and source trajectory values are shown for these variables (see Figure 14). As can be seen in Figures 12 and 13, the estimates of the eccentricity, ascending node, and perifocus have slight biases at epoch. The inclination parameter has a slight rate error. The mean anomaly and semi-major axis variations are only short-periodic and display essentially no growth characteristics. A plot of the difference in position between the source trajectory and the converged solution is shown in Figure 15. The 400 ft. bias between positions is relatable to the error bias in the estimated eccentricity parameter at epoch (e_o). The slight

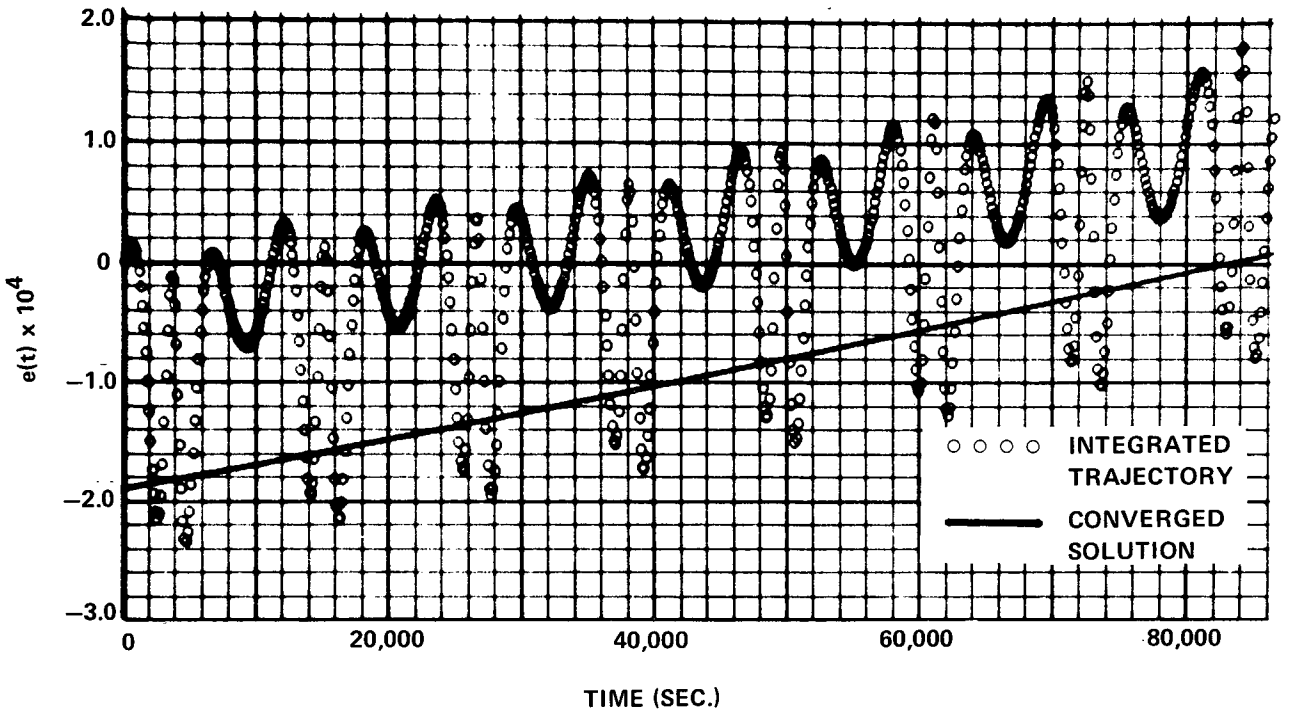

ECCENTRICITY AS A FUNCTION OF TIME
MINUS EPOCH VALUE

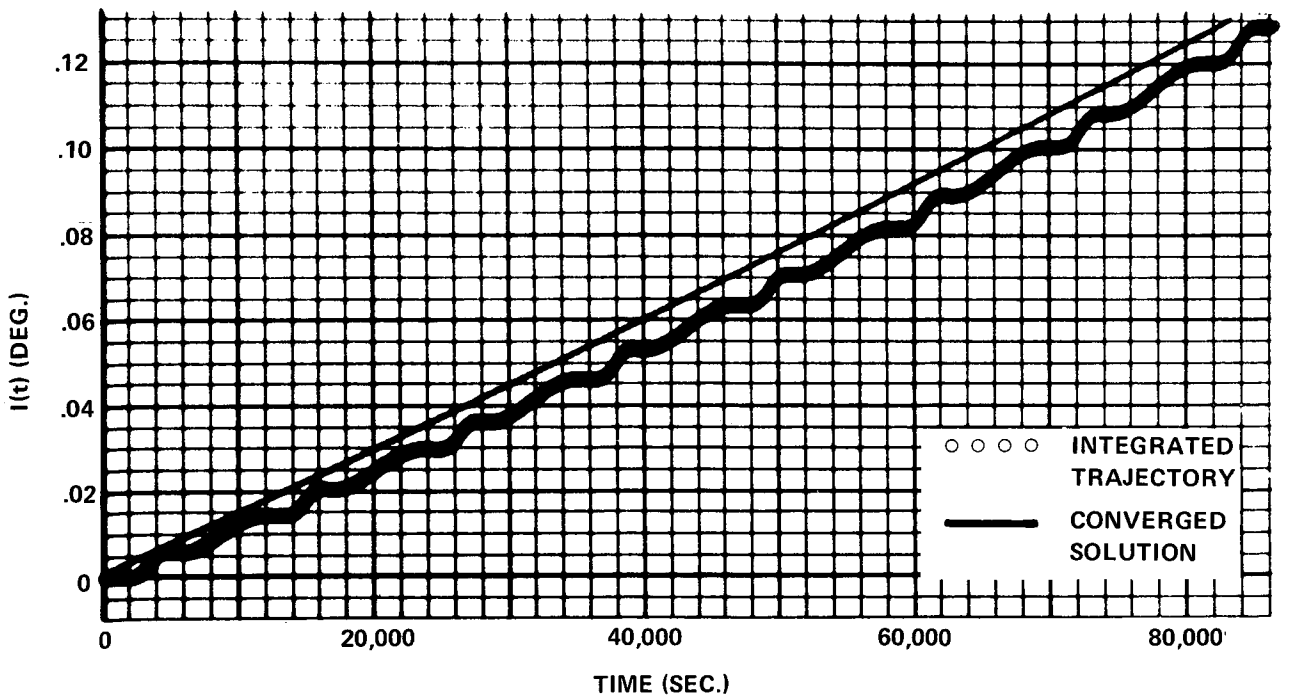

INCLINATION AS A FUNCTION OF TIME
MINUS EPOCH VALUE

FIGURE 12 - LUNAR ORBITER V ORBIT

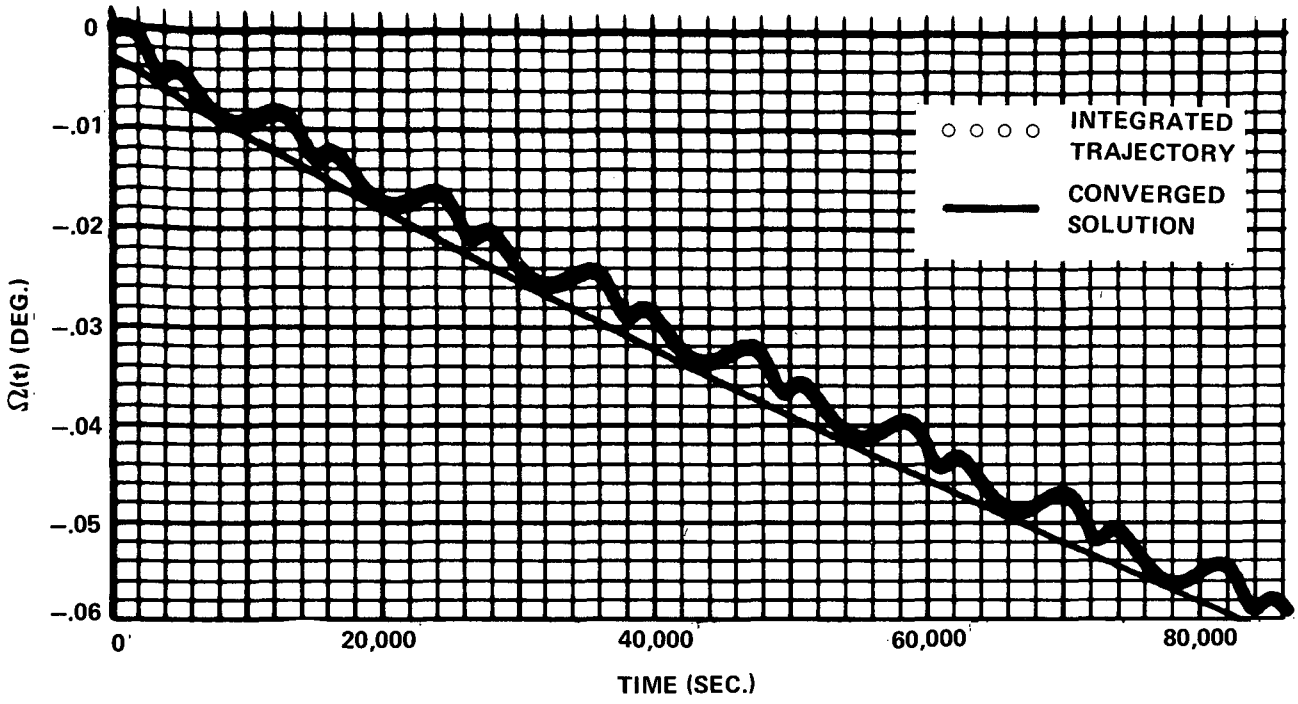

ASCENDING NODE AS A FUNCTION OF TIME
MINUS EPOCH VALUE

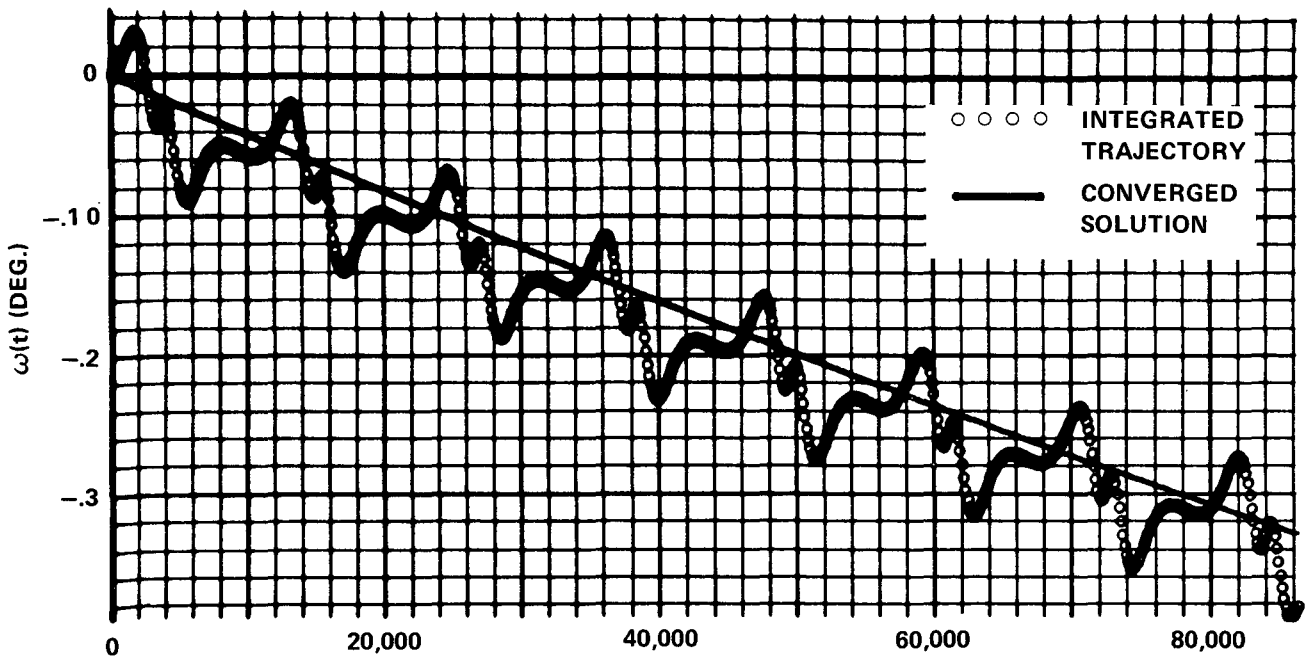

PERIFOCUS AS A FUNCTION OF TIME
MINUS EPOCH VALUE

FIGURE 13 - LUNAR ORBITER V ORBIT

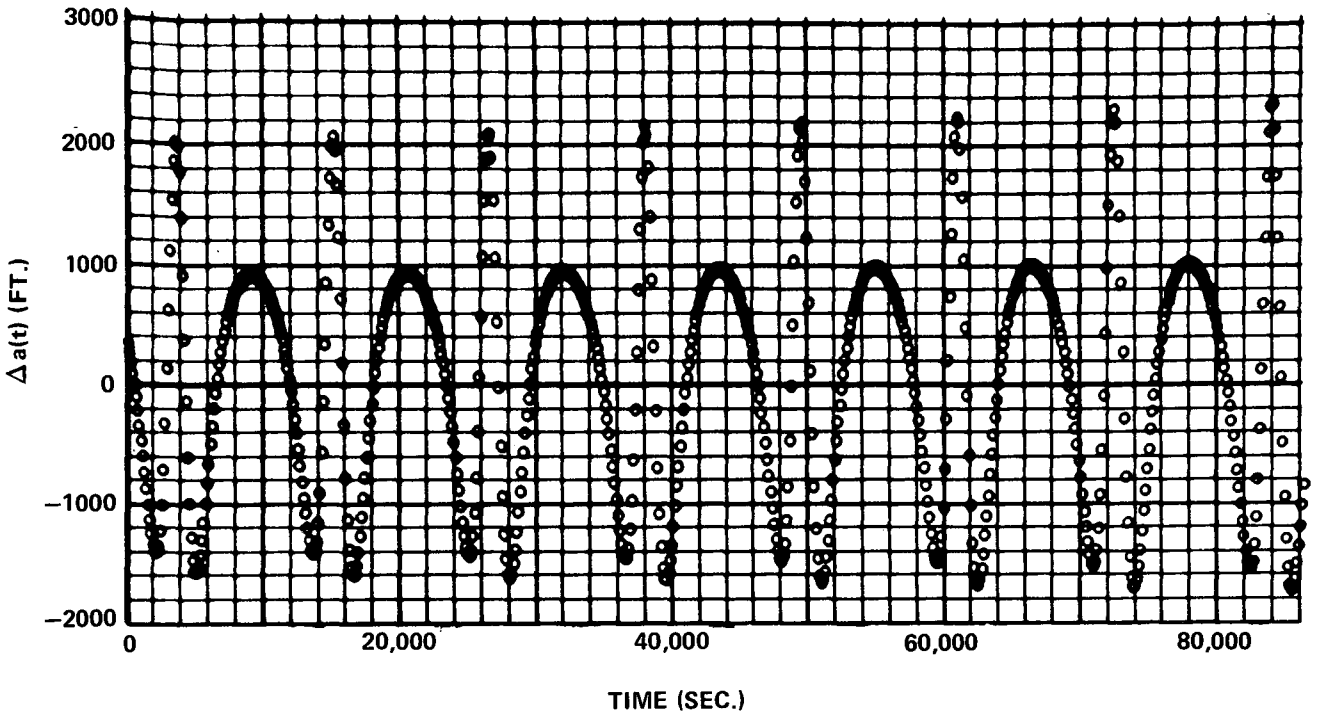

DIFFERENCE IN SEMI-MAJOR AXIS

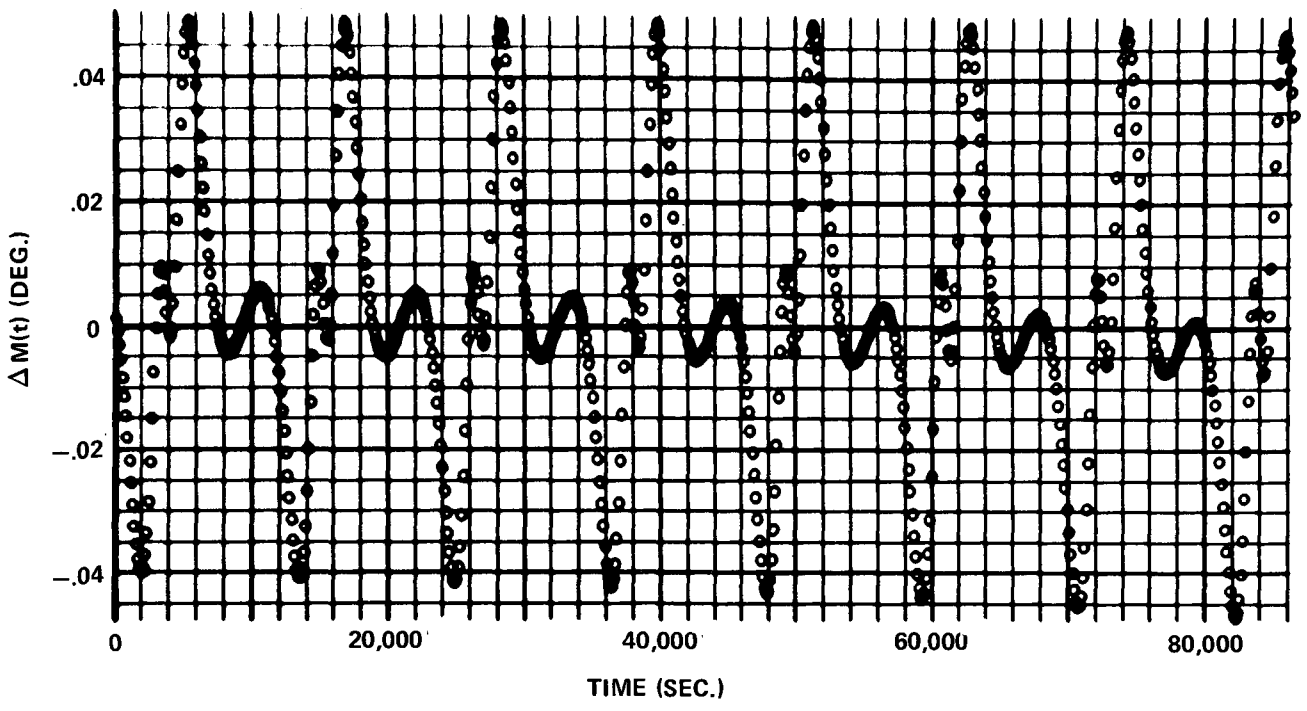

DIFFERENCE IN MEAN ANOMALY

FIGURE 14 - LUNAR ORBITER V ORBIT

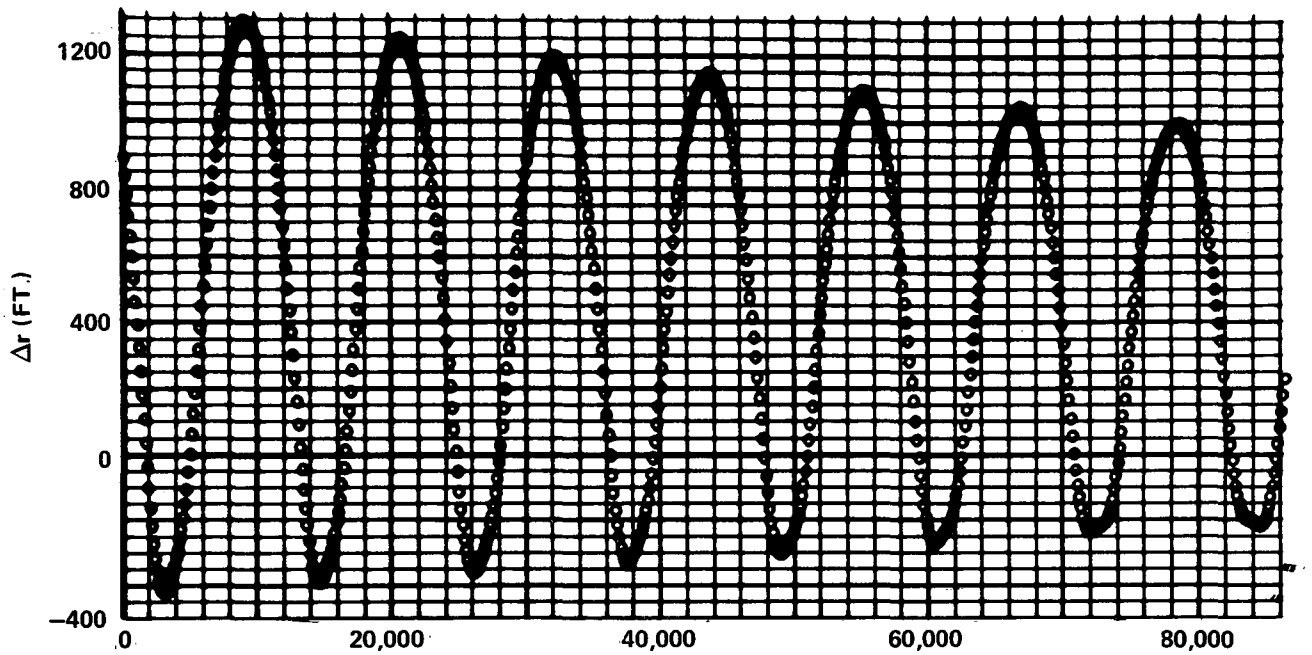

DIFFERENCE IN POSITION AS A FUNCTION OF TIME

FIGURE 15 - LUNAR ORBITER V ORBIT

time variations in the position differences arise from small errors in the eccentricity and mean anomaly rates.

Analysis of the functional properties of the partial derivatives used in the least-squares convergence shows that two of the state variables have similar sensitivities to the data;

$$\frac{\partial \dot{\rho}}{\partial \omega} \approx \frac{\partial \dot{\rho}}{\partial M} \tag{3.51}$$

This lack of separability arises primarily from the poor geometrical configuration from which the Doppler measurements are taken. Plots of the functional behavior of the five basic partial derivatives used in the solution are shown in Figures 16-18. The presence of these nearly equal sensitivities among the state parameters leads to high correlations in the $(H^T W H)^{-1}$ matrix. These correlations lead to linear combinations among the state parameters being estimated. For this particular solution very high correlations ($\rho \geq |.9|$) exist between the following sets of parameters:

Correlation Coefficient	Parameter Pair
-.98	I_o, Ω_o
.97	I_o, ω_o
.91	I_1, ω_1
-.97	Ω_o, ω_o
-.92	Ω_1, ω_1
.97	M_1, M_2

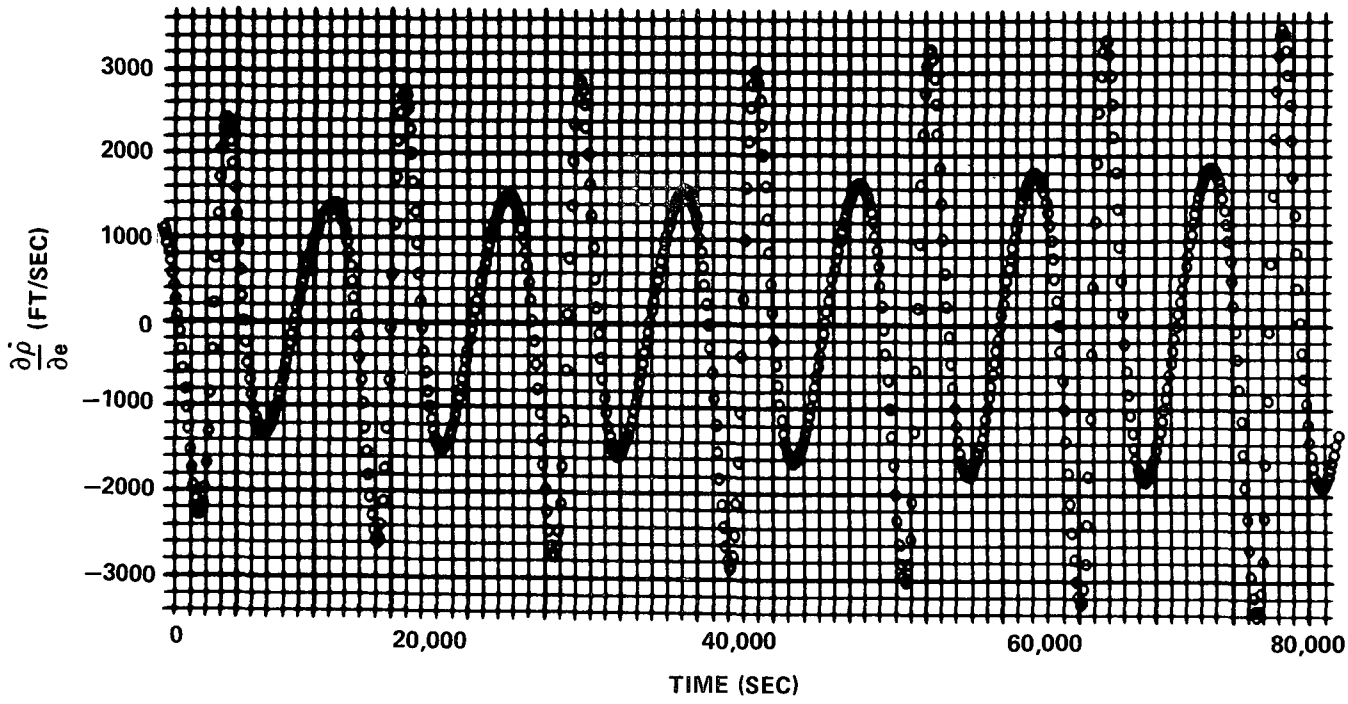

$\frac{\partial \dot{\rho}}{\partial e}$ AS A FUNCTION OF TIME

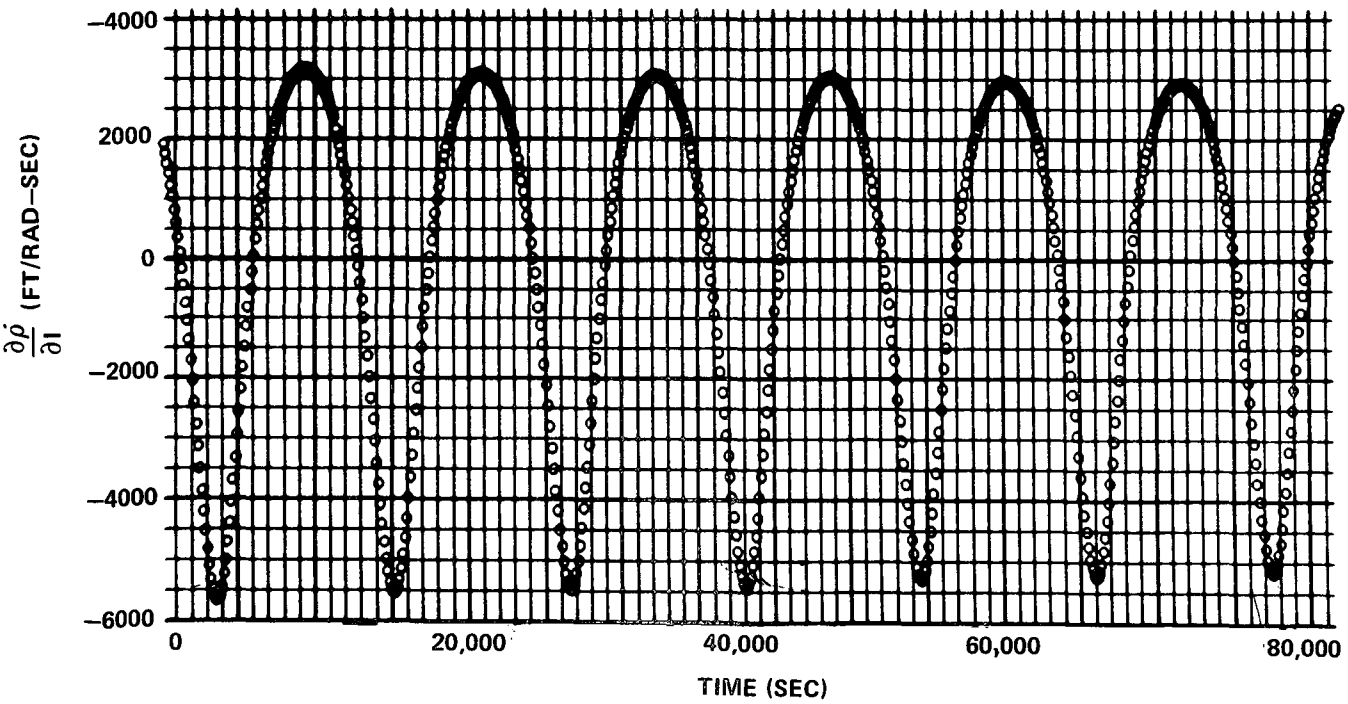

$\frac{\partial \dot{\rho}}{\partial I}$ AS A FUNCTION OF TIME

FIGURE 16 - LUNAR ORBITER V ORBIT

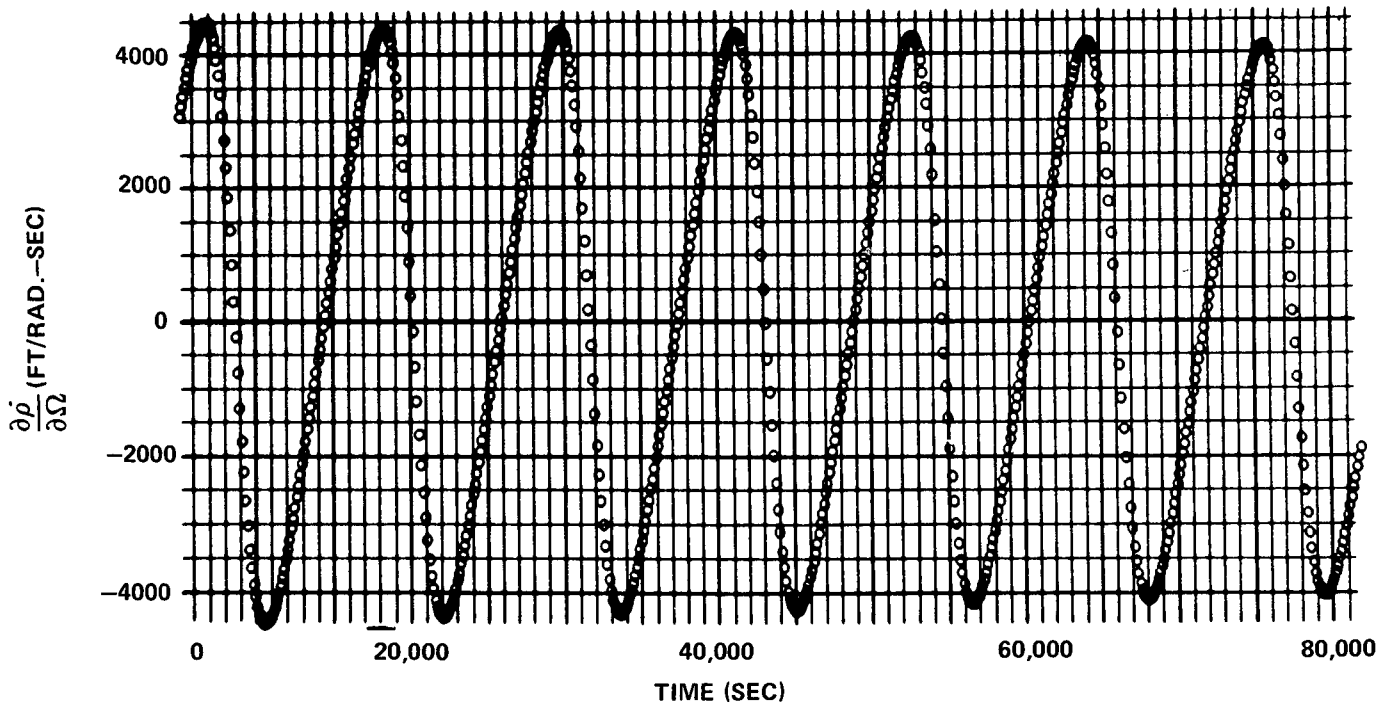

$\frac{\partial \dot{\rho}}{\partial \Omega}$ AS A FUNCTION OF TIME

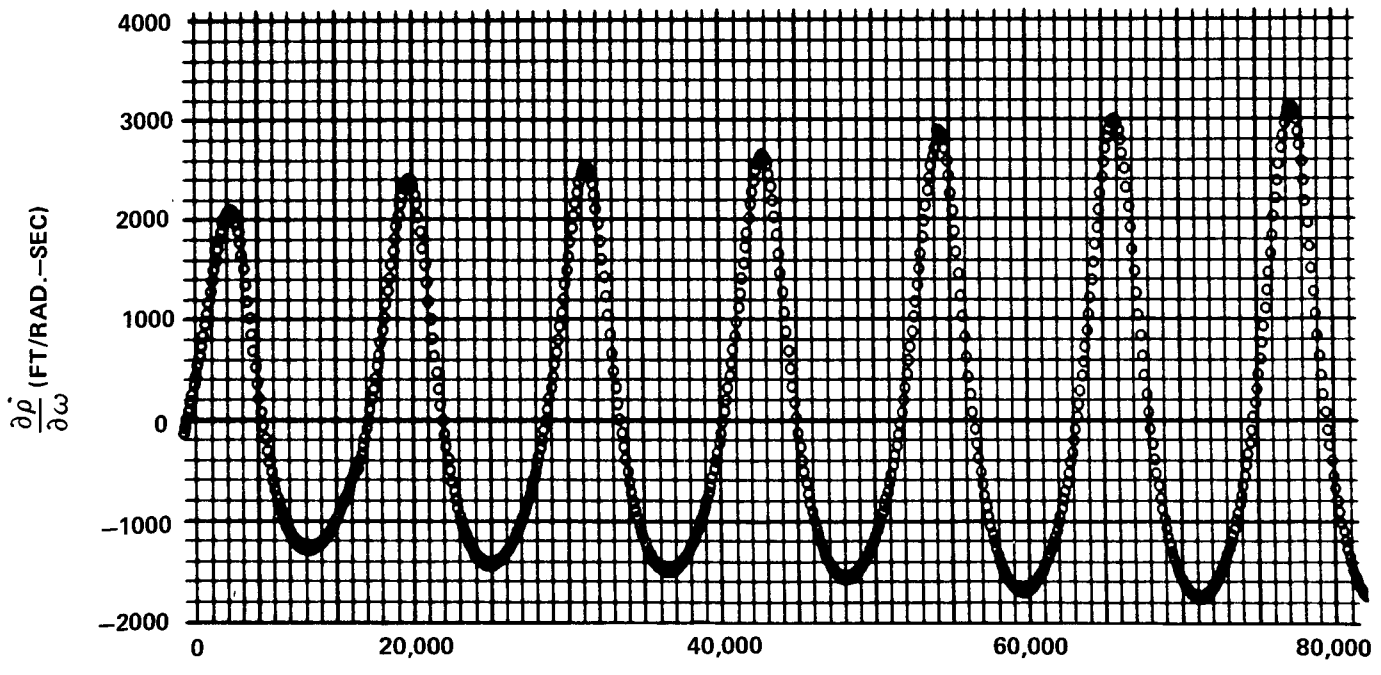

$\frac{\partial \dot{\rho}}{\partial \omega}$ AS A FUNCTION OF TIME

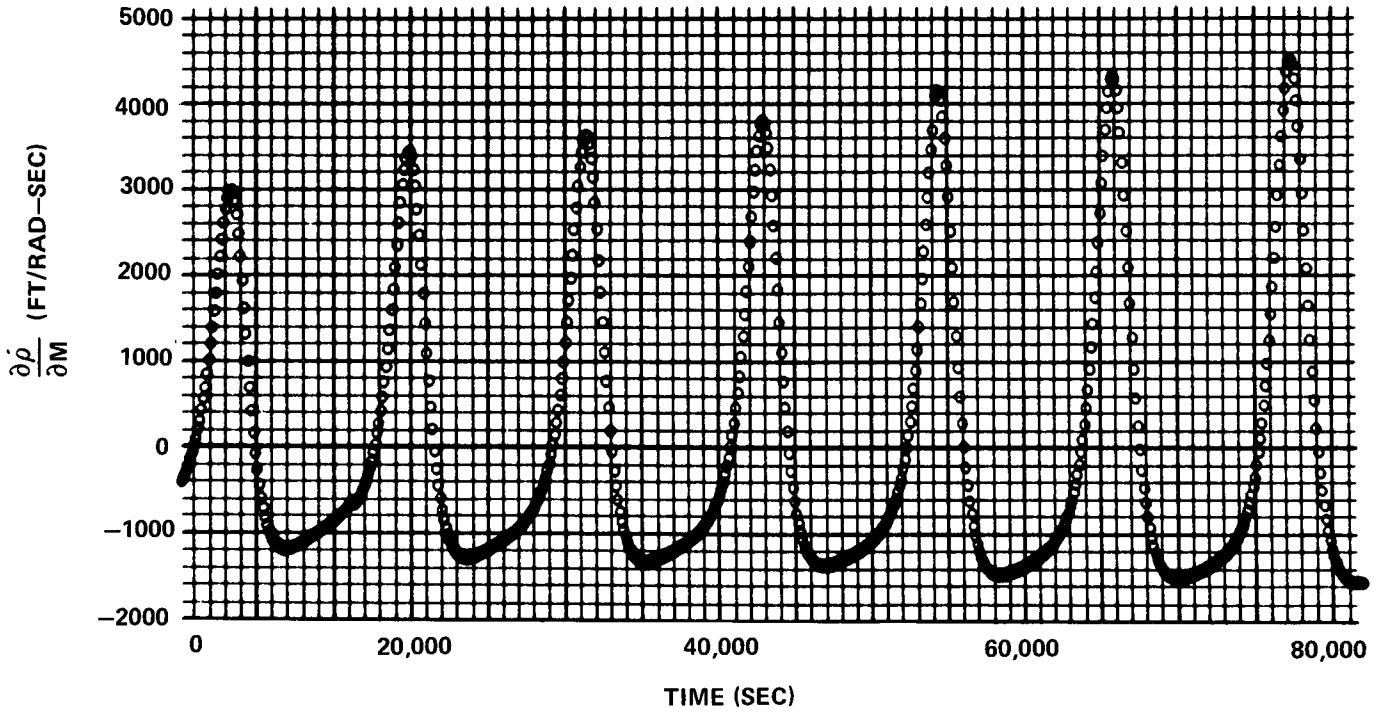

$\frac{\partial \dot{\rho}}{\partial M}$ AS A FUNCTION OF TIME

FIGURE 18 - LUNAR ORBITER V ORBIT

-.97	Ω_1, Ω_2
.91	ω_1, ω_2

Linear combinations among the Keplerian parameters can be viewed as a measure of observability. Hence the slight biases obtained in the converged solution can be ascribed to these equal sensitivites among some state variables and to the aliasing effects of the unmodeled short-period variations.

The second data simulation was generated for a Lunar Orbiter III (Apollo type) orbit. This data span contains tracking data from the same three stations and is approximately 10 hours in duration. The epoch date and initial conditions for this orbit are:

Epoch Date: August 30, 1967 20 hours 55 min.

Initial Conditions: (Selenographic)

a = 6,457,093 ft.	e = .04348376
I = 20°899211	Ω = 63°970000
ω = 354°05800	M = 194°90793

The Doppler residuals ($\Delta\dot{\rho}$) associated with this solution are shown in Figure 19. As in the previous solution, these residuals are systematic and have the general shape and form of the unmodeled short-period variations. The residuals have a mean of -.016 fps and a standard deviation σ= .08 fps.

The thirteen Keplerian parameters found for this solution are the following:

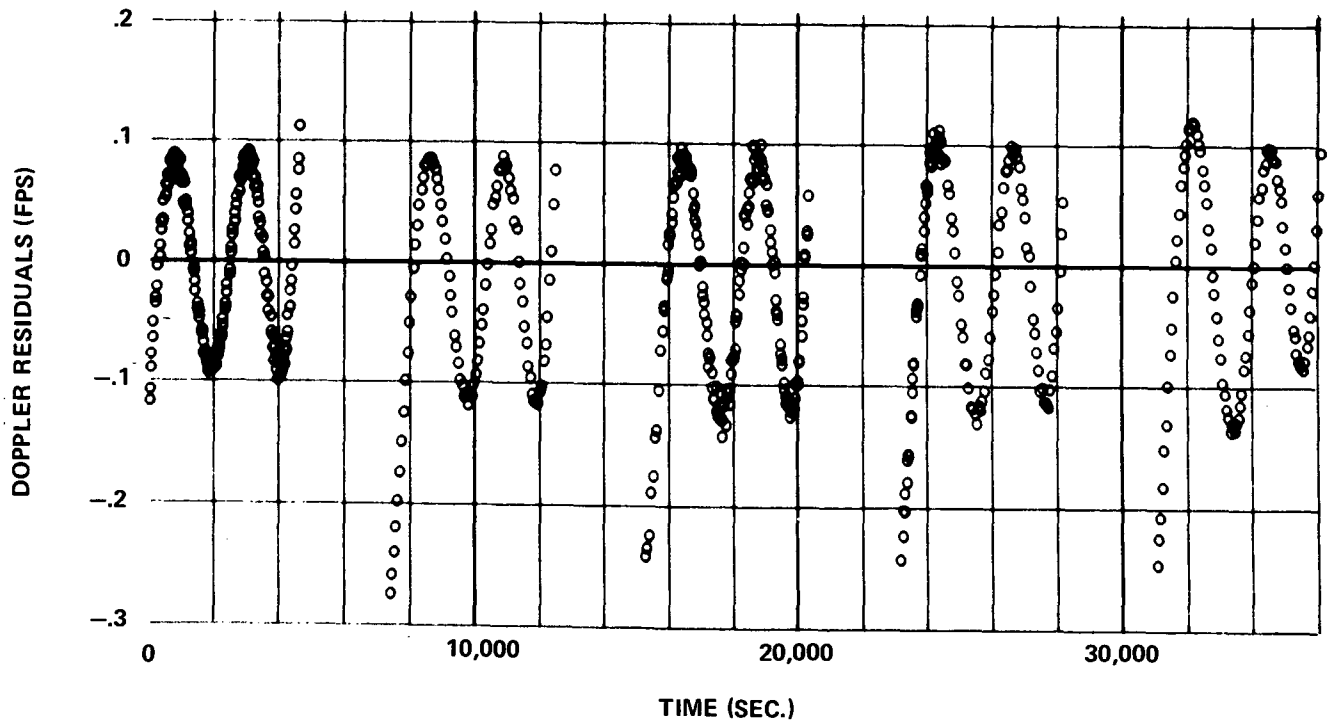

FIGURE 19 - LUNAR ORBITER III PSEUDO DATA DOPPLER RESIDUALS

$$e_o = .04363890$$

$$e_1 = -.22143541 \times 10^{-9}$$

$$I_o = 20°.902504$$

$$I_1 = .75197331 \times 10^{-6} \text{ deg/sec.}$$

$$\Omega_o = 63°.984837$$

$$\Omega_1 = -.14299451 \times 10^{-4} \text{ deg/sec}$$

$$\Omega_2 = .52154323 \times 10^{-10} \text{ deg/sec}^2$$

$$\omega_o = 354°.05553$$

$$\omega_1 = .23548454 \times 10^{-4} \text{ deg/sec}$$

$$\omega_2 = -.81426635 \times 10^{-10} \text{ deg/sec}^2$$

$$M_o = 194°.89384$$

$$M_1 = .045951285 \text{ deg/sec.}$$

$$M_2 = .26356956 \times 10^{-10} \text{ deg/sec}^2$$

The associated semi-major axes found are:

$$a_o = 6,457,426 \text{ ft.}$$

$$\bar{a} = 6,456,214 \text{ ft.}$$

Variations in the eccentricity and the Euler angles of this orbit are shown in Figures 20 and 21. Semi-major axis, mean anomaly, and position differences are shown in Figures 22 and 23. As can been seen from Figure 20 the inclination parameter has a bias error at epoch and a slight slope error. The ascending node parameter (see Fig. 21) has only a slight slope error. The semi-major axis difference has a bias of 150 ft. The position difference has a slight error trend and a bias of 150 ft.

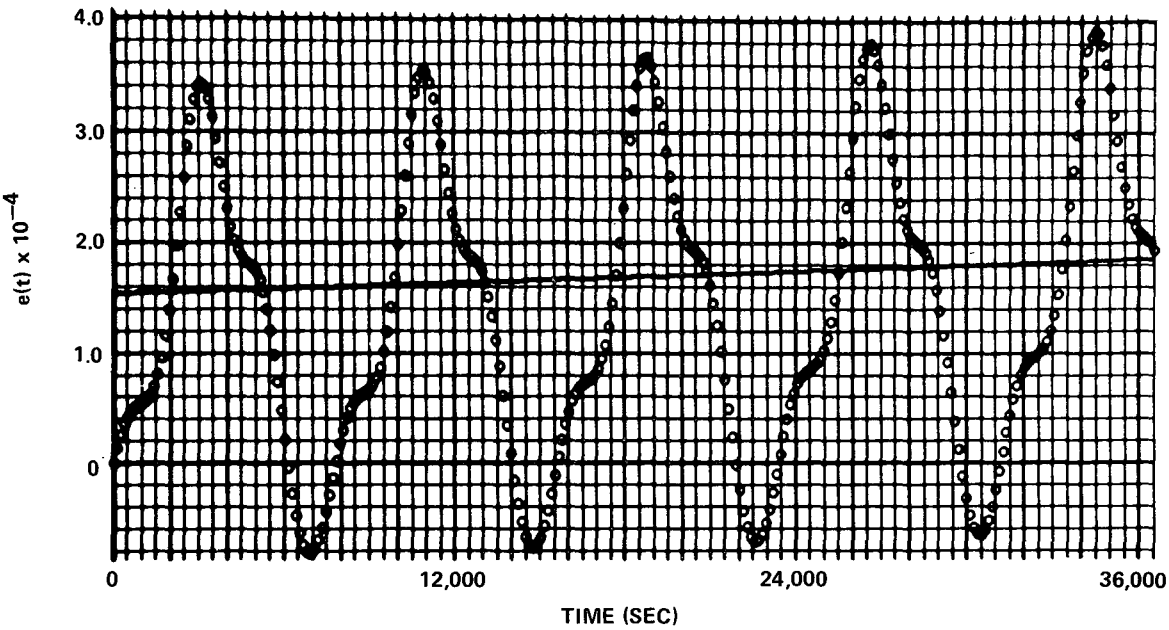

VARIATION IN ECCENTRICITY AS A FUNCTION OF TIME
MINUS EPOCH VALUE

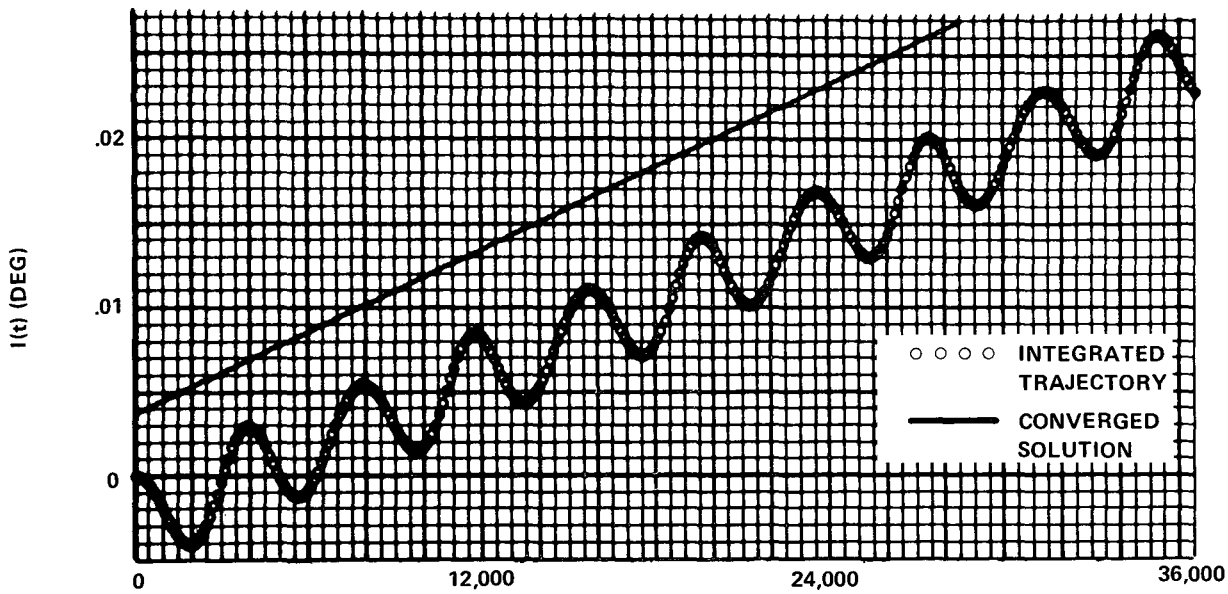

VARIATION IN INCLINATION AS A FUNCTION OF TIME
MINUS EPOCH VALUE

FIGURE 20 - LUNAR ORBITER III ORBIT

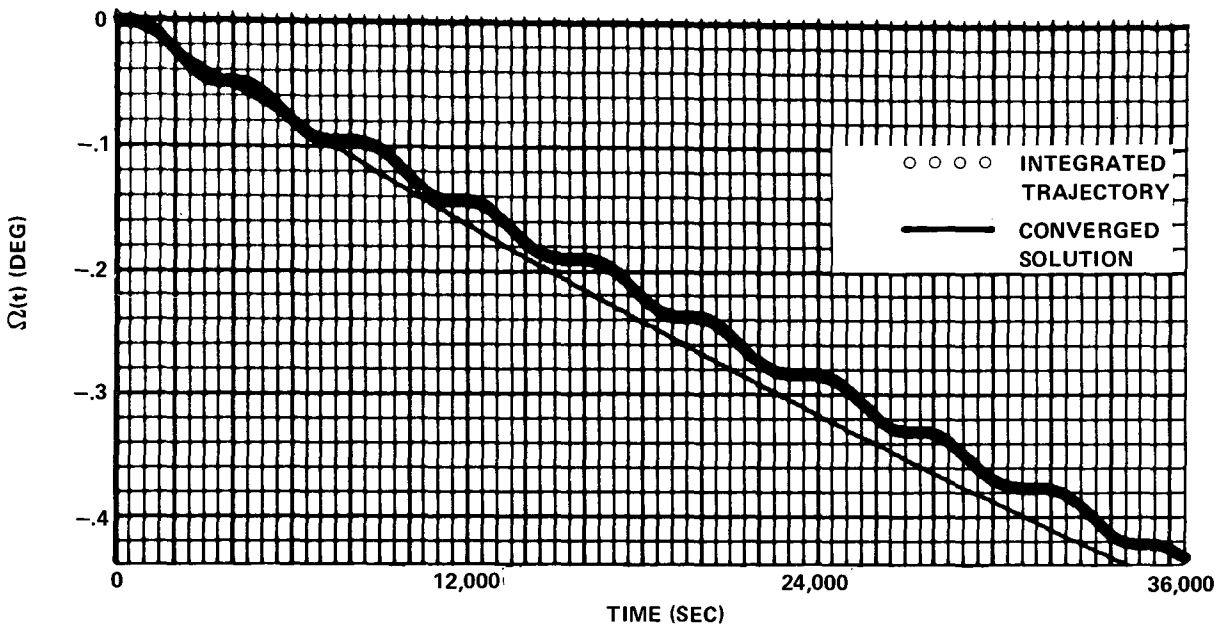

ASCENDING NODE AS A FUNCTION OF TIME
MINUS EPOCH VALUE

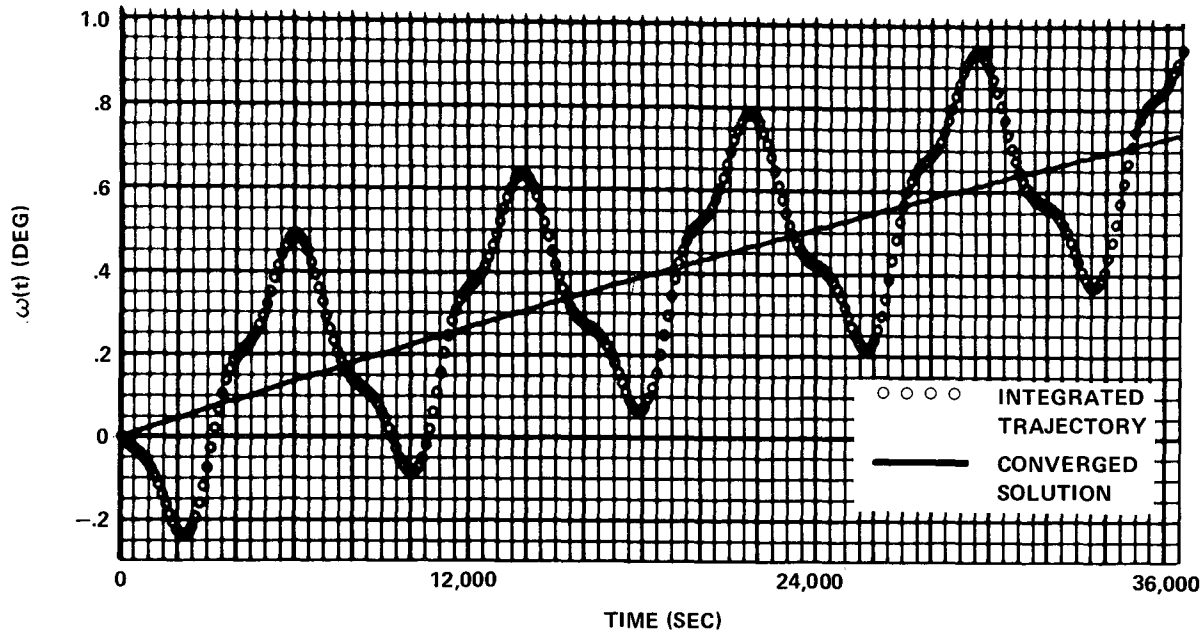

PERIFOCUS AS A FUNCTION OF TIME
MINUS EPOCH VALUE

FIGURE 21 - LUNAR ORBITER III ORBIT

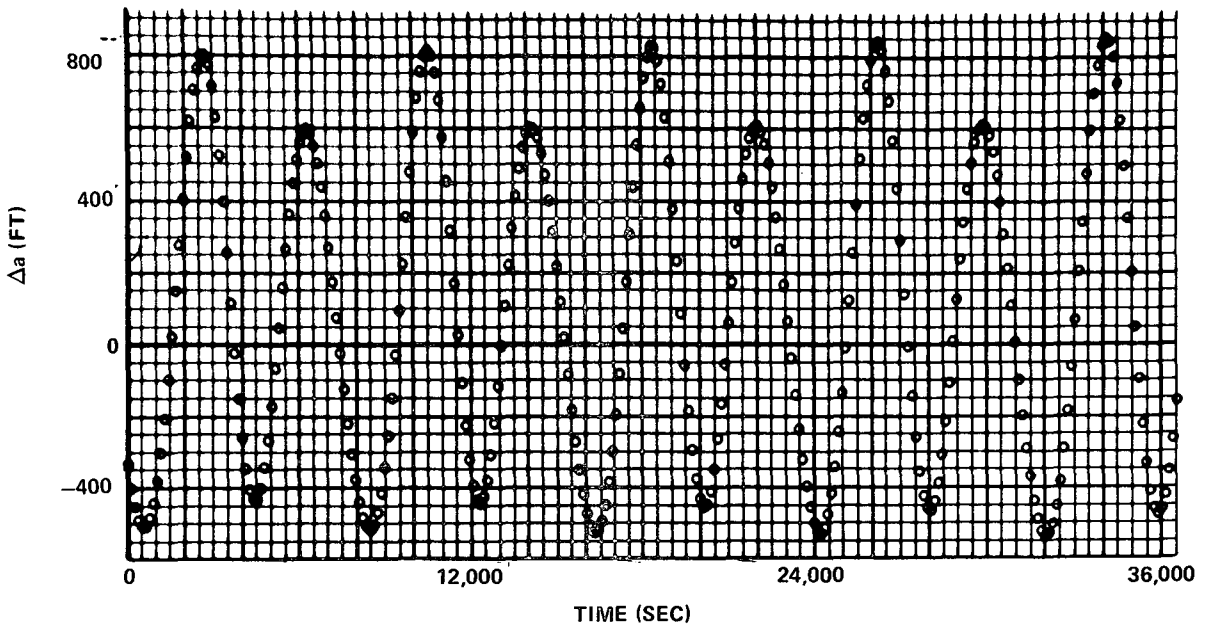

DIFFERENCE IN SEMI-MAJOR AXIS AS A FUNCTION OF TIME

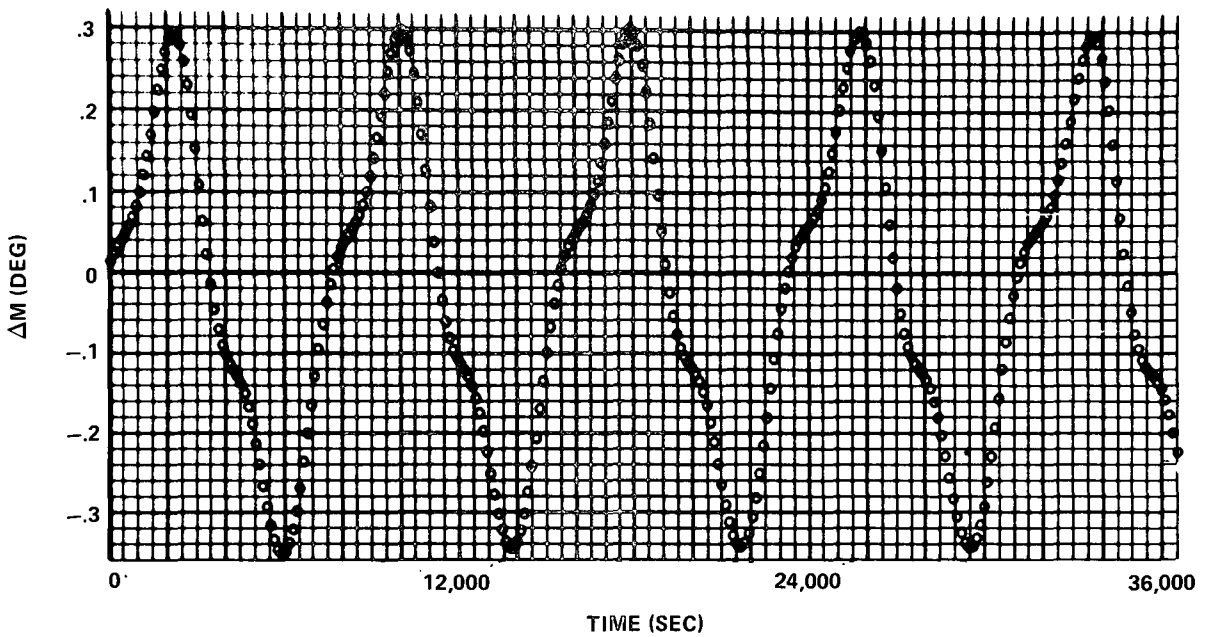

DIFFERENCE IN MEAN ANOMALY AS A FUNCTION OF TIME

FIGURE 22 - LUNAR ORBITER III ORBIT

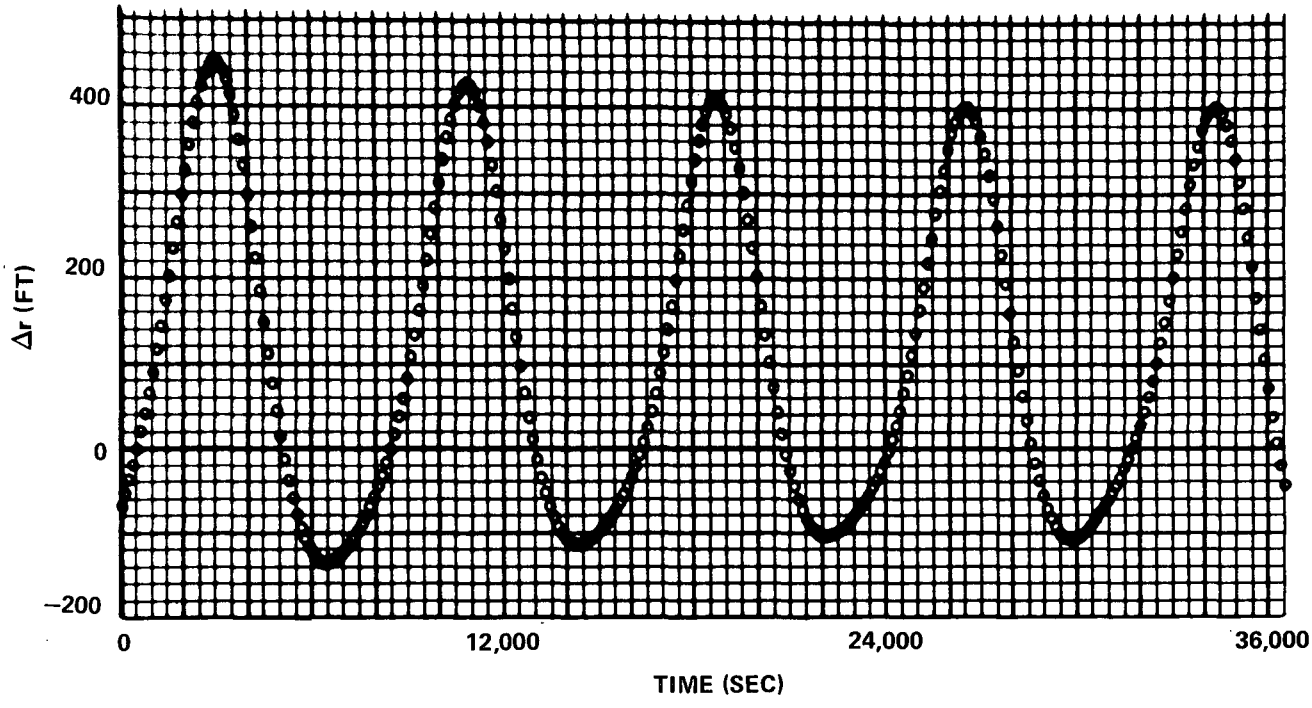

DIFFERENCE IN POSITION AS A FUNCTION OF TIME

FIGURE 23 - LUNAR ORBITER III ORBIT

Again an examination of the functional properties of the partial derivatives used in this solution reveals that three of the state variables have virtually identical sensitivities to the data (see Fig. 24-26)

$$\frac{\partial \dot{\rho}}{\partial \Omega} = \frac{\partial \dot{\rho}}{\partial \omega} = \frac{\partial \dot{\rho}}{\partial M} \tag{3.52}$$

High correlations in the solution $[H^T W H]^{-1}$ matrix were found to exist between the following sets of parameters:

Correlation Coefficient	Parameter Pair
-.95	M_1, M_2
.99	I_o, Ω_o
.98	I_o, ω_o
.98	I_1, Ω_1
.97	I_1, ω_1
.99	Ω_o, ω_1
.99	ω_o, Ω_o
.99	ω_1, Ω_1

Again the slight biases and trend errors experienced in the convergence are a reflection of the equal sensitivities among the state parameters and the aliasing effects of short period variations.

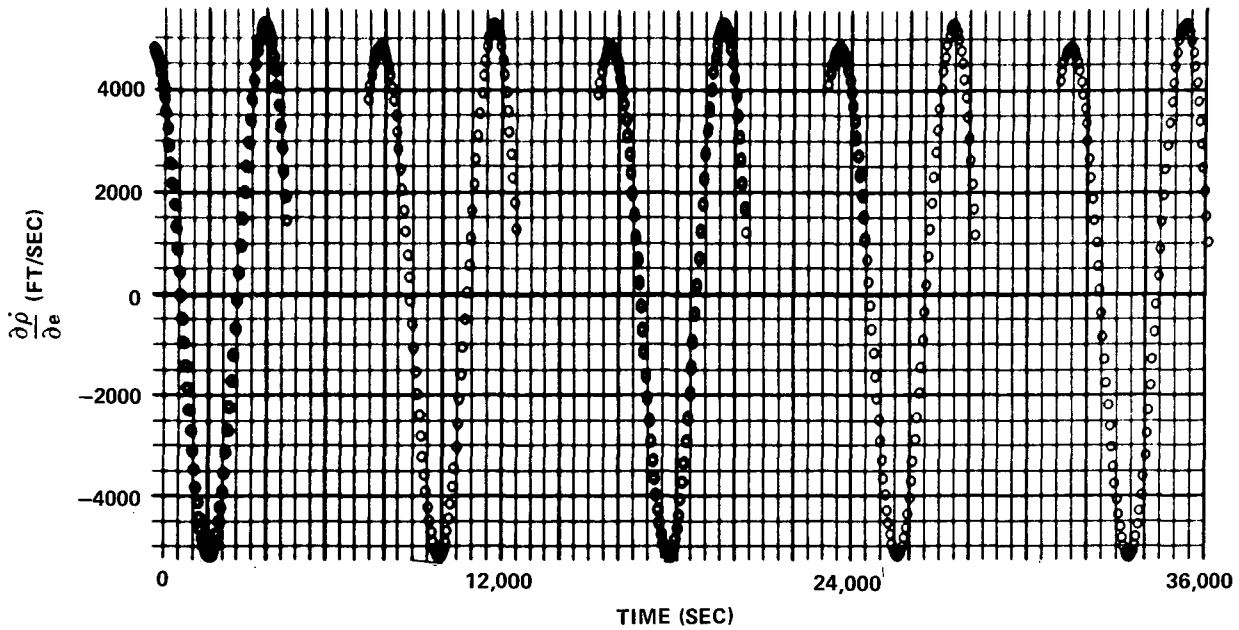

$\frac{\partial \dot{\rho}}{\partial e}$ AS A FUNCTION OF TIME

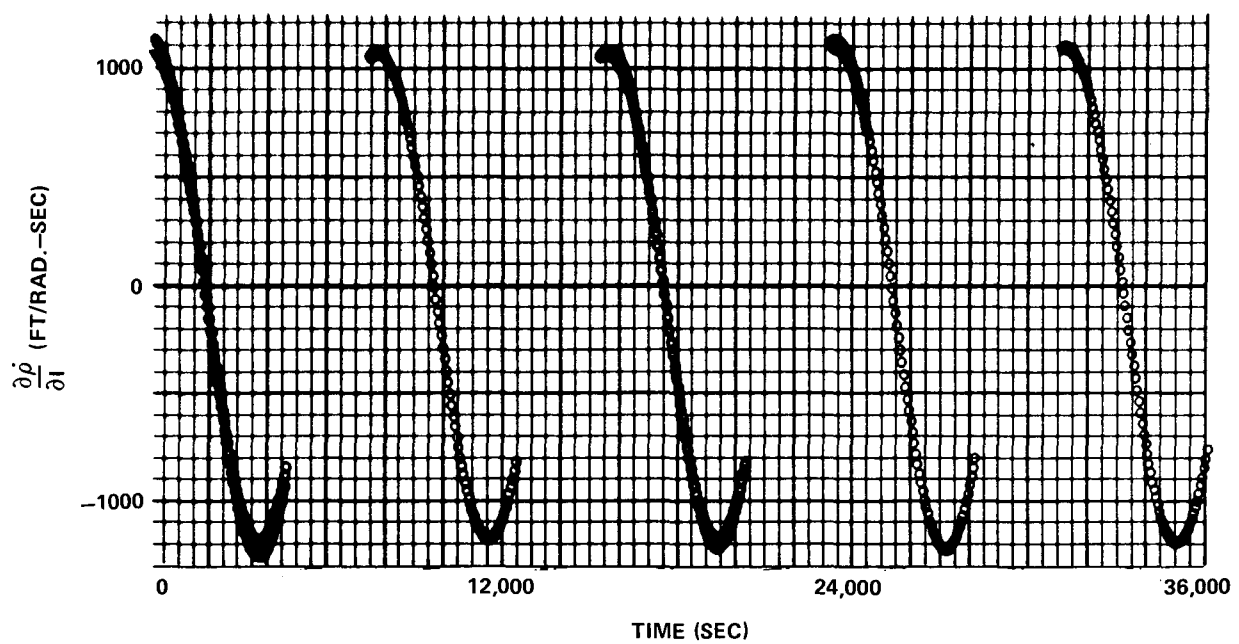

$\frac{\partial \dot{\rho}}{\partial I}$ AS A FUNCTION OF TIME

FIGURE 24 - LUNAR ORBITER III ORBIT

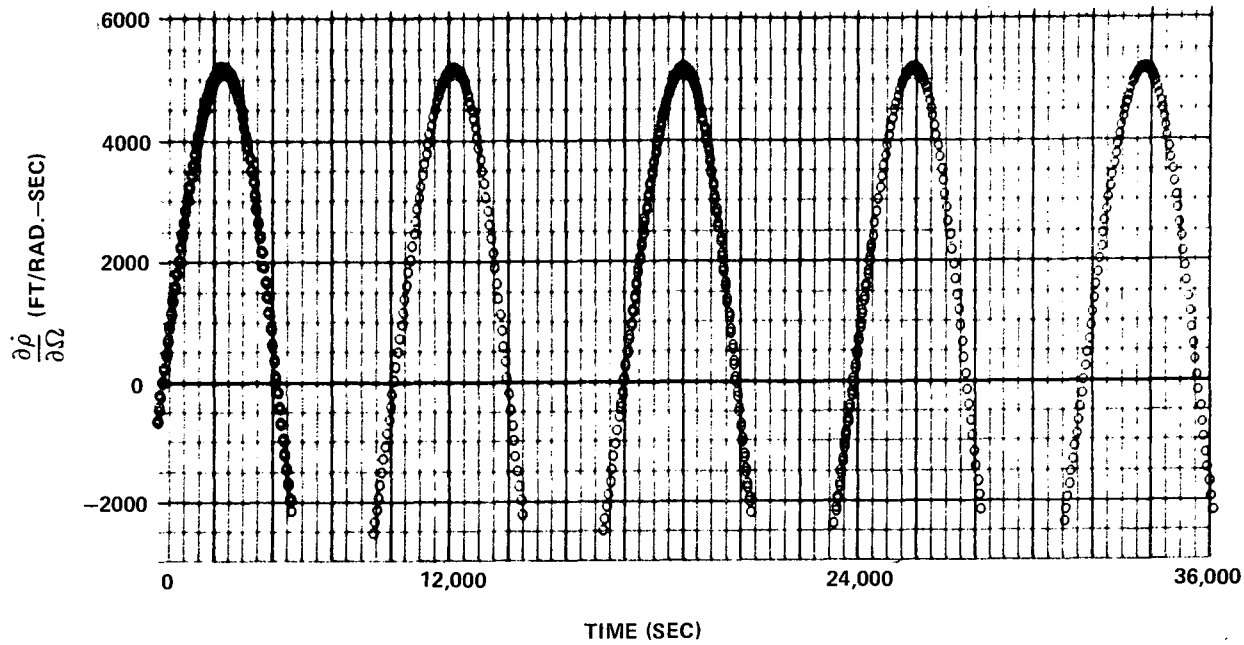

$\frac{\partial \dot{\rho}}{\partial \Omega}$ AS A FUNCTION OF TIME

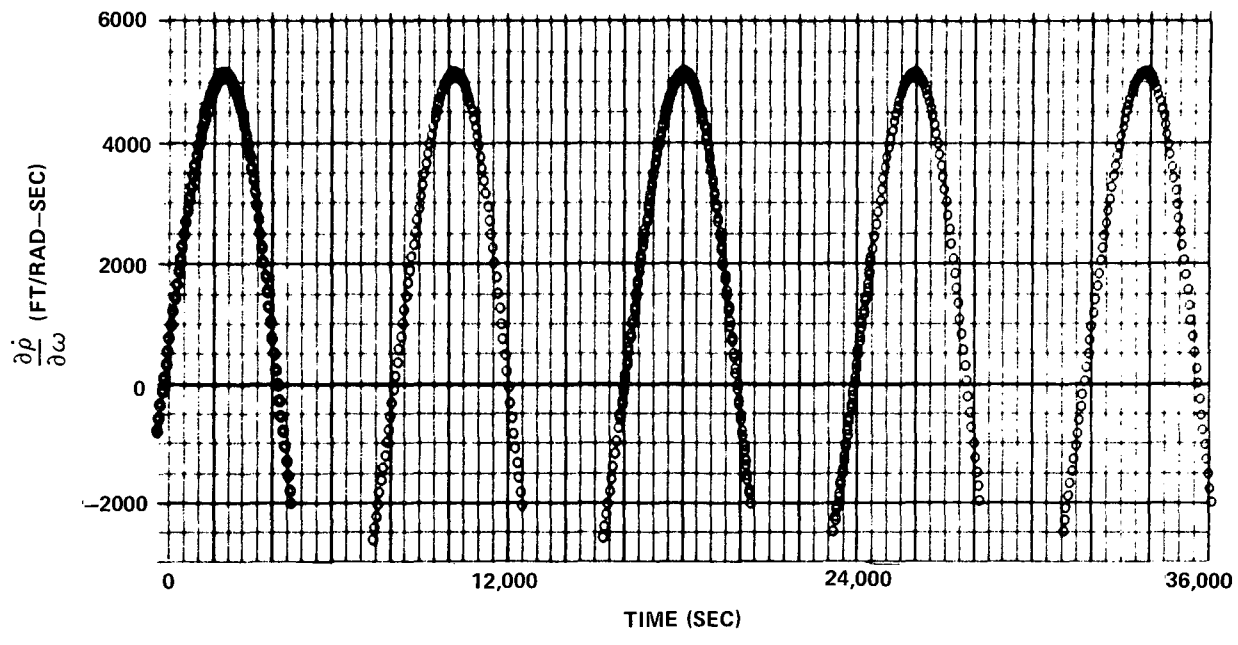

$\frac{\partial \dot{\rho}}{\partial \omega}$ AS A FUNCTION OF TIME

FIGURE 25 - LUNAR ORBITER III ORBIT

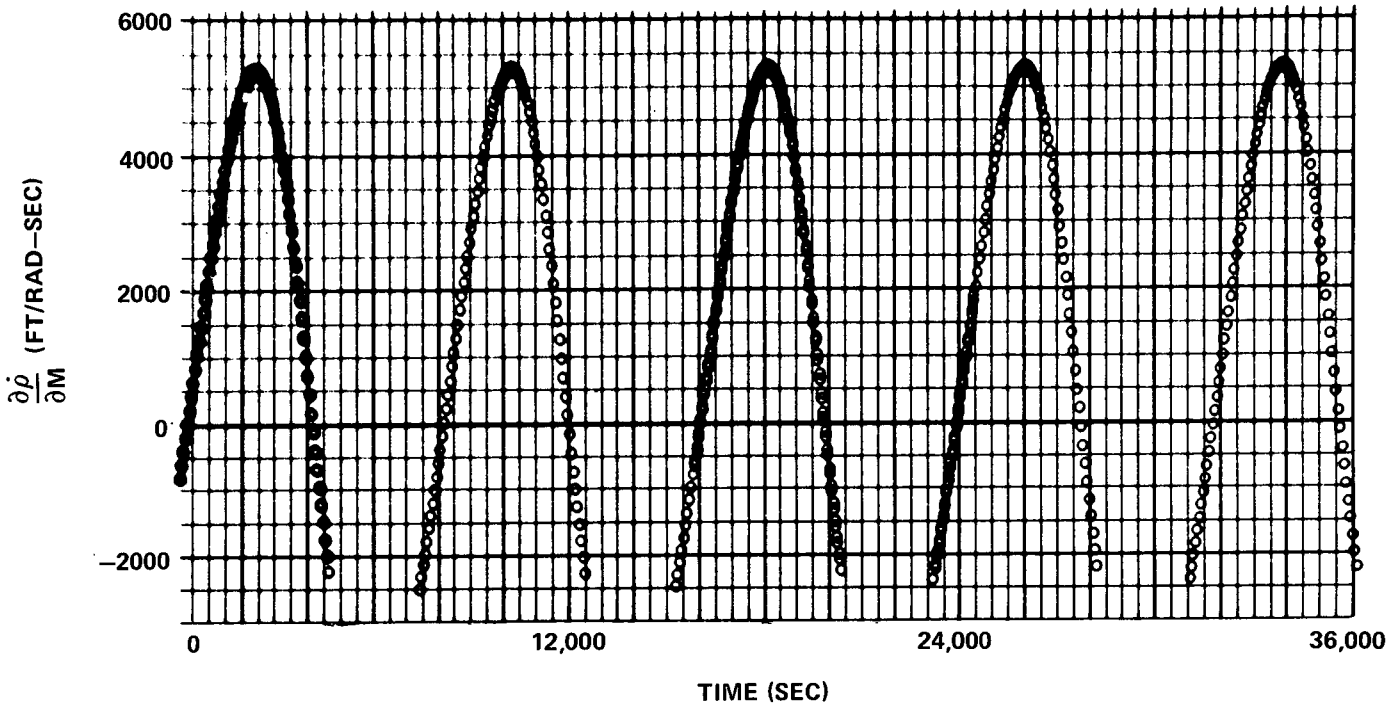

$\frac{\partial \dot{\rho}}{\partial M}$ AS A FUNCTION OF TIME

FIGURE 26 - LUNAR ORBITER III ORBIT

The overall results of these simulations show that the empirical orbit determination method can be used to accurately estimate long-period orbital element variations arising from the non-central features of the moon, from earth and sun perturbations, and from solar radiation. This analysis shows the largest single error source is the lack of separability of dynamical effects from the Doppler measurements. Analysis has shown (for Doppler data) the only way of enhancing these sensitivities is to choose earth based tracking stations with the greatest north-south separation relative to the lunar orbit and to have simultaneous tracking coverage from these stations whenever possible.

The set of Kepler element rates, orbital elements, and associated weighting matrices obtained from this pseudo data analysis will be used to determine a set of triaxial lunar coefficients. The results of that procedure will be discussed in the next chapter.

CHAPTER IV

HARMONIC ESTIMATION

The gravity field determination is performed in a second weighted least-squares processor which uses as input the Kepler element rates, the estimated Kepler elements, and a weighting matrix and outputs a set of spherical harmonic coefficients (see Figure 27). The perturbation equations are of the form

$$\dot{\bar{k}} = \bar{f}(\bar{k},\bar{p},t) \tag{4.1}$$

where $\bar{p}$ is the vector (n×1) of gravity coefficients.

$$\bar{p} = \begin{bmatrix} C \\ \hline S \end{bmatrix} \tag{4.2}$$

The error function to be minimized for this estimator is:

$$\varepsilon = (\dot{\bar{k}} - \dot{\bar{k}}^*)^T \; A(\dot{\bar{k}} - \dot{\bar{k}}^*) \tag{4.3}$$

where A is the (5×5) weighting matrix introduced in the previous chapter, $\dot{\bar{k}}^*$ is an estimate of $\dot{\bar{k}}$.

LEAST SQUARES PROCESSOR

Since the gravity parameters appear as linear functions in the perturbation equations, then (4.1) can be expressed in the following form:

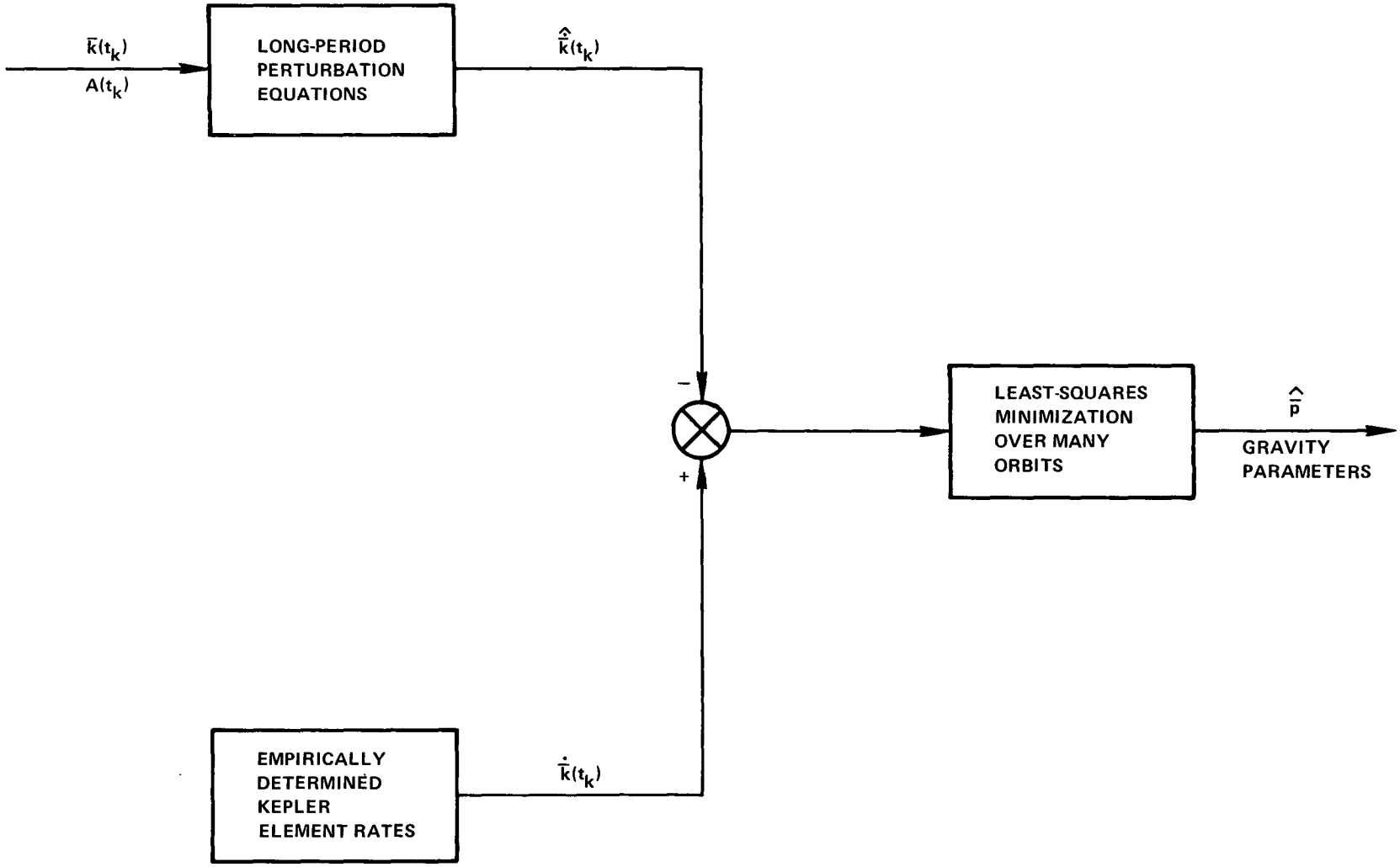

FIGURE 27 - GRAVITY COEFFICIENT ESTIMATION

$$\dot{\bar{k}}^* = F(\bar{k})\bar{p}^* \tag{4.4}$$

where F is a (5×n) matrix of partial derivatives of the Kepler element rates with respect to the gravity coefficients:

$$F(\bar{k}) = \begin{bmatrix} \frac{\partial \dot{e}}{\partial C_{20}} & \cdots & \frac{\partial \dot{e}}{\partial C_{\ell m}} & \frac{\partial \dot{e}}{\partial S_{21}} & \cdots & \frac{\partial \dot{e}}{\partial S_{\ell m}} \\ \\ \frac{\partial \dot{M}}{\partial C_{20}} & \cdots & \frac{\partial \dot{M}}{\partial C_{\ell m}} & \frac{\partial \dot{M}}{\partial S_{21}} & \cdots & \frac{\partial \dot{M}}{\partial S_{\ell m}} \end{bmatrix} \tag{4.5}$$

The error function can be written in terms of the gravity coefficients as follows:

$$\varepsilon = (\dot{\bar{k}} - F\bar{p}^*)^T A(\dot{\bar{k}} - F\bar{p}^*) \tag{4.6}$$

The minimum of the error function is found by setting $\delta\varepsilon = 0$. The resulting equations are:

$$\underbrace{\hat{\bar{p}}}_{(n\times 1)} = \underbrace{[F^T A F]^{-1}}_{(n\times n)} \quad \underbrace{F^T A \dot{\bar{k}}}_{(n\times 1)} \tag{4.7}$$

where $\hat{\bar{p}}$ is the best estimate of the lunar gravity parameters.

TRIAXIAL FIELD DETERMINATION (PSEUDO DATA)

In order to demonstrate the dynamical continuity between the empirical orbit determination and harmonic estimating processors, the two pseudo data convergences presented in the previous chapter will be used to find the triaxial (C_{20} and C_{22}) lunar coefficients assumed in the source trajectory. The nominal values of these terms used for pseudo data generation are as follows:

$$\left.\begin{aligned} C_{20} &= -2.07108\times10^{-4} \\ C_{22} &= .20716\times10^{-4} \end{aligned}\right\} \quad (4.8)$$

Since the orbital period of the Orbiter V satellite is 3.2 hours and the data span 21 hours, this converged solution contributes seven sets of Kepler element rates and elements to the harmonic estimator. The Orbiter III satellite has an orbital period of 2.1 hours and a data span of 10 hours, consequently this solution contributes five sets of Kepler elements and element rates.

The numerical values for the lunar triaxial coefficients as obtained from the pseudo data Orbiter III and Orbiter V convergences when used as input to the harmonic estimating processor are as follows:

$$\begin{aligned} \hat{C}_{20} &= -2.09\times10^{-4} \\ \hat{C}_{22} &= .209\times10^{-4} \end{aligned} \quad (4.9)$$

Since this entire process is one of parameter identification (See Appendix E) and many of the state variables are subject to systematic errors and biases, it is questionable whether the terms on the diagonal of the $[F^TAF]^{-1}$ matrix can be regarded as variances of the $\hat{C}_{20}$ and $\hat{C}_{22}$ estimates. The principal detriment to making this assumption is the fact that A weighting matrix used in the process is not truly the covariance matrix of the input Kepler element rates. The normalized non-diagonal terms in the $[F^TAF]^{-1}$ matrix do reflect the true measure of correlation between the $\hat{C}_{20}$ and $\hat{C}_{22}$ terms. The correlation coefficient between these two terms for this harmonic determination is $\rho = .08$.

Analysis shows when each of these solutions was used separately for a coefficient determination the numerical results obtained varied. The most significant aspect of using only single satellite solutions for gravity determination is that the correlation coefficient between the parameters increases. The harmonic estimation results from using each satellite independently are given below:

SATELLITE NUMBER	ESTIMATED HARMONICS	CORRELATION COEFFICIENT
ORBITER V	$\hat{C}_{20} = -2.056\times10^{-4}$ $\hat{C}_{22} = .219\times10^{-4}$	$\rho=.98$
ORBITER III	$\hat{C}_{20} = -2.044\times10^{-4}$ $\hat{C}_{22} = .668\times10^{-5}$	$\rho=.99$

The small correlation coefficient associated with the multi-satellite solution has an important physical interpretation. Basically a high correlation reflects the inseparability of gravity effects in the harmonic estimator. Since the gravity coefficients each affect different orbits in different ways, using solutions from as many orbits as possible reduces this inseparability. Optimum separation of dynamical effects is achieved by using data from orbits of many different inclinations. The gravity estimation errors associated with multi-orbit solutions are then largely a function of the degree of accuracy of the estimated Keplerian states and rates. For the case of single orbit solutions, the presence of high correlations in the $[F^TAF]^{-1}$ matrix also tends to confuse the estimation process. This notion of separability of dynamical effects becomes very important in the actual determination of the lunar field.

In order to obtain a quantitative measure of the triaxial solution given by (4.9) a comparison is made between it and the nominal triaxial values (4.8) using numerically integrated equations of motion. The comparisons, covering a one day period, are made both for the Lunar Orbiter III and V orbits. Differences in each of the Kepler elements, position, and velocity are shown in Figures (28-35). The position errors developed over the Lunar Orbiter V trajectory are small and attain a maximum value of 60 ft. The velocity errors are also

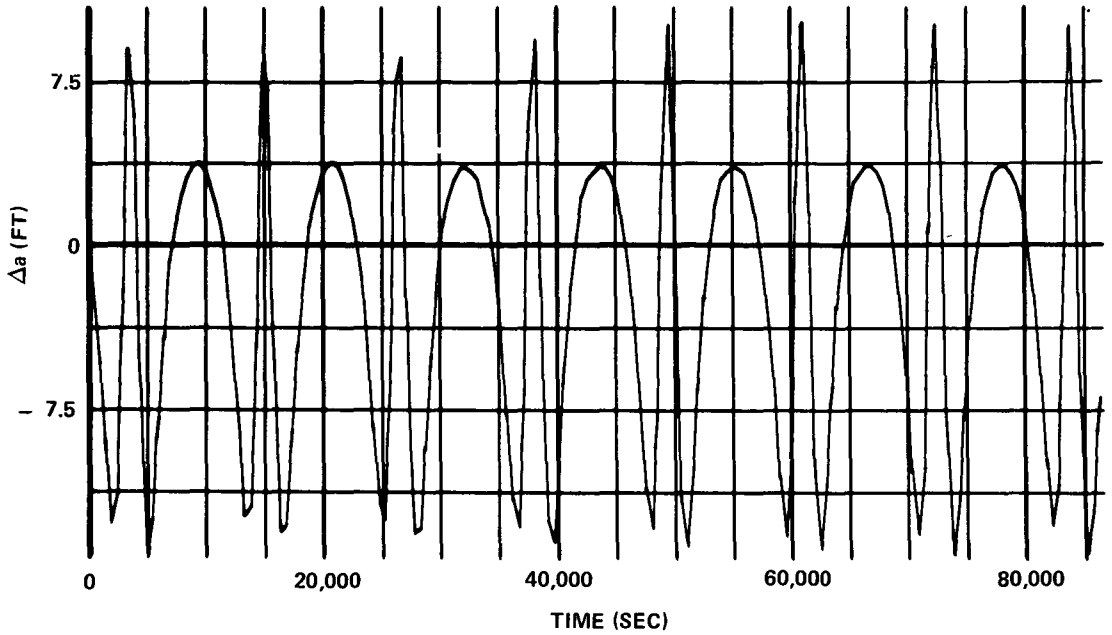

SEMI-MAJOR AXIS DIFFERENCE VS. TIME

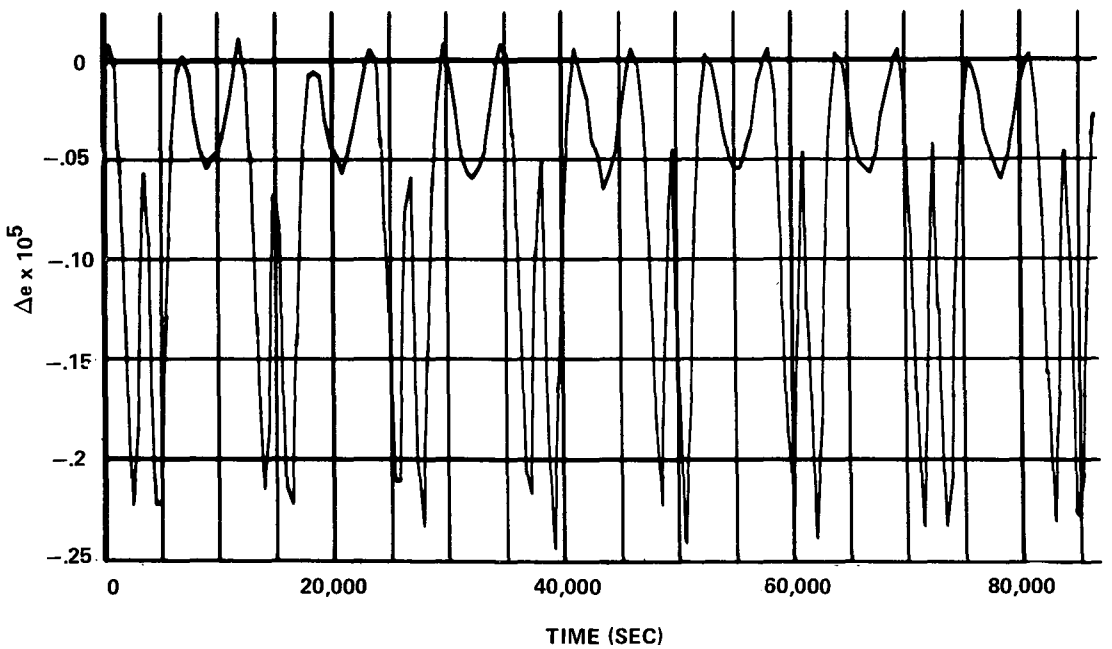

ECCENTRICITY DIFFERENCE VS TIME

FIGURE 28 - LUNAR ORBITER V ORBIT

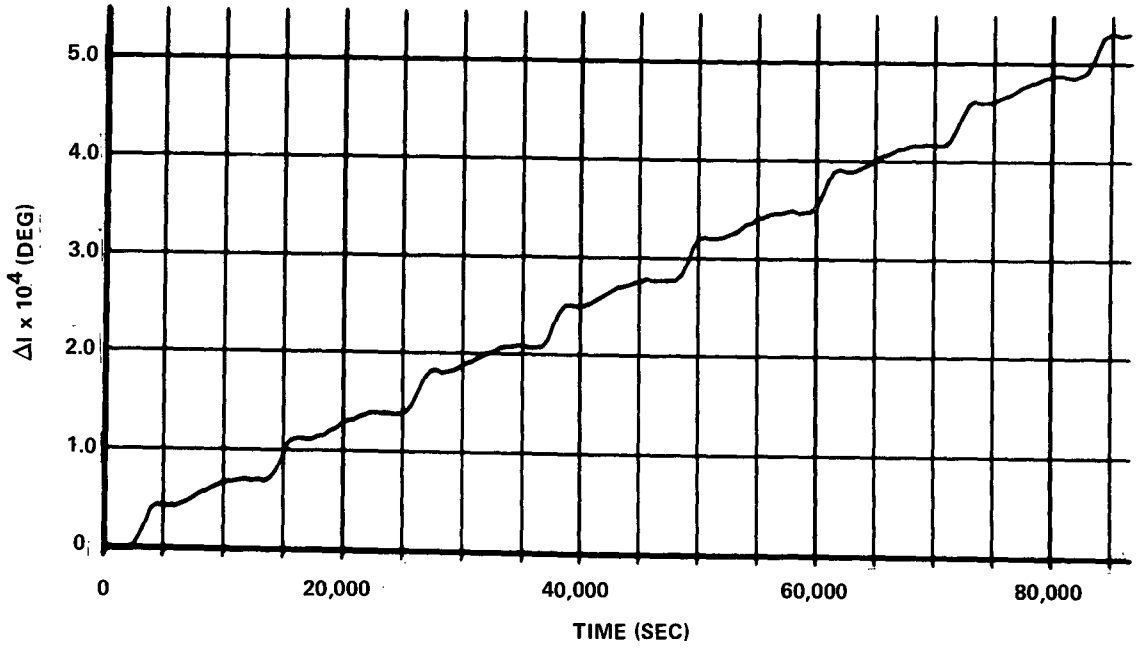

INCLINATION DIFFERENCE VS. TIME

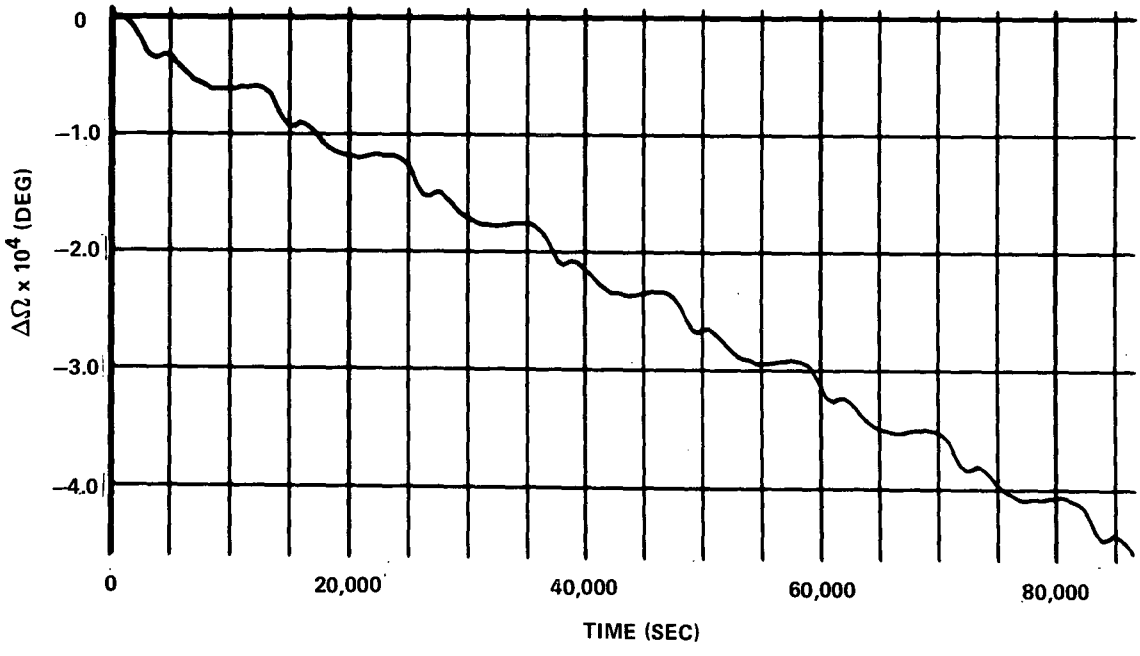

ASCENDING NODE DIFFERENCE VS. TIME

FIGURE 29 - LUNAR ORBITER V ORBIT

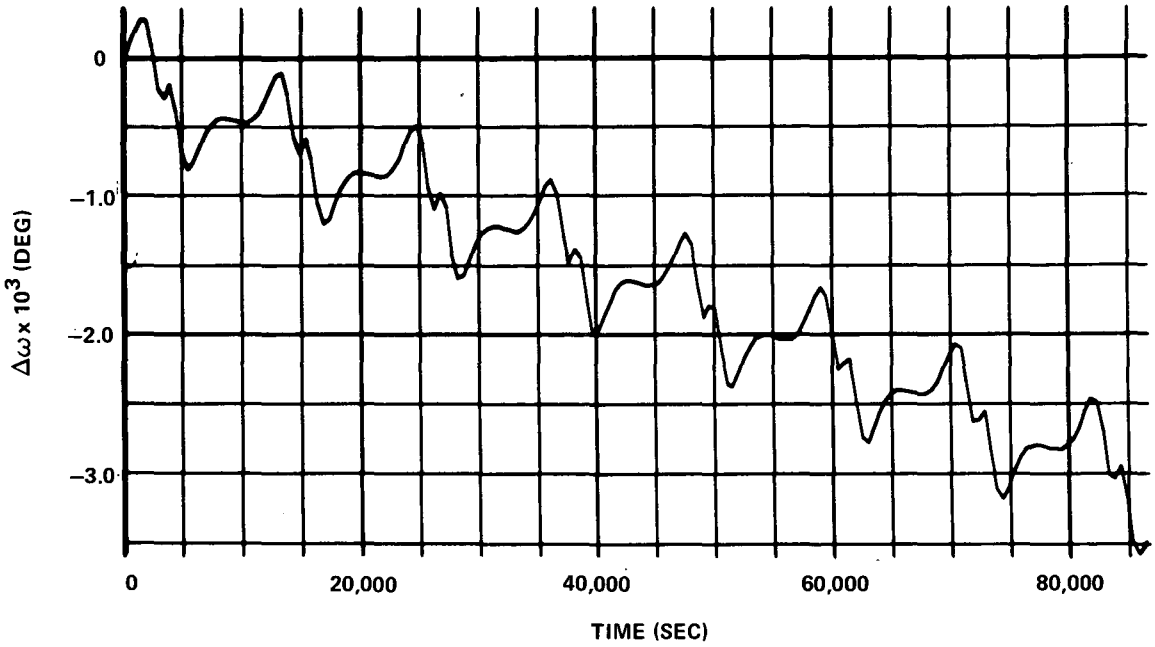

PERIFOCUS DIFFERENCE VS. TIME

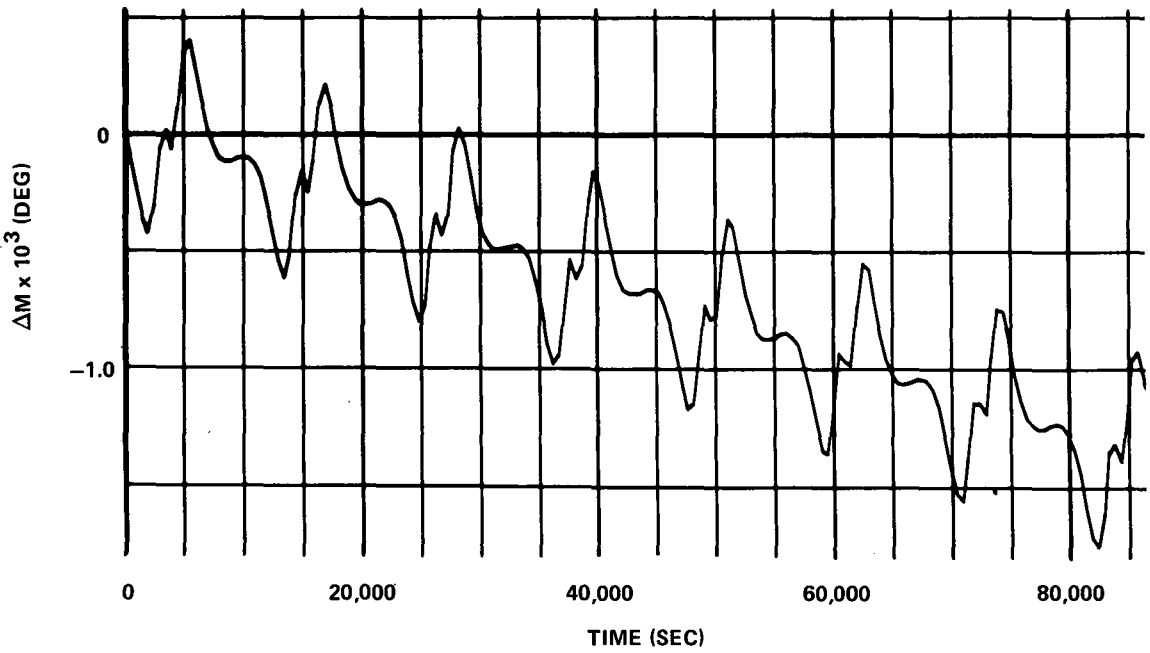

MEAN ANOMALY DIFFERENCE VS. TIME

FIGURE 30 - LUNAR ORBITER V ORBIT

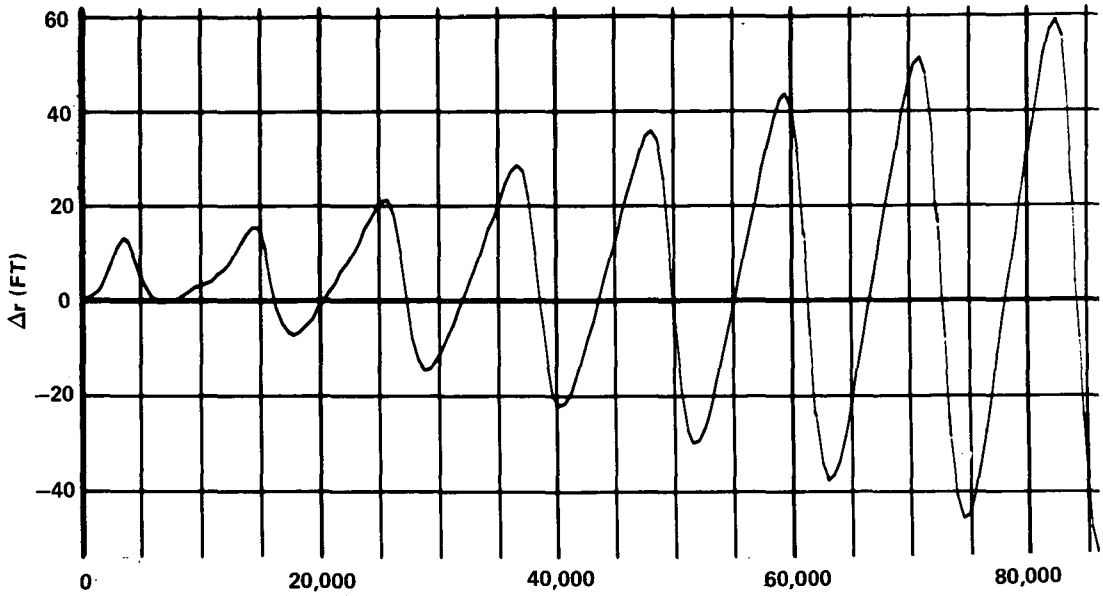

POSITION DIFFERENCE VS. TIME

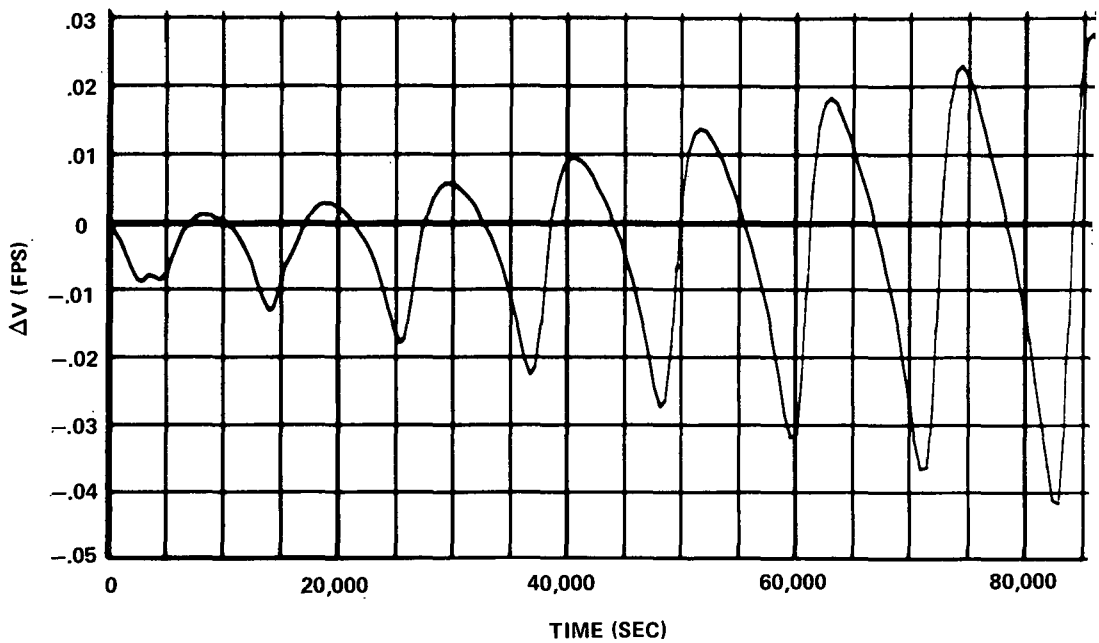

VELOCITY DIFFERENCE VS. TIME

FIGURE 31 - LUNAR ORBITER V ORBIT

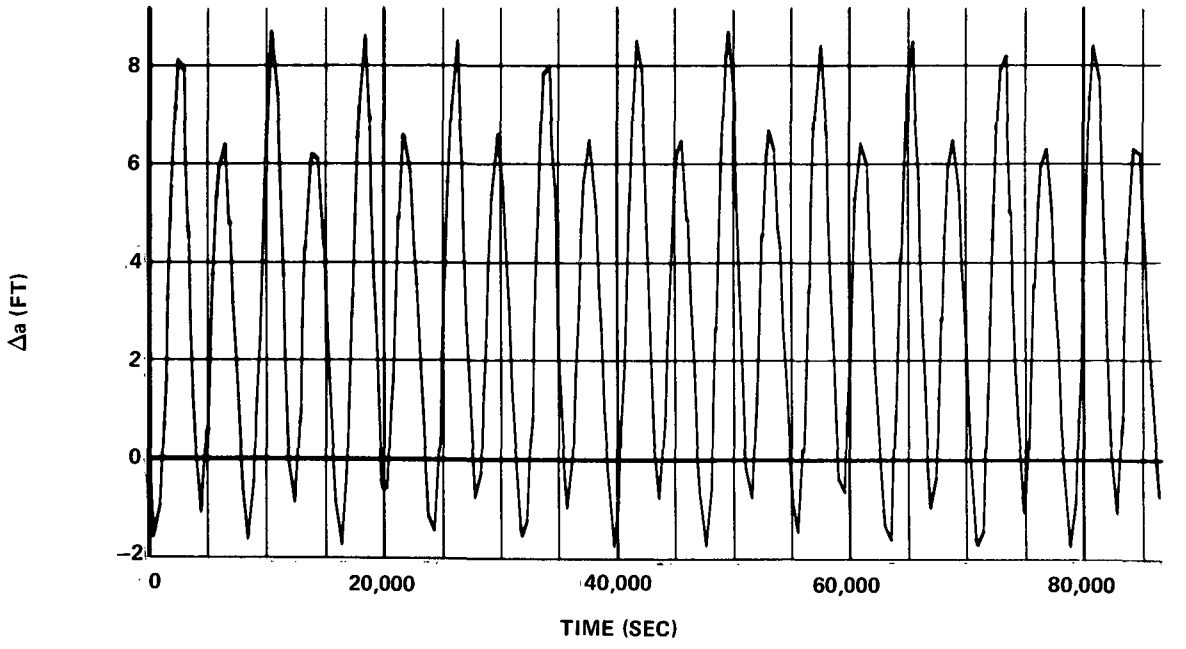

SEMI-MAJOR AXIS DIFFERENCE VS TIME

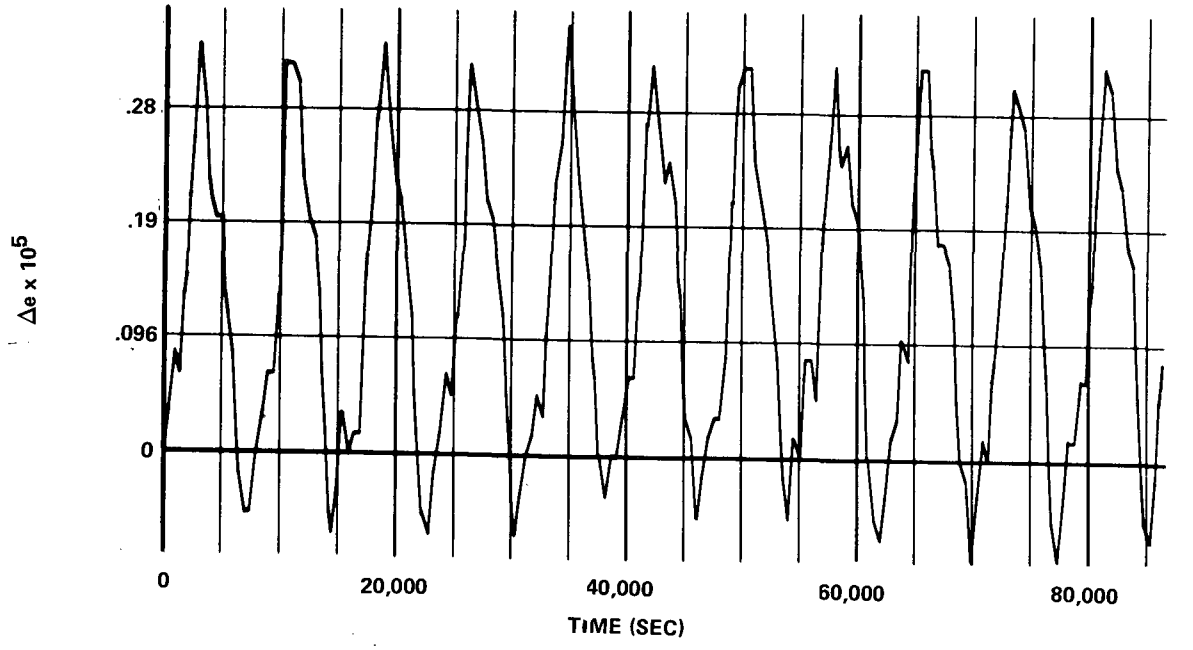

ECCENTRICITY DIFFERENCE VS TIME

FIGURE 32 - LUNAR ORBITER III ORBIT

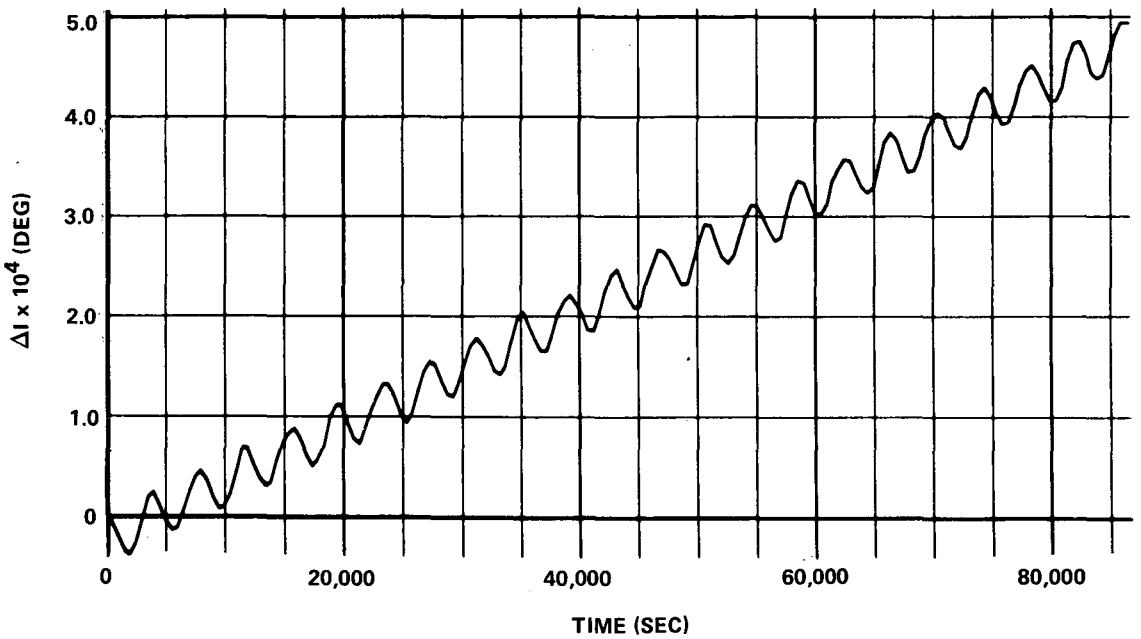

INCLINATION DIFFERENCE VS TIME

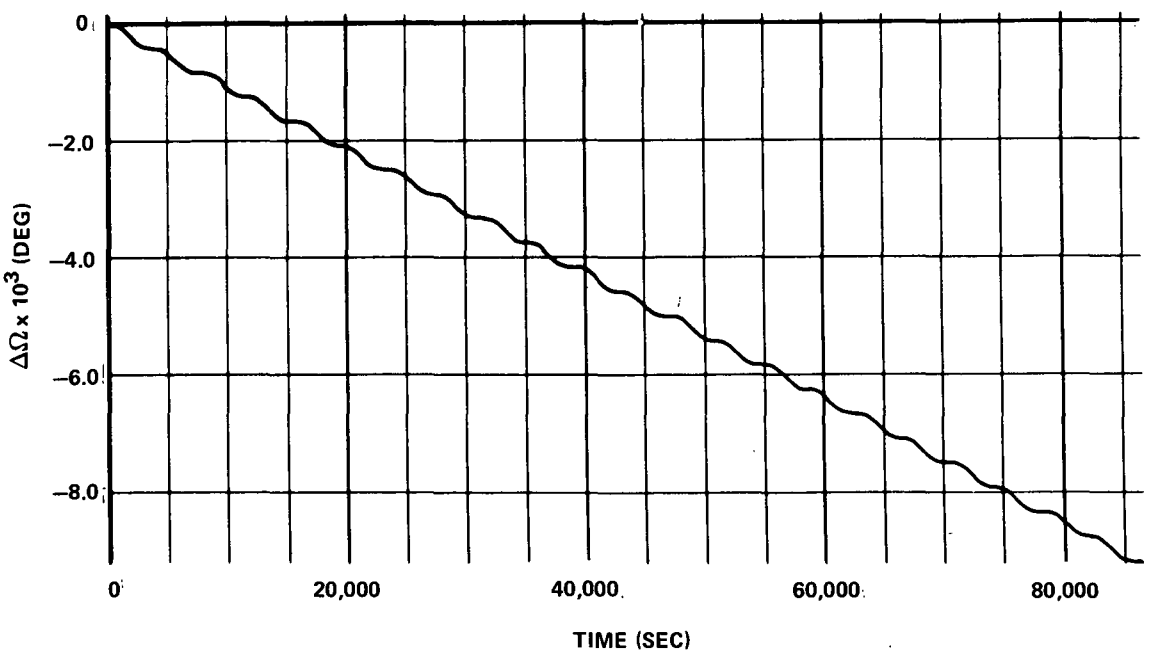

ASCENDING NODE DIFFERENCE VS TIME

FIGURE 33 - LUNAR ORBITER III ORBIT

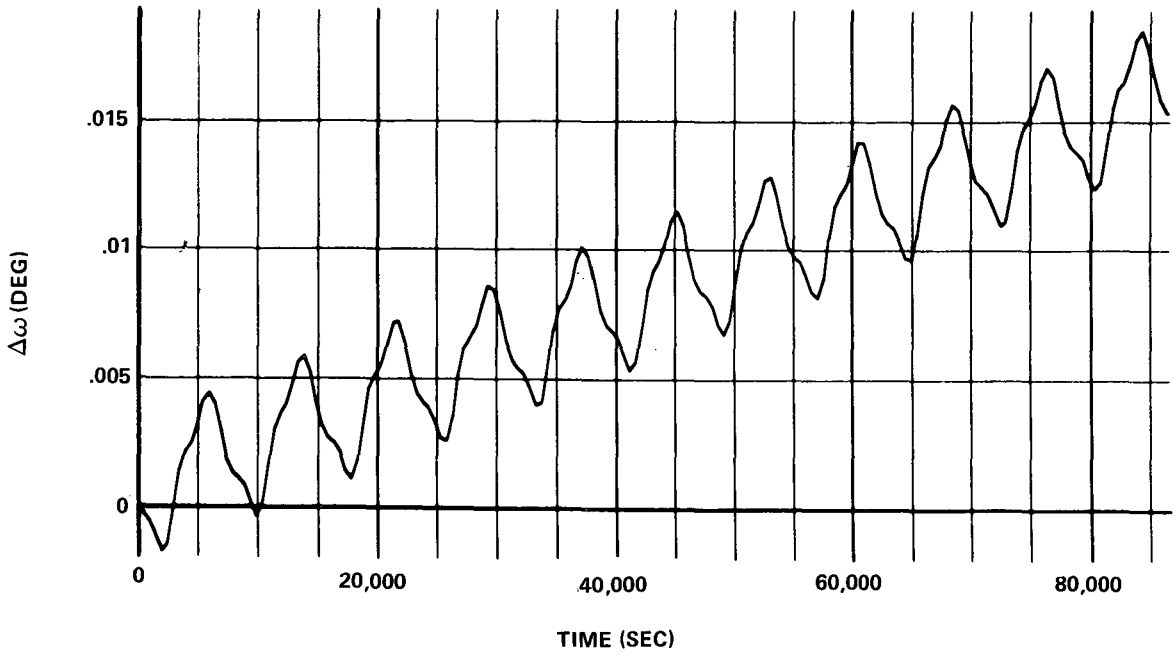

PERIFOCUS DIFFERENCE VS TIME

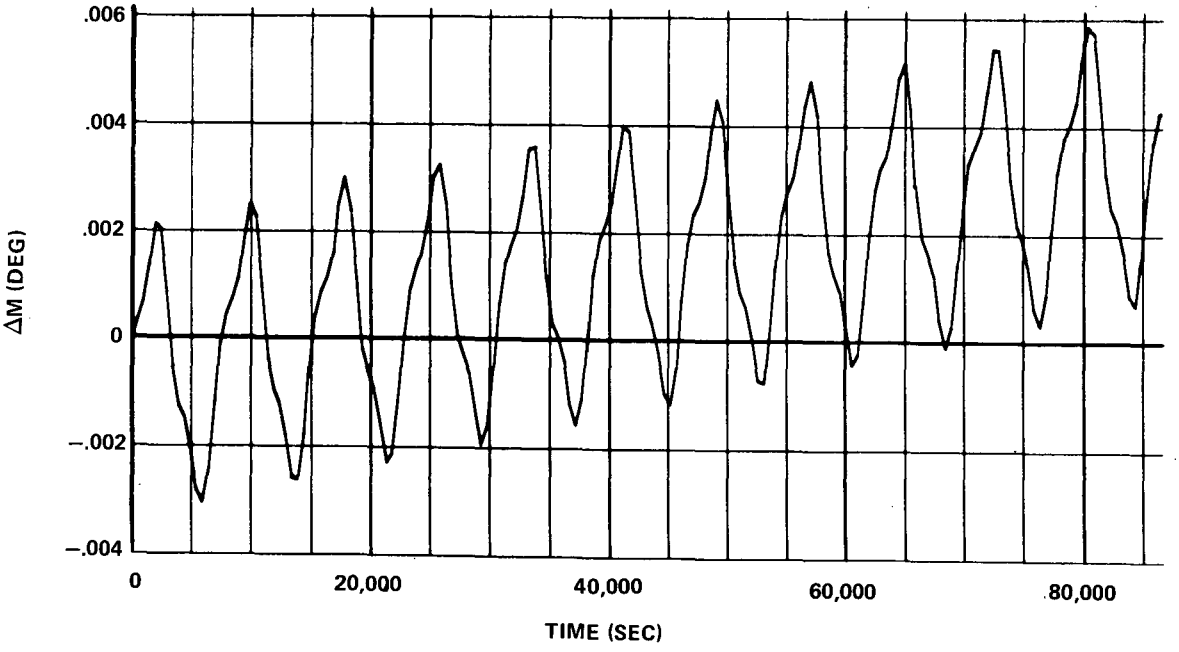

MEAN ANOMALY DIFFERENCE VS TIME

FIGURE 34 - LUNAR ORBITER III ORBIT

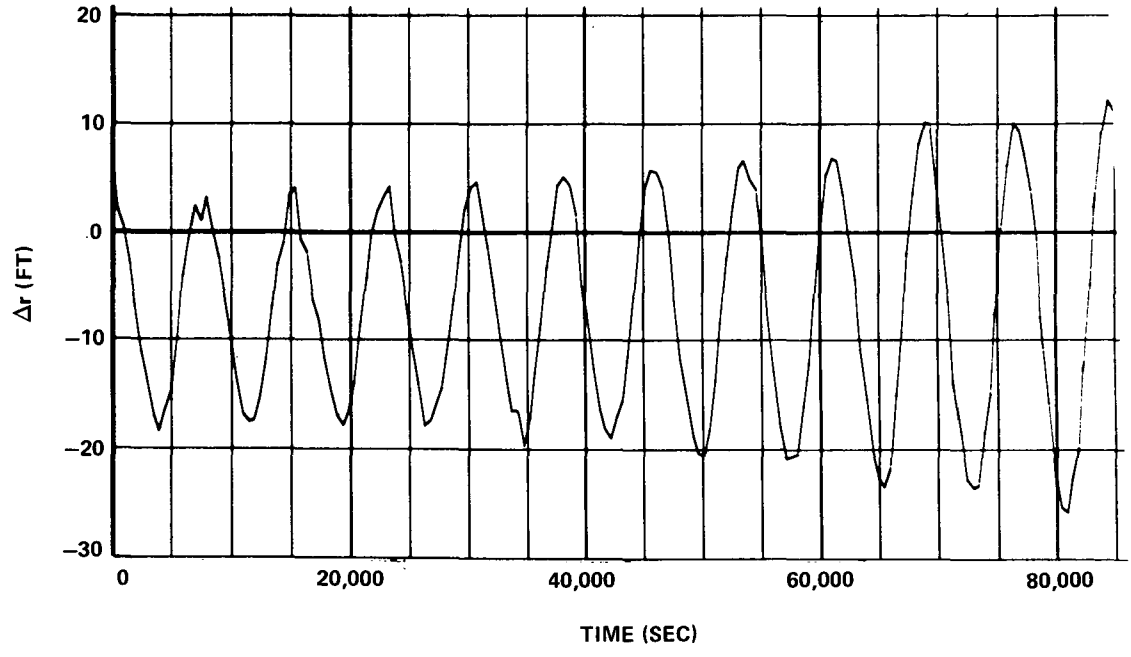

POSITION DIFFERENCE VS TIME

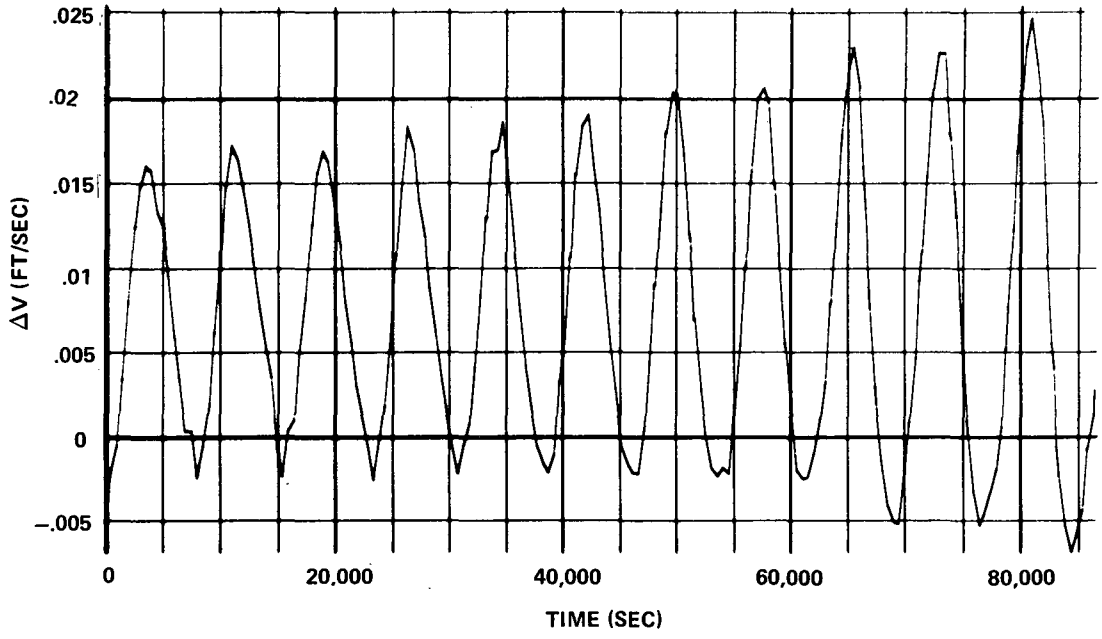

VELOCITY DIFFERENCE VS TIME

FIGURE 35 - LUNAR ORBITER III ORBIT

small, reaching a peak value of .05 fps. For the case of the Lunar Orbiter III trajectory the position errors are even smaller, attaining a peak value of 25 ft. and the velocity errors attaining a value of .025 fps.

DISCUSSION

The dynamical compatibility of this empirical selenodesy method has been established in this chapter. It is significant to note at this point that the method is dependent on the following:

1. Doppler tracking data of free-flight quality (thrust-free).
2. Tracking coverage relative to the satellite orbit which provides the best geometrical configuration possible (good north-south station separation).
3. Tracking of satellites from many different inclinations so as to attain the best overall coverage of the moon.

These points are re-emphasized since in the next chapter of this investigation the empirical method is applied to actual Doppler data. Of the three points mentioned, none are actually achieved for the case of real data.

CHAPTER V

DATA ANALYSIS

In the previous two chapters, the theory and equations for this empirical selenodesy method have been developed and a controlled pseudo data analysis has been presented to illustrate the dynamical consistency of the method. The purpose of this chapter is to present and discuss the results obtained when this method was applied to actual Doppler tracking data.

DATA SET UTILIZED

As mentioned earlier in this study, large amounts of Doppler tracking data were acquired during the lunar orbits of both the Lunar Orbiters (I-V) and the Apollo (8, 10, 11, 12, 14, and 15) missions. Almost all the tracking data acquired during the photographic portions of the Lunar Orbiter missions includes propulsive attitude control maneuvers performed at such a high frequency (about every three hours) that these data cannot be used for selenodesy purposes. Even the Lunar Orbiter data from the extended mission phases (primarily that used in this analysis) contains some minor propulsive thrusts. Data from all the Apollo 8 mission and large portions of the Apollo 10, 11, and 15 missions contain propulsive thrusting. The extended mission phase Lunar Orbiter data was used to determine the lunar gravity field presented in this study since it is not only the largest but also the most complete (but far from complete in an absolute sense) data set gathered to date.

The free-flight quality data from parts of the Apollo 11, 12 and 14 missions were used as control data to test the quality of the lunar field obtained. The small amount of Apollo data which is of free-flight quality cannot be used in the method since these data are from either nearly circular, or nearly equatorial orbits and the method as it has been developed becomes near singular for orbits of this type.

The epoch times, length, and number of tracking stations of the various data arcs used in this analysis are listed in Table III. No data from the Orbiter IV satellite were included; since earth perturbations were the most dominant for this orbit, it was assumed to have only minimal lunar gravity information content. The length of the data arcs used in orbit determination solutions varies from a minimum of about eight hours to a maximum of thirty-six hours.

ANALYSIS OF ORBIT DETERMINATION SOLUTIONS

Two different sized parameter sets representing the satellite Keplerian state in lunar orbit were used. The first set contains eleven parameters $\{e_o, e_1, I_o, I_1, \Omega_o, \Omega_1, \omega_o, \omega_1, M_o, M_1, M_2\}$ and was used exclusively when the Doppler data span was twelve hours or less. The second solution set contains thirteen parameters $\{e_o, e_1, e_2, I_o, I_1, \Omega_o, \Omega_1, \Omega_2, \omega_o, \omega_1, \omega_2, M_o, M_1, M_2\}$ and was used when the data span was greater than twelve hours. Analysis with pseudo data showed that this choice of parameters should be adequate to model the long-period variations of the satellite.

TABLE III

LUNAR ORBITER DATA ARCS

SATELLITE	EPOCH (DAY, MO., YR.)	LENGTH (SEC)	STATIONS
ORBITER I	31.41180556 Aug. 1966	75,989	3
	1.32430556 Sept. 1966	88,889	3
	4.22916667 Sept. 1966	84,000	3
	13.84722222 Sept. 1966	81,000	3
	14.81597222 Sept. 1966	81,000	3
	15.78263889 Sept. 1966	108,670	3
ORBITER II	8.85938421 Dec. 1966	92,700	3
	10.55208333 Dec. 1966	32,760	3
	29.61805556 June 1967	34,260	2
ORBITER III	20.60000000 Feb. 1967	93,290	3
	21.68055556 Feb. 1967	86,000	3
	27.97222222 Feb. 1967	89,280	3
	2.38194444 Mar. 1967	75,000	3
	5.16666667 Mar. 1967	110,800	3
	6.83958333 Mar. 1967	97,740	3
	24.21527778 Mar. 1967	31,380	2
	11.48611111 April 1967	46,080	2
ORBITER V	18.31111111 Aug. 1967	63,000	3
	19.09027778 Aug. 1967	88,000	3
	20.11111111 Aug. 1967	119,450	3
	21.49652778 Aug. 1967	119,068	3
	24.21180556 Aug. 1967	87,928	3
	25.22847222 Aug. 1967	59,340	3
	26.25208333 Aug. 1967	85,000	3
	27.28819444 Aug. 1967	70,468	3
	2.52777778 Oct. 1967	29,880	2
	3.54166667 Oct. 1967	43,200	2
	17.38194444 Nov. 1967	38,040	2
	21.31944444 Nov. 1967	33,568	2
	29.86111111 Jan. 1968	112,618	3

TABLE IV PHYSICAL CONSTANTS

I. ASTRODYNAMIC CONSTANTS

Gravitational Parameters:

$$\mu_{\text{☾}} = .1731300417087798 \times 10^{15} \quad Ft^3/sec^2$$
$$\mu_{\oplus} = .1407646853278542 \times 10^{17} \quad Ft^3/sec^2$$
$$\mu_{\odot} = .4686697671960888 \times 10^{22} \quad Ft^3/sec^2$$

Mean Lunar Radius:

$$R_e = .570239501312336 \times 10^{7} \quad Ft.$$

Angular Velocity of Moon's Rotation:

$$\gamma = .2661703316891657 \times 10^{-5} \quad Rad/sec$$

Velocity of Light in a Vacuum:

$$c = .9835711942257218 \times 10^{9} \quad Ft/sec$$

II. STATION LOCATIONS

STATION	GEOCENTRIC COORDINATES		
	Radius, Ft.	Latitude, Deg.	Longitude, Deg.
Goldstone, Calf. (DSS12)	20,905,479	35.118640	243.19483
Woomera, Australia (DSS41)	20,907,326	-31.211390	136.88779
Madrid, Spain (DSS61)	20,898,911	40.238540	355.75129
Madrid, Spain (DSS62)	20,898,927	40.263490	355.63246

III. DOPPLER DATA WEIGHT

$$W = \frac{1}{\sigma^2}, \quad \sigma = .00213 \ Ft/sec$$

IV. SOLAR ACCELERATION

$$F = 3.973 \times 10^{-7} \ Ft/sec^2$$

Table IV contains a list of the tracking station locations[30] and all the astrodynamical constants[31] assumed known and fixed in the orbit determination program. The positions and relative velocities of the earth, sun, and moon are obtained from Jet Propulsion Laboratory Ephemeris Tape DE-19.[32] The least-squares orbit determination program reads the necessary information from this tape during the convergence process.

The rate of convergence for each orbit determination solution varied as a function of the orbit, the data arc length, and the number and locations of earth based stations used. In general each convergence process took about five to six iterations. The numerical particulars associated with a typical solution for each of the Lunar Orbiters (I, II, III, and V) will now be discussed.

Representative residuals from Lunar Orbiter I, II, III, and V orbit determination solutions are given in Figures 36 and 37. The residuals associated with each of these convergences have the statistical properties listed in Table V.

TABLE V

SATELLITE	RESIDUAL MEAN (fps)	RESIDUAL STD. DEVIATION (fps)
ORBITER I	-.010	.108
ORBITER II	-.012	.090
ORBITER III	.006	.053
ORBITER V	.003	.068

As can be seen from the figures the residuals associated with the Lunar Orbiter I and II convergences presented have a larger

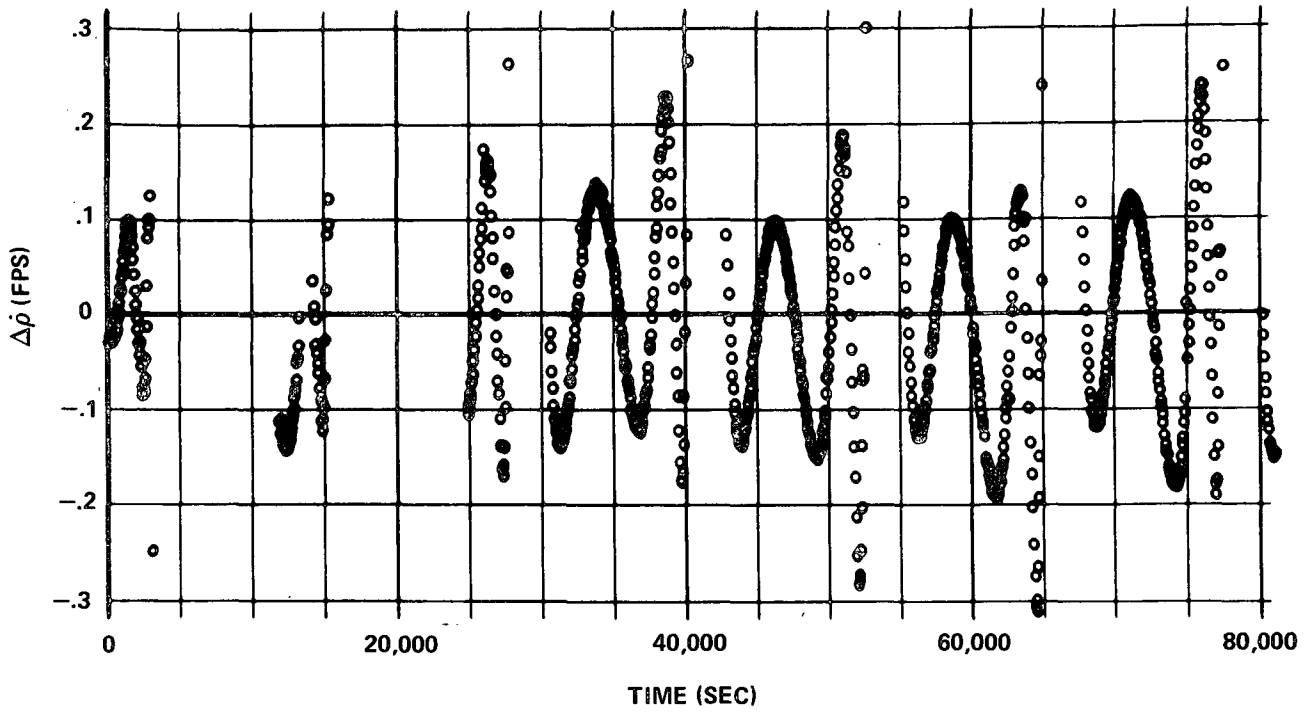

LUNAR ORBITER I DOPPLER RESIDUALS VS. TIME

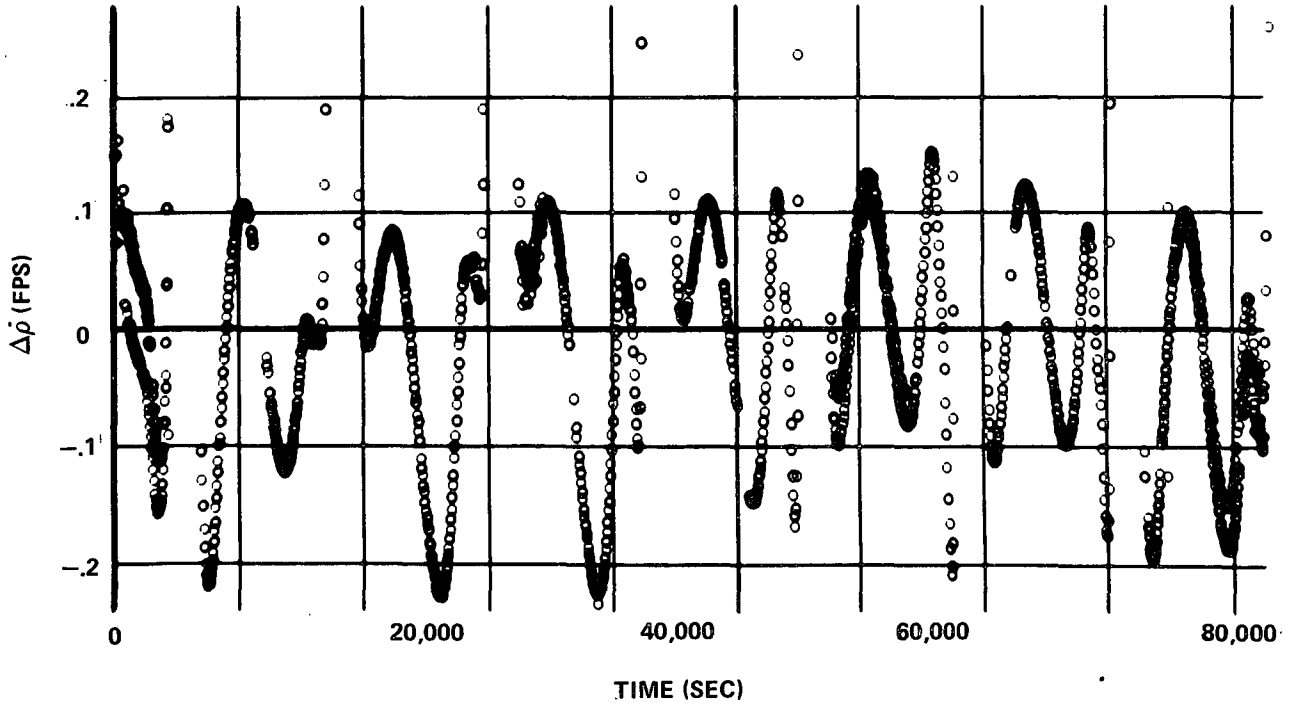

LUNAR ORBITER II DOPPLER RESIDUALS VS. TIME

FIGURE 36

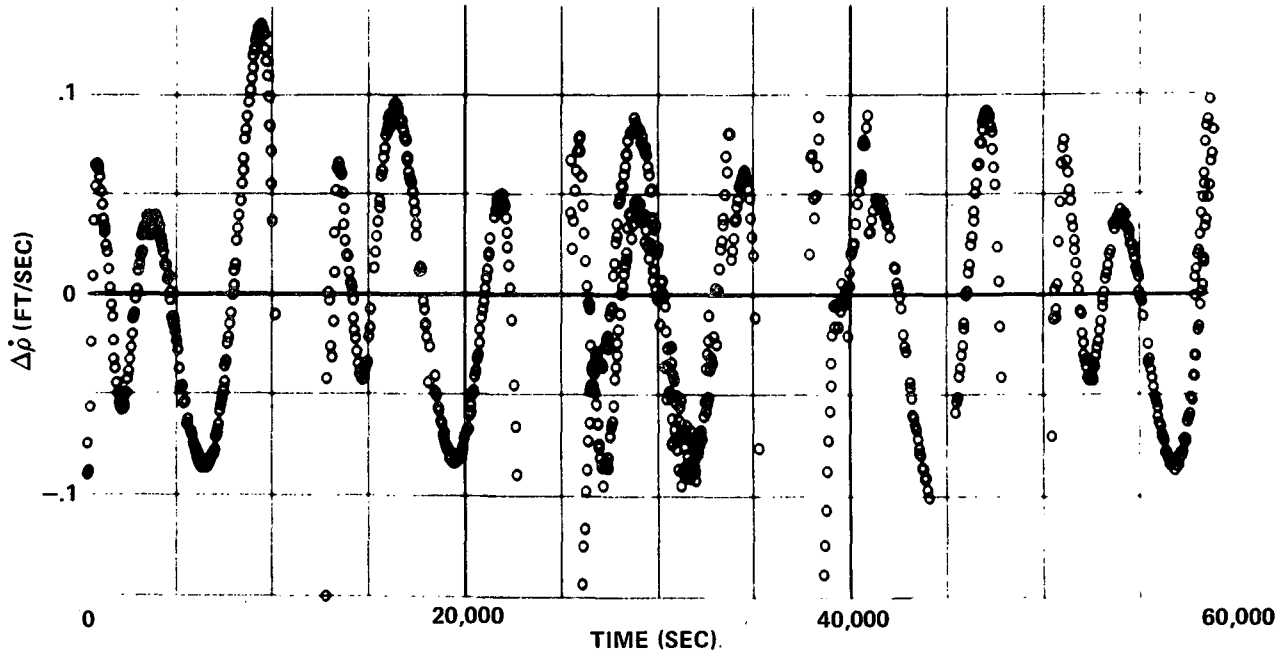

LUNAR ORBITER III DOPPLER RESIDUALS

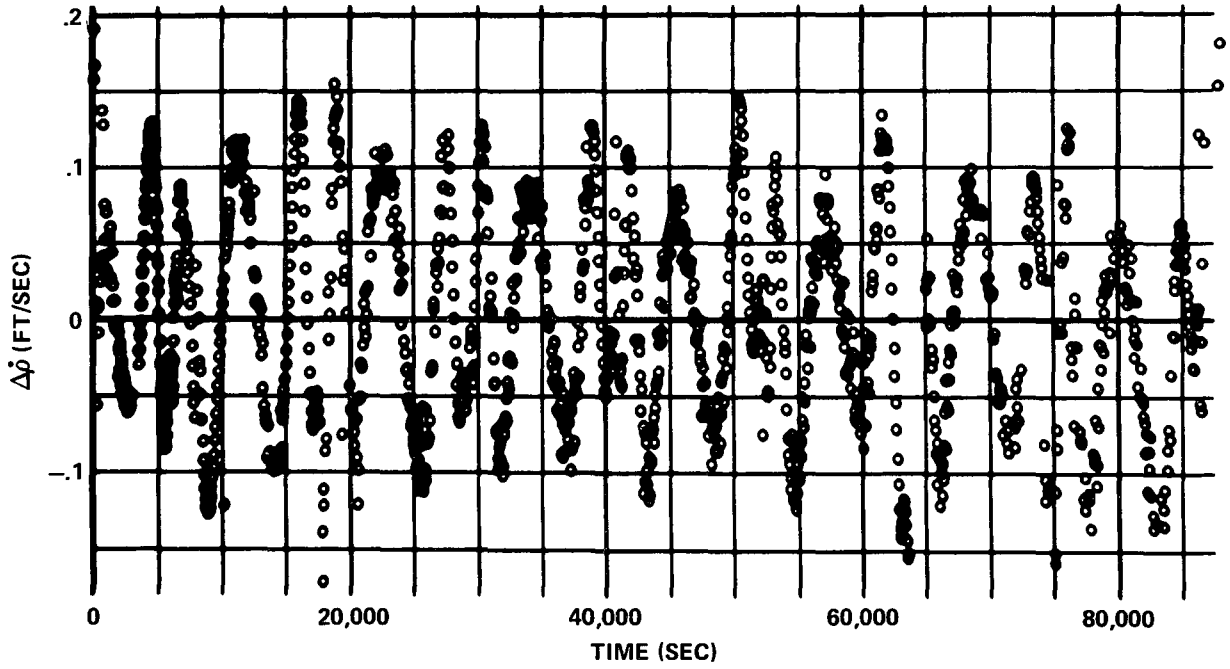

LUNAR ORBITER V DOPPLER RESIDUALS

FIGURE 37

peak amplitude. Each of these residual plots also possesses points of irregularly large amplitude relative to the remainder of the span. These irregularities in the residuals most likely correspond to low thrust attitude control maneuvers performed by the spacecraft.

An analysis of the $[H^T WH]^{-1}$ matrix for each of these solutions shows that many of the Keplerian parameters are extremely highly correlated. Table VI presents a summary of the highest correlations for each of these four convergences.

TABLE VI SOLUTION CORRELATIONS

SATELLITE	PARAMETER PAIR	CORRELATION COEF.
ORBITER I	Ω_o, ω_o	-.9999
	Ω_1, ω_1	.9999
ORBITER II	I_o, Ω_o	-.9908
	Ω_o, ω_o	-.9998
	Ω_1, ω_1	-.9995
ORBITER III	I_o, Ω_o	-.9938
	I_o, ω_o	-.9946
	Ω_o, ω_o	-.9998
	Ω_1, ω_1	-.9985
ORBITER V	I_o, Ω_o	.9948
	I_o, ω_o	-.9903
	Ω_o, ω_o	-.9843
	Ω_1, I_1,	.9948

These correlations represent the largest found in each $[H^T WH]^{-1}$ matrix. There were other correlations present of large magnitude ($\rho = |.9|$). For the case of each Lunar Orbiter

satellite presented almost the identical correlation pairs reoccur. These correlations reflect the basic difficulty of using Doppler measurements at lunar distances to separate the dynamical properties of the Euler angles of the orbit. It should be noted that this situation is particularly amplified for the case of the Lunar Orbiters since in most cases the satellite was only tracked by one earth-based station, thus losing the geometrical enhancement of a second or third tracker.

The thirty data arcs used for orbit determination solutions contributed one hundred ninety-nine sets of states and rates for lunar gravity determination. The factors used in defining the degree and order of the lunar field to be determined from these sets of Keplerian rates and elements will now be discussed.

A PRIORI COEFFICIENT SELECTION

The work of Muller and Sjogren[33] has provided conclusive evidence that rather large near-surface mass concentrations ("mascons") are present in the near-side lunar maria regions. The existence of these non-central mass concentrations has a significant impact on the application of Equation (2.20) for describing lunar gravity. Accurately representing a "mascon" moon would require spherical harmonic coefficients of high order and degree. In mathematical terminology, the presence of "mascons" causes the convergence rate of (2.20) to be very slow.

In theory then the proper approach to modeling the lunar gravity field is to seek a spherical harmonic coefficient set large enough in degree and order to represent all the non-central lunar features. In practice however, due to the

incomplete Doppler data set and due to a lack of far side Doppler measurements, lunar gravity solutions involving large numbers of harmonic coefficients have high correlations in the $[F^TAF]^{-1}$ matrix and in general have poor overall numerical characteristics.

Analyses were made using the harmonic estimating program with pseudo data input from numerically integrated long-period perturbation equations (assuming a nominal seventh degree and order field). Long-period trajectories for each of the Lunar Orbiter missions were simulated. When a solution set of degree and order seven or larger was sought, the nominal values of the field (as could be expected) were recovered with good accuracy. An analysis of the correlations in the $[F^TAF]^{-1}$ matrices for these solutions (for Lunar Orbiter tracking coverage) showed that a great many harmonic coefficient pairs (C_{20} & C_{40}, C_{30} & C_{50} etc) were very highly correlated. This correlation is totally a consequence of the incomplete data set used. When subset gravity solutions (for example a complete fifth degree and order field) were sought from the Keplerian rate data generated from the seventh degree and order field, the numerical values obtained were very different from their nominal values. Basically, the higher degree harmonics which had been omitted from the solution set were aliased into the lower ones due to the existing large correlations. Had a complete data set (data covering all latitudes and longitudes) been used, then orthogonality would be induced in the $[F^TAF]^{-1}$ matrix and the subset values recovered would be the nominal ones. Since the

spherical harmonic expansion (2.20) is essentially a three dimensional Fourier series in spherical coordinates, this orthogonality can only be achieved when:[34]

$$\int_{\text{sphere}} Y_{\ell m}\, Y_{hk}\, d\sigma = \begin{cases} 0 & \text{if } \ell \neq h \text{ or } m \neq k \\ \dfrac{4\pi\,(\ell+m)!}{(1-m)!\,(2\ell+1)\,(2-\delta_{om})} & \text{for } \ell = h \text{ and } m = k \end{cases} \tag{5.1}$$

where: $Y_{\ell m}(\phi,\lambda) = P_{\ell}^{m}(\sin\phi)\,[C_{\ell m} \cos m\lambda + S_{\ell m} \sin m\lambda]$

and where the Kronecker delta δ_{om} is equal to 1 for $m=0$ and 0 for $m\neq 0$.

This discussion of the "mascons" and the lack of orthogonality associated with the existing Doppler data is introduced as background for the rational process used in choosing a harmonic coefficient solution set. The basic strategy assumed in this analysis is to obtain the largest coefficient set possible while incurring a minimum of high correlations in the $[F^{T}AF]^{-1}$ matrix. It is a foregone conclusion that, with the data available at this time, it is not possible to determine a lunar gravity field which truly represents all the localized fine structure near-surface mass inhomogeneities. The only attainable goal of this data analysis then is to derive a more accurate global lunar gravity model.

A LUNAR GRAVITY FIELD

Solutions varying from degree and order three to degree and order seven were attempted from the one hundred ninty-nine sets of Kepler element rates. All solutions obtained above degree and order four contained very large numbers of parameter correlations in the solution $[F^TAF]^{-1}$ matrices. When these solutions were applied to the tracking data from the Apollo orbits, both the fit and prediction characteristics obtained were very poor. As a result of this situation, the lunar harmonic coefficient set determined in this study is of order and degree four.

Analysis of the numerical characteristics of the full fourth degree and order solution revealed two important points. First, the C_{20} and C_{40} zonal coefficients were still highly correlated (ρ = .86). Second, the solution contained very little direct information in determining the C_{22} harmonic. In performing the least-squares gravity estimation, the entry in the $F^TA\dot{\bar{k}}$ vector associated with C_{22} was essentially zero (other components were of significantly larger magnitudes). Hence the estimate of C_{22} was dominated by correlations present in the $[F^TAF]^{-1}$ matrix.

In order to circumvent these numerical problems, both the C_{20} and C_{22} terms were fixed in the gravity determination to values obtained by Koziel[35] in studying the physical librations of the moon. The values used are the following:

$$\left.\begin{aligned} C_{20} &= -.2056 \times 10^{-3} \\ C_{22} &= \ .2258 \times 10^{-4} \end{aligned}\right\} \qquad (5.2)$$

The fourth order and degree field lunar gravity field (with C_{20} and C_{22} fixed) is given in Table VII. The correlation matrix associated with this solution is given in Table VIII. As in the pseudo data analysis previously presented, this gravity estimation process is subject to systematic errors and biases. Hence the diagonal terms of the $[F^TAF]^{-1}$ matrix cannot be regarded as variances of the estimated terms.

The residuals associated with each of the five element rates and this fourth order field are shown in Figures 38-40. These residuals have the statistical properties listed in Table IX.

TABLE VII

GRAVITATIONAL FIELD DETERMINED FROM LUNAR ORBITERS I, II, III, AND V

ℓ	m	$C_{\ell m} \times 10^4$	$S_{\ell m} \times 10^4$
2	0	-2.0560*	---
	1	.0537	.0617
	2	.2258*	-.0017
3	0	.2216	---
	1	.3575	.0820
	2	.0210	.0340
	3	.0301	.0055
4	0	.0543	---
	1	-.0677	.1195
	2	.0443	.0106
	3	.0136	.0066
	4	.0027	.0043

*Fixed in solution.

TABLE VIII

GRAVITY SOLUTION CORRELATION MATRIX

	C_{30}	C_{31}	C_{32}	C_{33}	C_{40}	C_{41}	C_{42}	C_{43}	C_{44}	S_{21}	S_{22}	S_{31}	S_{32}	S_{33}	S_{41}	S_{42}	S_{43}	S_{44}
C_{21}	-.02	.06	-.11	.11	.25	.59	-.69	.41	-.14	.18	.15	.03	.43	-.08	.3	-.21	.05	.25
C_{30}		-.09	-.08	.01	-.39	.17	.08	.01	-.03	.04	.05	-.05	.19	-.01	-.05	.06	.01	.07
C_{31}			-.03	.04	-.34	.18	-.1	.05	.05	.33	-.08	.06	.17	-.05	.56	.01	.29	.002
C_{32}				.06	.01	-.13	.22	.01	.09	-.18	.33	-.01	-.15	-.04	-.2	.81	.23	.13
C_{33}					.03	.07	-.01	-.01	.28	.04	-.18	.001	-.02	-.06	.08	.02	.39	.43
C_{40}						.06	-.11	.21	-.08	-.12	.07	.01	-.35	-.02	-.03	-.24	-.15	.02
C_{41}							-.53	.43	-.13	.38	.04	-.64	.4	-.06	.34	-.11	.17	.15
C_{42}								-.07	.3	-.15	-.18	.11	-.66	.12	-.20	.19	.07	-.11
C_{43}									-.26	.21	.01	-.16	-.15	-.34	.36	-.22	-.01	.04
C_{44}										-.15	-.13	.02	-.16	-.4	-.22	.21	.21	.09
S_{21}											-.23	-.13	.18	.09	.84	-.25	.4	.05
S_{22}												.04	.09	.16	-.18	-.14	-.12	.33
S_{31}													-.06	.06	.03	-.02	-.08	.02
S_{32}														-.06	.06	.08	.1	.04
S_{33}															.07	.04	.05	.11
S_{41}																-.32	.26	.03
S_{42}																	.24	.21
S_{43}																		-.06

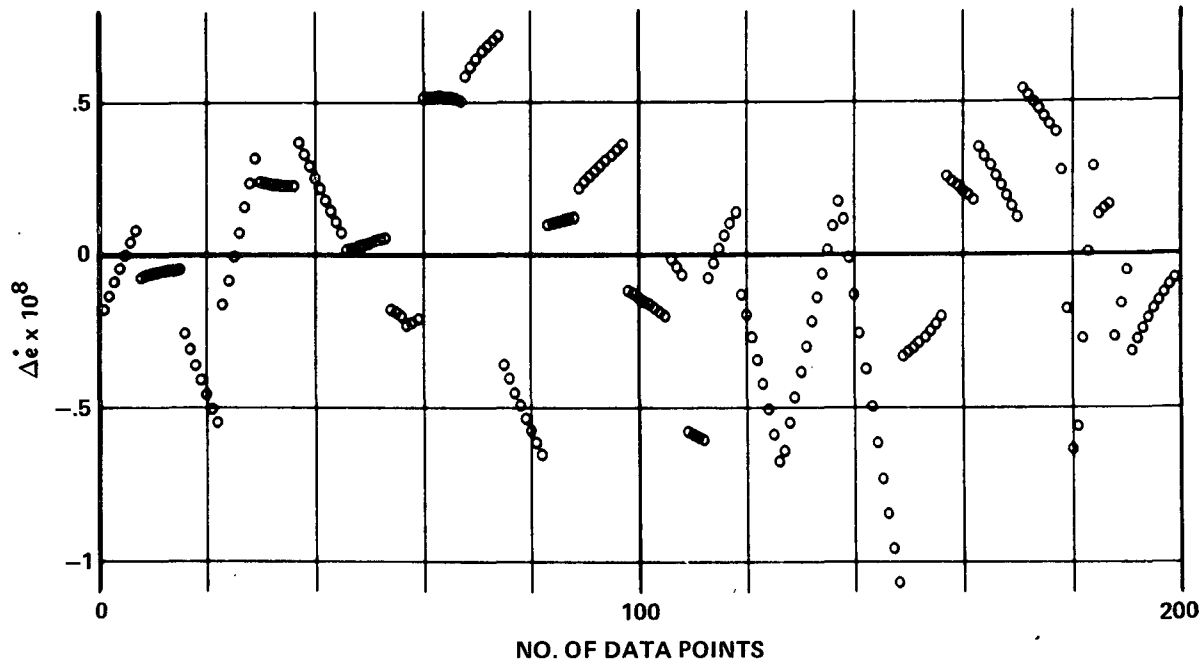

$\Delta\dot{e}$ VS NUMBER OF DATA POINTS

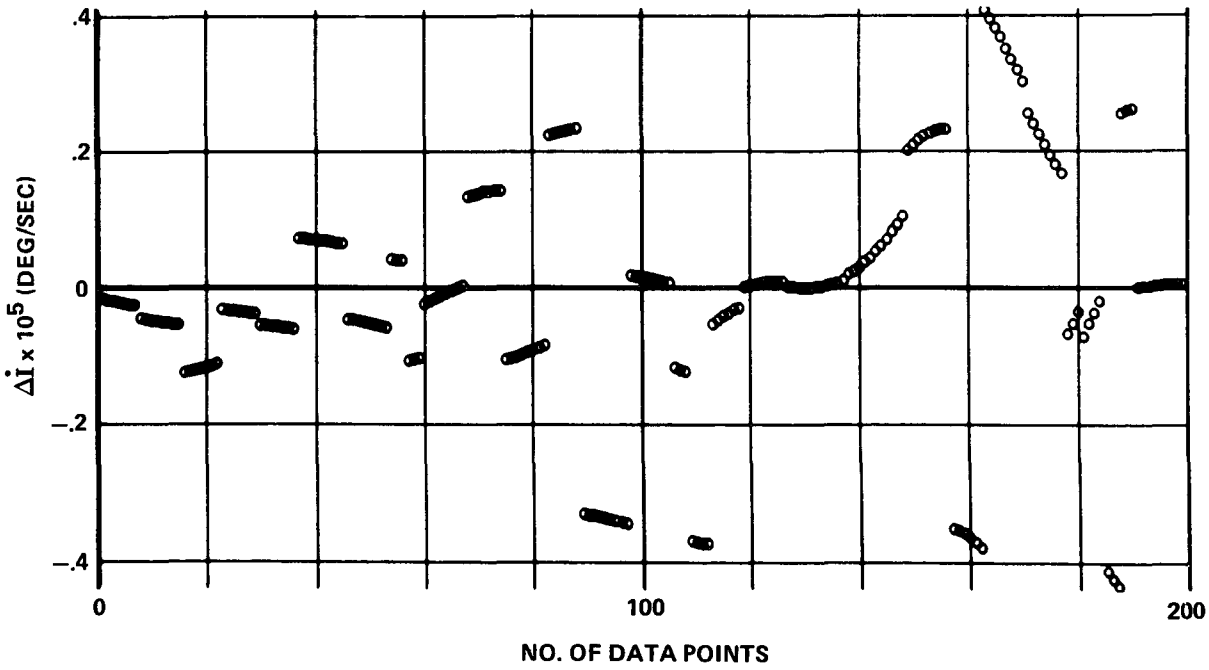

$\Delta\dot{i}$ VS NUMBER OF DATA POINTS

FIGURE 38

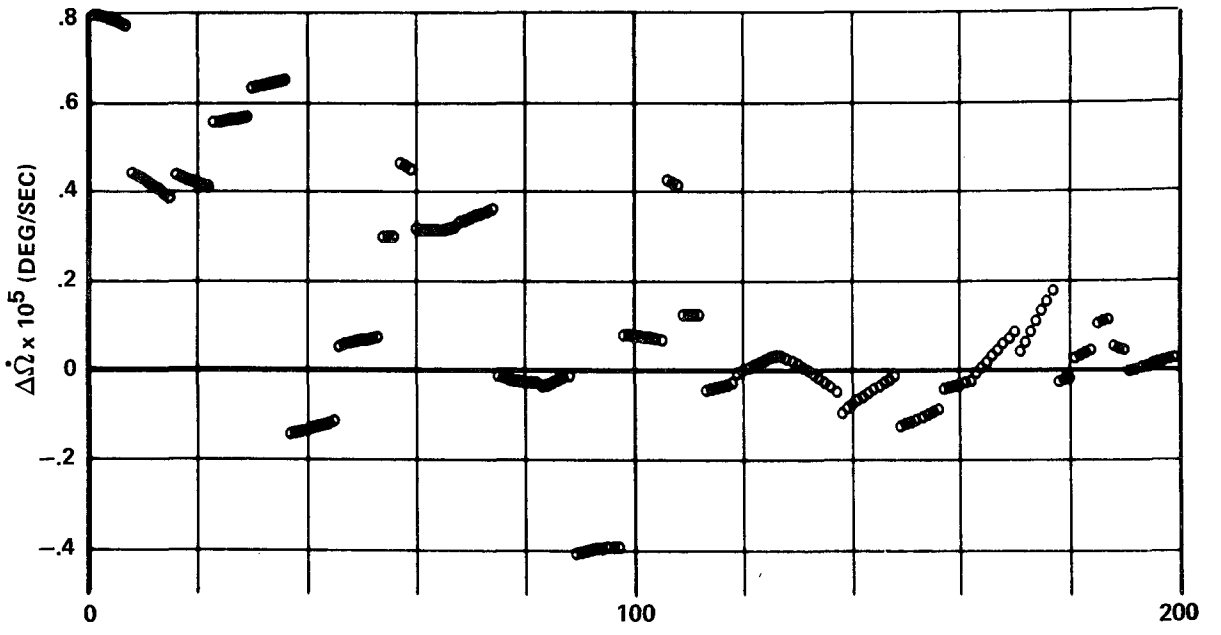

$\Delta\dot{\Omega}$ VS NUMBER OF DATA POINTS

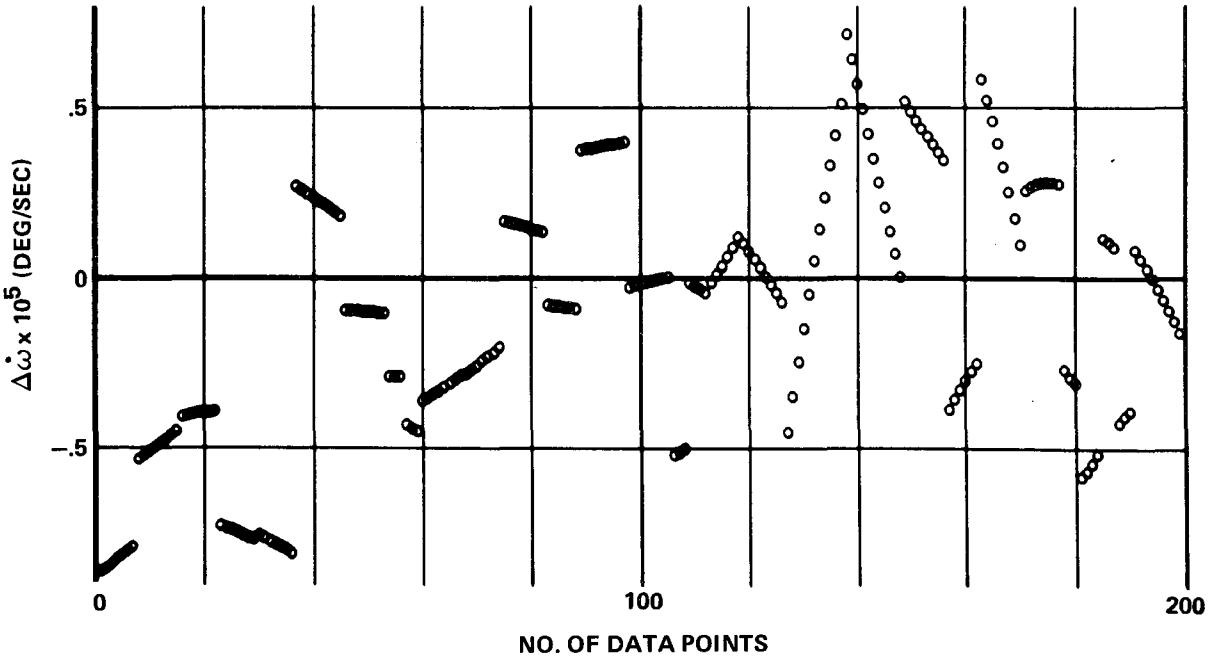

$\Delta\dot{\omega}$ VS NUMBER OF DATA POINTS

FIGURE 39

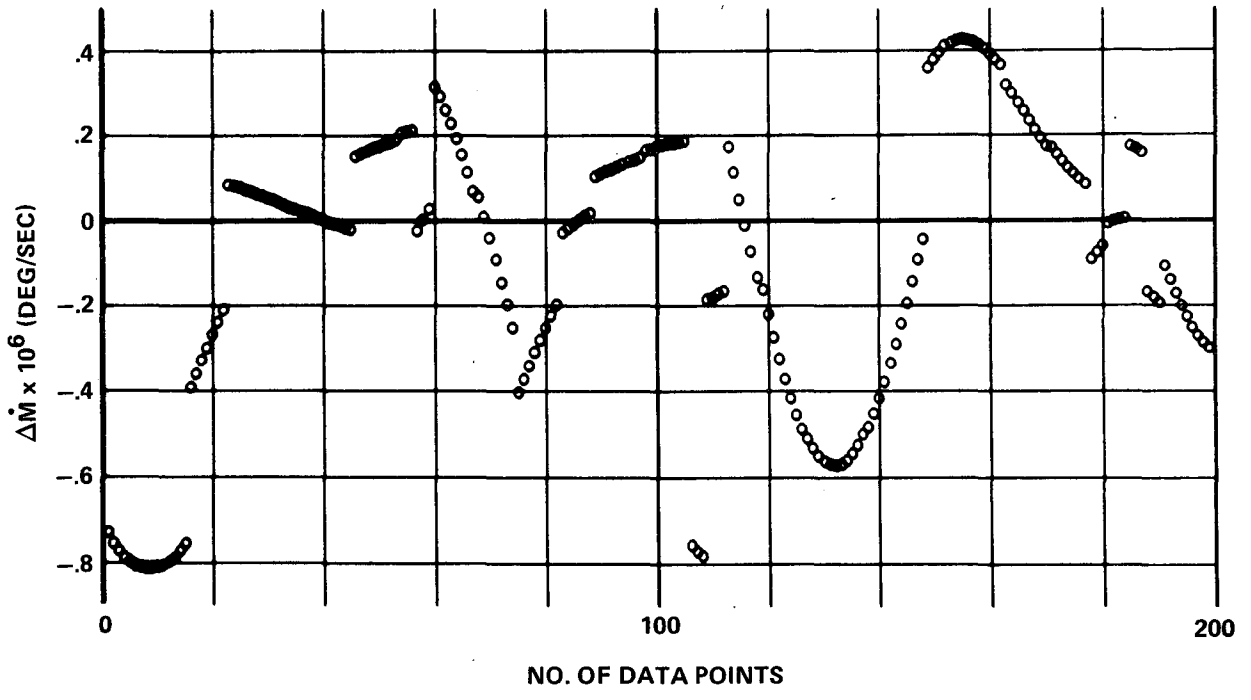

$\Delta\dot{M}$ VS NUMBER OF DATA POINTS

FIGURE 40

TABLE IX

Kepler Element Rate	Residual Mean	Residual Std. Deviation
$\dot{e}$	$-.272 \times 10^{-9}$	$.345 \times 10^{-8}$
$\dot{I}$	$-.836 \times 10^{-7}$ Deg/Sec	$.170 \times 10^{-5}$ Deg/Sec
$\dot{\Omega}$	$.127 \times 10^{-5}$ Deg/Sec	$.265 \times 10^{-5}$ Deg/Sec
$\dot{\omega}$	$-.965 \times 10^{-6}$ Deg/Sec	$.374 \times 10^{-5}$ Deg/Sec
$\dot{M}$	$-.915 \times 10^{-7}$ Deg/Sec	$.327 \times 10^{-6}$ Deg/Sec

As can be seen from the Kepler element rate residual plots, the errors are systematic in each case.

Equipotential surfaces have been calculated for this lunar gravity field and are shown in Figures 41 and 42. These surfaces are computed by finding the radial deviations to a spherical potential (generated with the field point at the mean lunar radius). The variations are quantized in thousand foot increments. The basic equipotential surfaces of this gravity field are those of a triaxial ellipsoid. The solid line on the surfaces indicates the equipotential line for the reference potential (zero deviation from spherical potential). These surfaces show three large areas of potential excess. The first of these is centered about latitude ϕ = 25°N and longitude λ = 10°E. This region very closely corresponds to the Mare Serenitatis region of the moon. The two other areas of potential excess are located at latitude ϕ = 5°S, longitude λ = 117°E

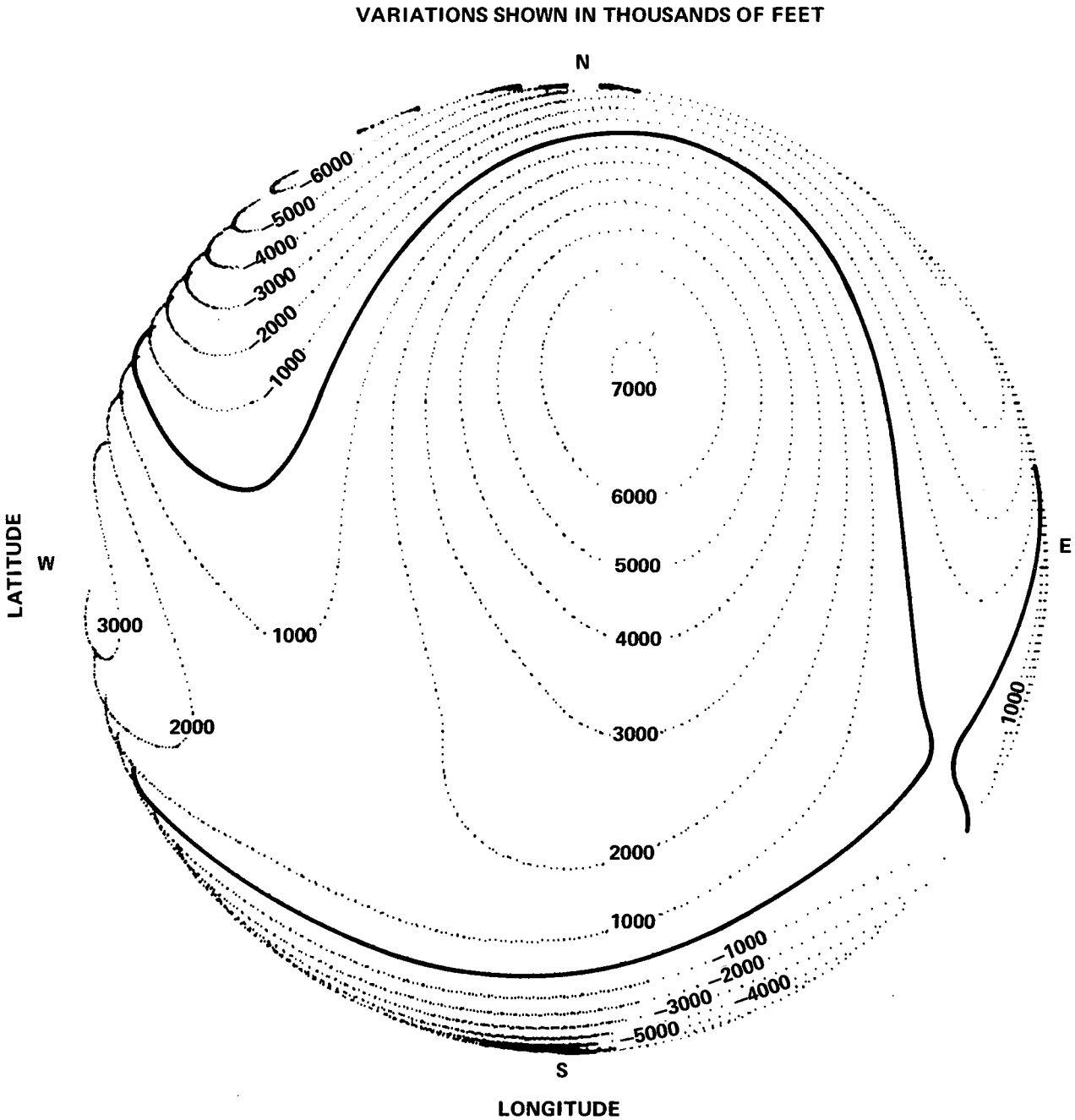

LUNAR NEAR SIDE EQUIPOTENTIAL SURFACES

FIGURE 41

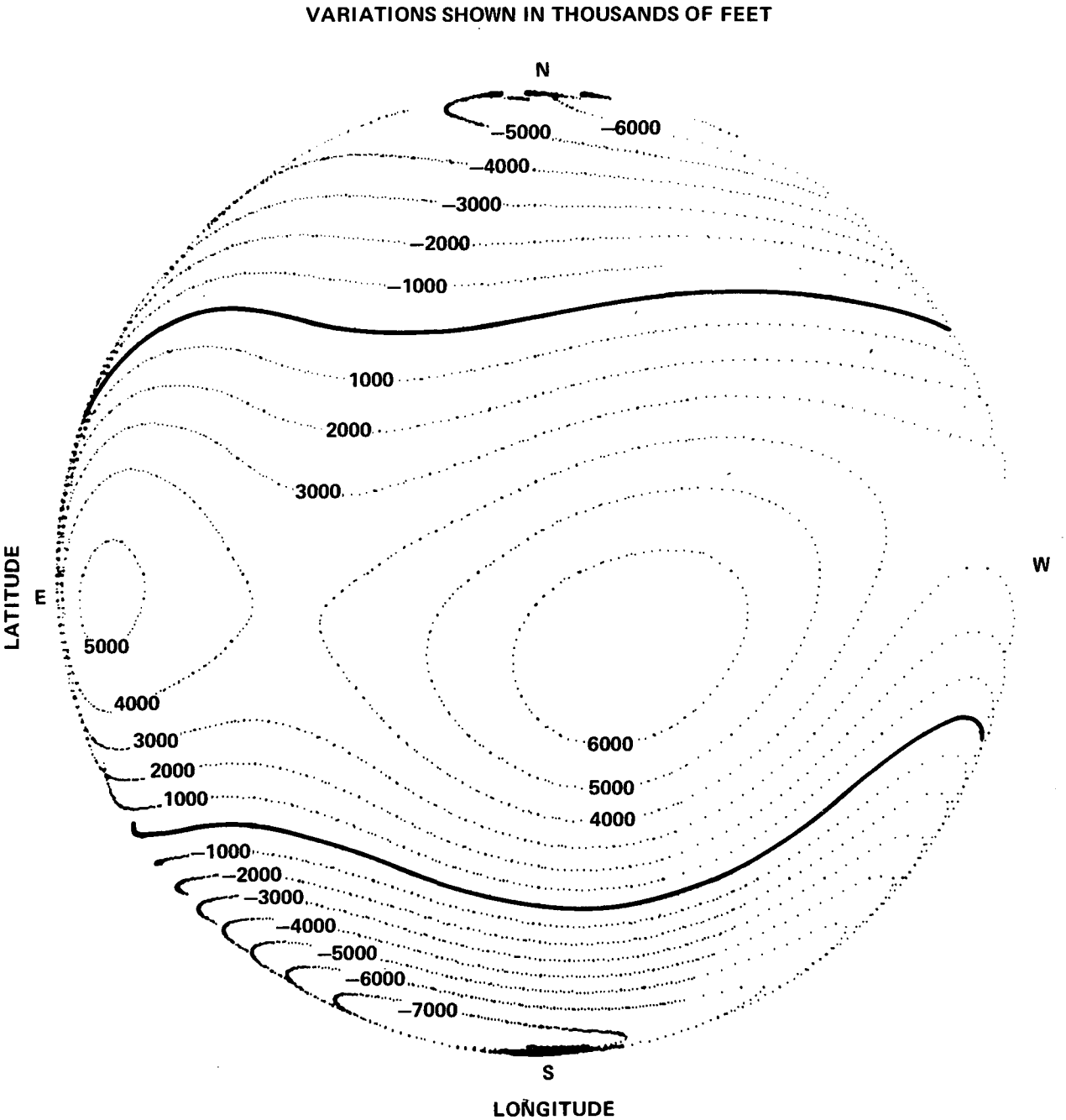

LUNAR FAR SIDE EQUIPOTENTIAL SURFACES

FIGURE 42

and latitude ϕ = 10°S, longitude λ = 170°W respectively. Neither of these two areas corresponds to an identified lunar maria region.

The second-degree harmonics in the potential are directly related to the moments and products of inertia of the moon. The relations between the gravity coefficients and the moments and products of inertia are:[36]

$$\left.\begin{aligned} C_{20} &= \frac{1}{m_{\mathbb{C}} R_e^2}\left[\frac{A+B}{2} - C\right] \qquad C_{22} = \frac{1}{4m_{\mathbb{C}} R_e^2}(B-A) \\ C_{21} &= \frac{E}{m_{\mathbb{C}} R_e^2} \qquad S_{21} = \frac{D}{m_{\mathbb{C}} R_e^2} \qquad S_{22} = \frac{F}{m_{\mathbb{C}} R_e^2} \end{aligned}\right\} \tag{5.3}$$

where A, B, C are the three principal moments of inertia ($A = I_{xx}$, $B = I_{yy}$, $C = I_{zz}$) and D, E, F are the products of inertia ($D = I_{yz}$, $E = I_{xz}$, $F = I_{xy}$). Since equation 5.3 contains five equations in six unknowns (A,B,C,D,E,F) one additional relationship is needed. From studies of the lunar physical librations the quantity

$$\beta = \frac{C-A}{B} \tag{5.4}$$

has been determined. The numerical value used is that computed by Koziel[37] from heliometer observations ($\beta = 6.294 \times 10^{-4}$). Hence given the five second degree harmonics and β, the following set of principal moments and products of inertia are found:

$$A = .3983208\ m_{\mathbb{C}} R_e^2 \qquad D = .617 \times 10^{-5}\ m_{\mathbb{C}} R_e^2$$
$$B = .39841118\ m_{\mathbb{C}} R_e^2 \qquad E = .537 \times 10^{-5}\ m_{\mathbb{C}} R_e^2$$
$$C = .39857195\ m_{\mathbb{C}} R_e^2 \qquad F = -.17 \times 10^{-6}\ m_{\mathbb{C}} R_e^2$$

The imprecision in the harmonics and the simplifications in the theory relating β to the inertias make the quality of these numbers somewhat poor.

EXTRAPOLATIONS

In order to measure the orbit determination and prediction qualities of the field obtained, it was applied to Doppler data not used in its generation. Specifically, the data used was acquired during the orbits of the Apollo 11, 12, and 14 missions (Apollo 15 data is not available at this time). The orbit determinations were performed using a standard least-squares processor which obtains a best estimate of a rectangular state vector at some epoch.

$$\hat{\bar{x}}_o = [H^T\ WH]^{-1}\ H^T\ W\ \overline{\Delta\dot{\rho}} \tag{5.5}$$

This process is identical to that given by (3.31) with the exception that $\hat{\bar{x}}_o$ is a six vector of position and velocity and the H matrix contains the partial derivatives of the Doppler with respect to the rectangular state at epoch. This best estimate of the state is then used to predict the Doppler outside the span of data used for the convergence.

Orbit determination solutions were obtained by fitting one front side pass of Doppler data from several stations. This

particular data length was chosen since it puts maximum stress on the orbital period prediction capability of the model. Once a converged solution is obtained, the Doppler data is predicted for the next three orbital periods to test the extrapolation capabilities of the model.

The data used from the Apollo 11 and 12 flights are from near-circular orbits with radius vectors of about 60 nautical miles (n.m.) above the lunar surface. The Apollo 14 data is from a slightly elliptical orbit (e = .0258) with an apolune of 60 n.m. above the surface and a perilune of 8 n.m. above the surface. The data from the Apollo missions, since they are collected from orbits very near the lunar surface, reveal many gravitational perturbations not present in the Lunar Orbiter data.

Converged solutions were obtained using the fourth degree and order gravity field. Doppler residuals for both the one pass fit and three passes of prediction for each of these Apollo orbits are shown in Figure 43. The Doppler residuals in each of these convergences are still systematic and an order of magnitude above the noise level of the data. The three orbital period prediction is characterized by a secular growth (period errors) in the residuals for each case. Both the systematic nature of the regressed Doppler and the growth in Doppler residuals during prediction reflect the incomplete nature of this fourth order field.

In order to obtain a relative perspective on the quality of orbit determination and prediction attainable,

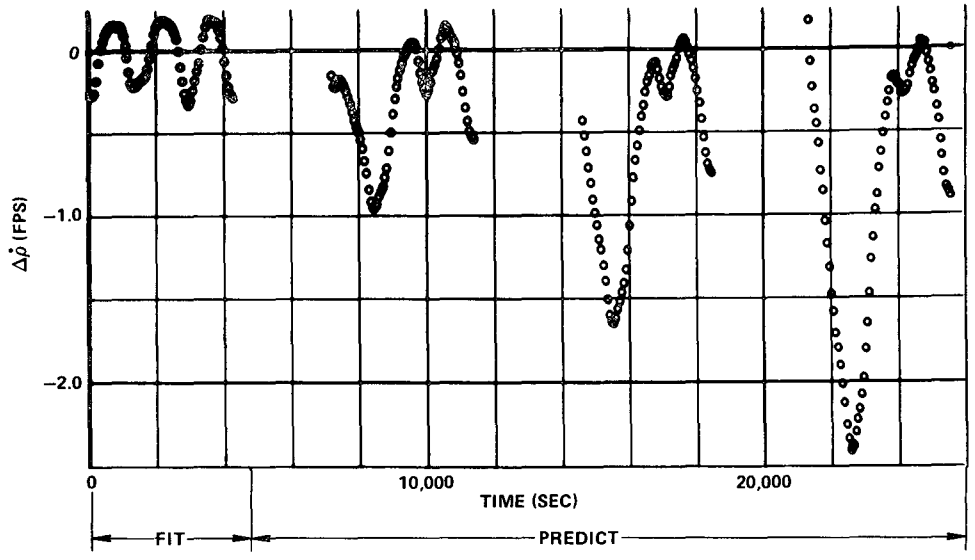

APOLLO 11 DOPPLER RESIDUALS

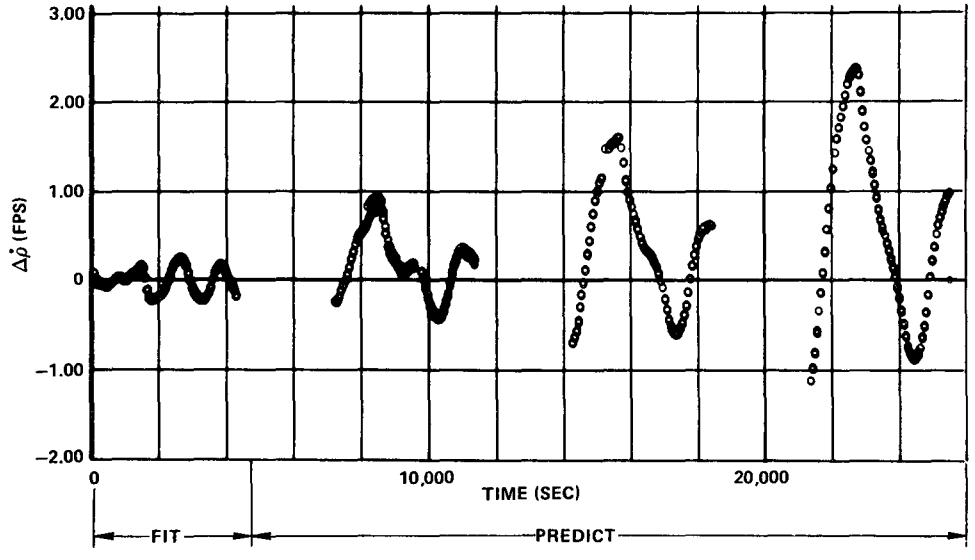

APOLLO 12 DOPPLER RESIDUALS

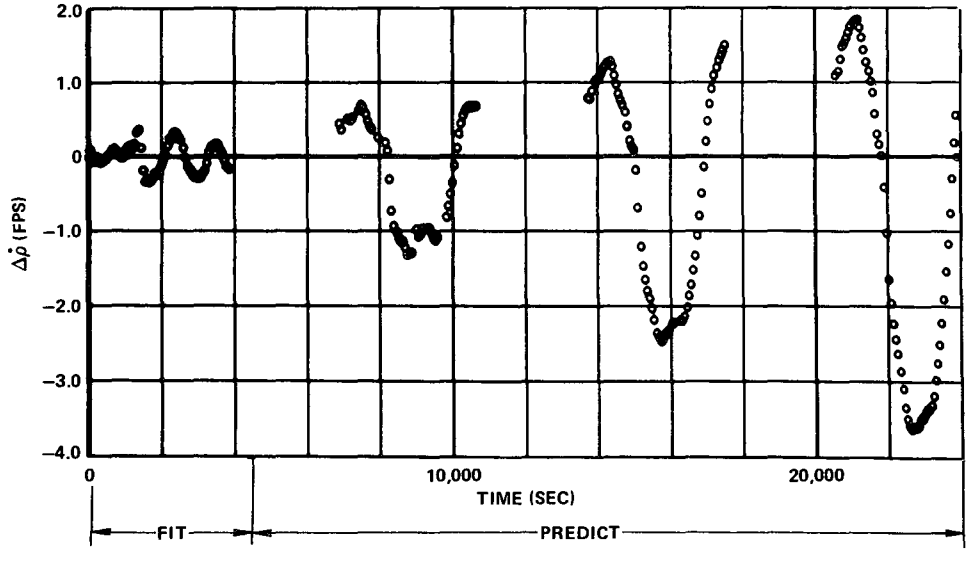

APOLLO 14 DOPPLER RESIDUALS

FIGURE 43 - FOURTH DEGREE AND ORDER LUNAR GRAVITY FIELD

convergences were also performed on these data using two other gravity models. The first model, the L1 field (see Table II), is used by the Manned Spacecraft Center for Apollo mission planning. The second model, developed by Liu and Laing,[38] is a fifteenth degree zonal and eighth order tesseral model (84 harmonics). This model represents the latest result from the indirect (long-period) analysis method.

The orbit determinations were again performed by fitting one pass of data and predicting the Doppler for the next three periods. The residuals associated with each of the fit and predictions for these two gravity fields are shown in Figures 44 and 45. Again both the Doppler residuals for the fit and prediction, for each field, have systematic errors. Both of these models, especially the fifteenth degree field, are characterized by secular growth in Doppler residuals of the prediction. Table X lists the statistical properties of the one pass Doppler residuals for all three models.

TABLE X

ORBIT	MODEL	RESIDUAL MEAN (FPS)	STD. DEVIATION (FPS)
Apollo 11	4 × 4*	-.011	.166
	L1	-.0015	.039
	15 × 8†	-.023	.463
Apollo 12	4 × 4	-.0029	.136
	L1	-.0042	.104
	15 × 8	-.022	.353
Apollo 14	4 × 4	-.0016	.187
	L1	-.0055	.159
	15 × 8	-.0304	.526

*Fourth degree and order model
†Fifteenth degree and eigth order model

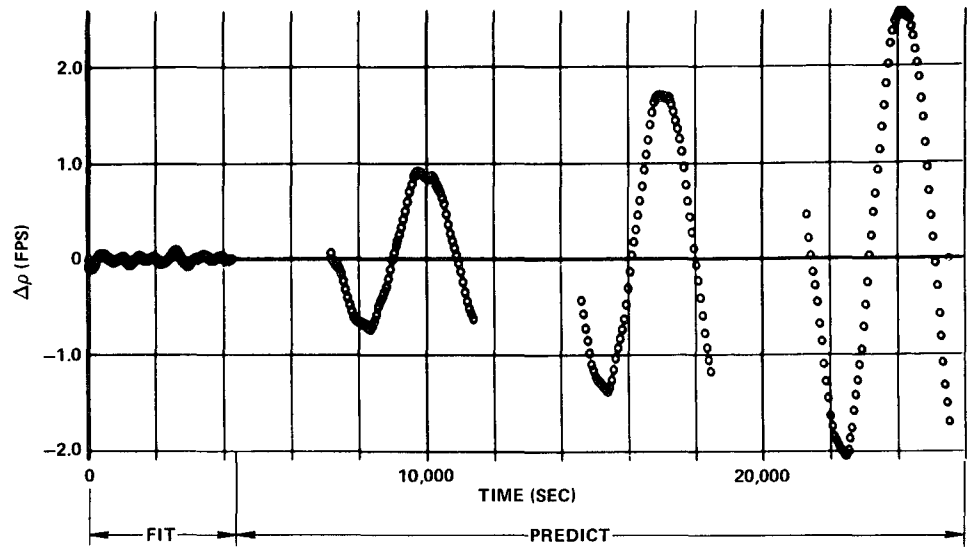

APOLLO 11 DOPPLER RESIDUALS

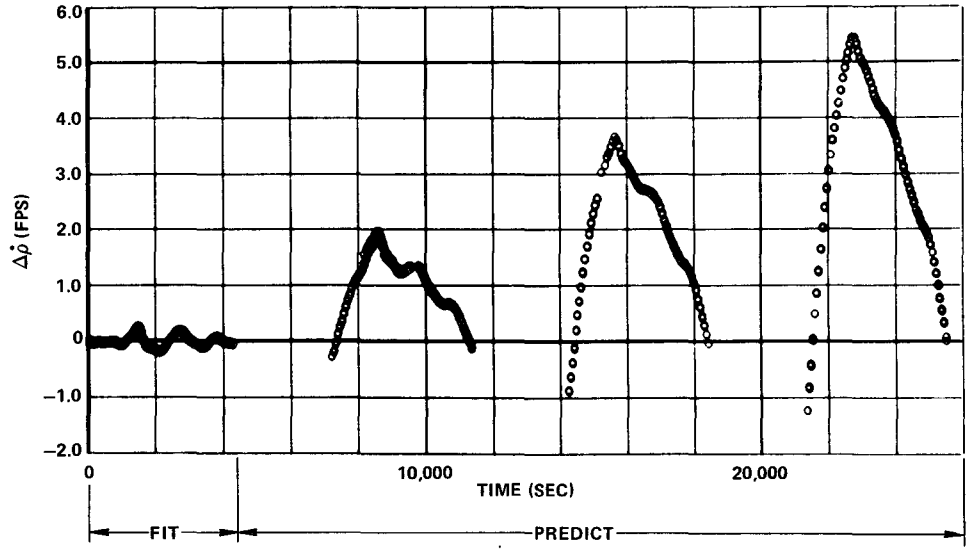

APOLLO 12 DOPPLER RESIDUALS

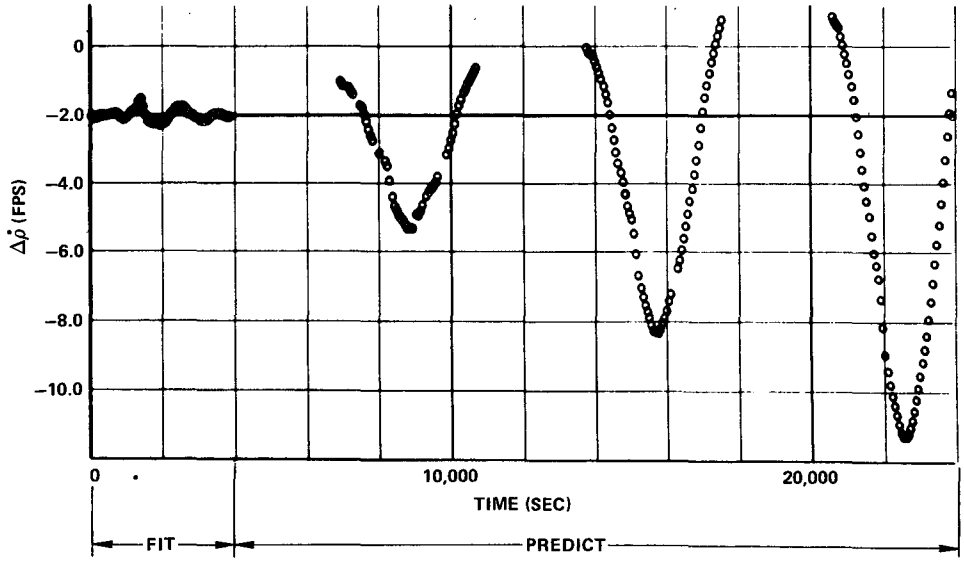

APOLLO 14 DOPPLER RESIDUALS

FIGURE 44 - L1 LUNAR GRAVITY FIELD

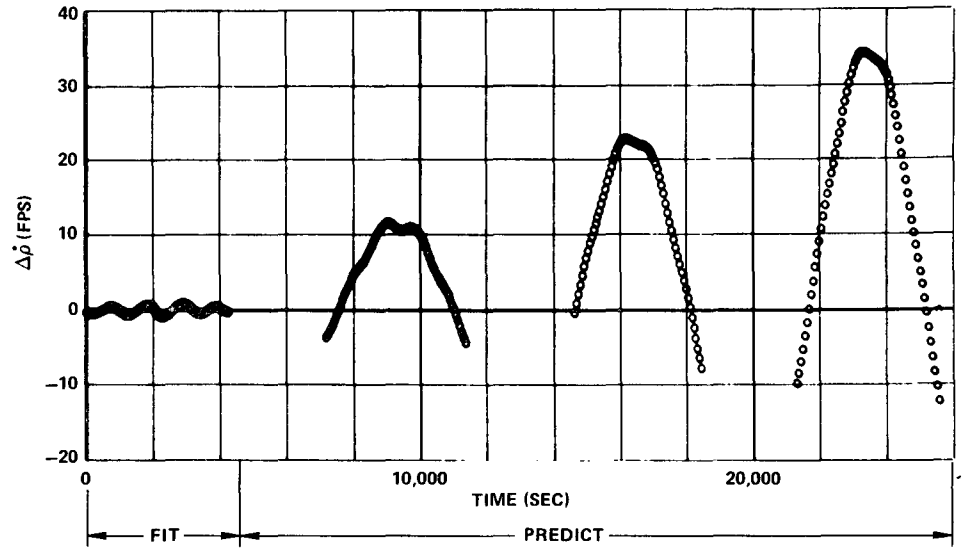

APOLLO 11 DOPPLER RESIDUALS

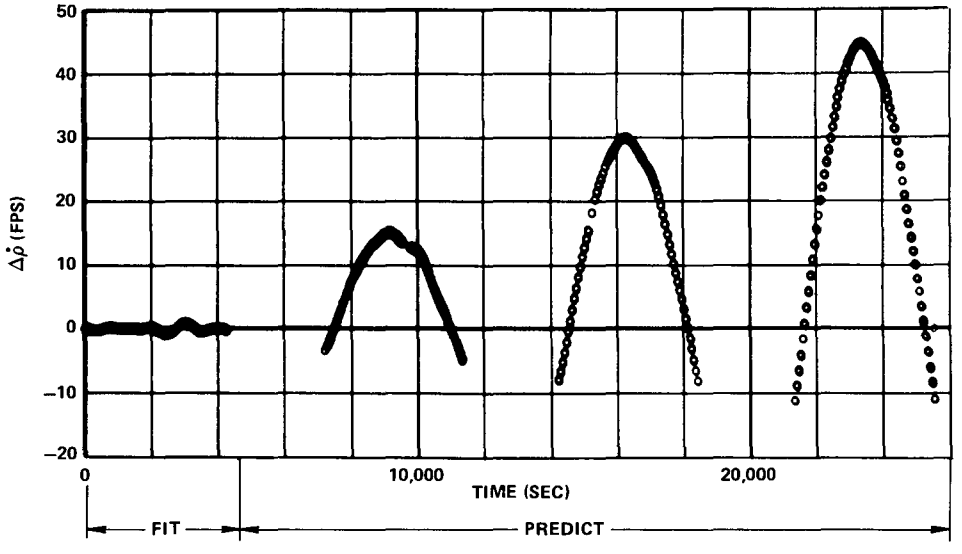

APOLLO 12 DOPPLER RESIDUALS

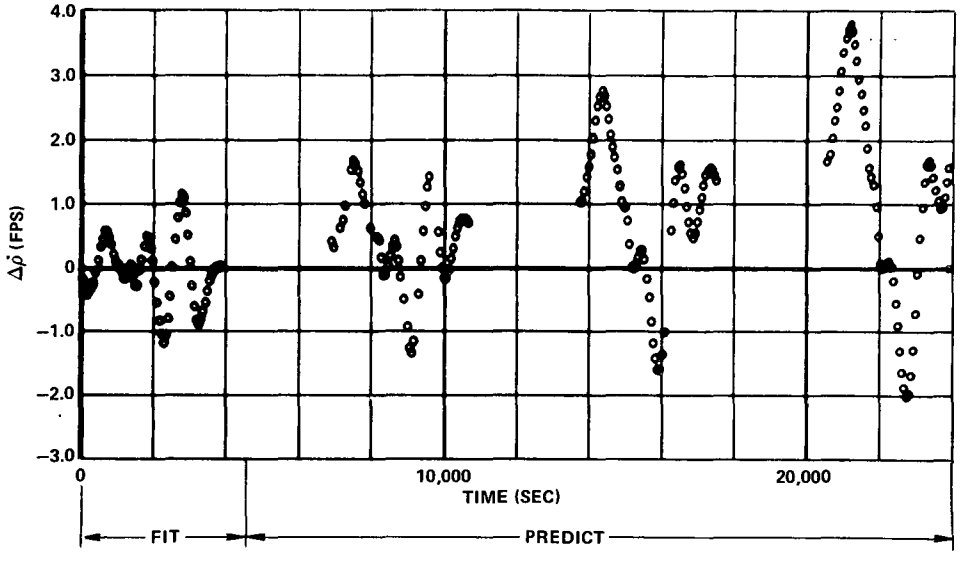

APOLLO 14 DOPPLER RESIDUALS

FIGURE 45 - FIFTEENTH DEGREE EIGHTH ORDER LUNAR GRAVITY FIELD

For these Apollo orbits, the L1 field achieves slightly better convergence statistics than the fourth degree field. However, the fourth degree field predicts the Doppler with an error rate of about 50% less than L1. Of the three fields compared, the fourth degree field most accurately describes the orbital variations arising from the non-central features of the moon.

CHAPTER VI

SUMMARY AND CONCLUSIONS

This study has presented an empirical method for determining the spherical harmonic coefficients of the lunar gravity field. This method uses a two-step data reduction and estimation process. In the first step, a weighted least-squares empirical orbit determination process is applied to Doppler tracking data to estimate long-period Kepler orbital elements and rates. Each of the Kepler elements is represented by an independent time function. The long-period perturbing effects of the earth, sun, and solar radiation are modeled explicitly in this orbit determination process. Kepler element variations estimated by the process are ascribed to non-central lunar gravitational features. Doppler data are reduced in this manner for as many orbits as are available. In the second step, lunar gravity coefficients are determined using another weighted least-squares processor which fits the long-period Lagrange perturbation equations to the estimated Keplerian rates.

Pseudo Doppler data have been generated simulating two different lunar trajectories. The perturbations included were triaxial lunar gravity harmonics, the earth, sun, and solar radiation pressure. Orbit determinations were performed using the empirical processor and the long-period orbital element variations obtained. The Kepler element rates from these convergences were used to recover the triaxial lunar gravity coefficients. The overall results of this controlled

experiment show that lunar gravity coefficients can be accurately determined and that the method as a whole is dynamically consistent. The pseudo data analysis shows the necessity of having Doppler data from different orbital inclinations for good selenodesy results.

The method has been applied to Doppler data from the Lunar Orbiter I, II, III, and V missions. One hundred ninety-nine sets of Kepler element rates were obtained for lunar gravity field determination. A gravity field of degree and order four is derived from these Kepler element rates. Equipotential surfaces from this gravity field show the lunar mass distribution to be that of a triaxial ellipsoid with three large areas of mass concentration. The largest and by far the most dominant of these areas is centered very near the Mare Serenitatis region and covers a large portion of the near side of the moon. The other two regions of mass concentration are located on the far side of the moon but do not correspond to any specific mare region.

This gravity field has been investigated using data from several of the Apollo missions. Orbit determination solutions (using a standard least-squares processor) from these data show that this fourth degree field results in improved orbit predictions as compared to those using other lunar gravity fields. All solutions indicate the lunar field models are still incomplete.

There are three major areas of this investigation which are original. The first is the development and application of an empirical orbit determination method for lunar orbits. The second is the derivation of a selenodesy method based on empirically determined Kepler element rates. The third is the generation of a fourth degree and order lunar gravity field (presented in this study) from Lunar Orbiter data using this method. This is the only indirect type selenodesy method that truly estimates long-period orbital element variations.

This study demonstrates the necessity of obtaining more tracking data from lunar satellites at different orbital inclinations (specifically in the I = 26° to 85° gap). Only when this has been accomplished will correlations diminish between the various spherical harmonic coefficients and then an accurate gravity field will be determined.

It is recommended that a version of this method which is determinate for both near-circular and near-equatorial orbits orbits be applied to Doppler tracking data from the Apollo 15 Sub-satellite and any future lunar orbiters.

APPENDIX A

TRANSFORMATION FROM ORBITAL ELEMENTS TO STATE

The rectangular state components $(\bar{r},\bar{v})$ are found from the orbital elements, $\bar{k}$, using the following set of non-linear relationships:

$$\bar{r} = [R_T]\ \bar{q} \tag{A-1}$$

where the entries to the R_T matrix are:

$$\left.\begin{aligned}
r_{11} &= \cos\Omega\cos\omega - \sin\Omega\cos I\sin\omega \\
r_{12} &= -\cos\Omega\sin\omega - \sin\Omega\cos I\cos\omega \\
r_{13} &= \sin\Omega\sin I \\
r_{21} &= \sin\Omega\cos\omega + \cos\Omega\cos I\sin\omega \\
r_{22} &= -\sin\Omega\sin\omega + \cos\Omega\cos I\cos\omega \\
r_{23} &= -\cos\Omega\sin I \\
r_{31} &= \sin I\sin\omega \\
r_{32} &= \sin I\cos\omega \\
r_{33} &= \cos I
\end{aligned}\right\} \tag{A-2}$$

and:

$$\bar{q} = \begin{bmatrix} a(\cos E - e) \\ a\sqrt{1-e^2}\,\sin E \\ 0 \end{bmatrix} \tag{A-3}$$

The eccentric anomaly, E, used in these equations is found, given M and e, by solving Kepler's equation.

$$E - e \sin E = M \tag{A-4}$$

The velocity is found as follows:

$$\bar{v} = [R_T]\ \dot{\bar{q}} \tag{A-5}$$

where:

$$\dot{\bar{q}} = \begin{bmatrix} -\sin E \\ \sqrt{1-e^2}\cos E \\ 0 \end{bmatrix} \frac{\sqrt{\mu_\oplus / a}}{(1-e\cos E)} \tag{A-6}$$

Hence the state $\bar{x}$ can be found from $\bar{k}$ at any time using A-1 and A-5.

TRANSFORMATION FROM STATE TO ORBITAL ELEMENTS

Given $(\bar{r},\bar{v})$, the orbital elements are obtained as follows:

$$\bar{h} = \bar{r} \times \bar{v} \tag{A-7}$$

$$\Omega = \tan^{-1}\left[h_1 \ / \ -h_2\right] \tag{A-8}$$

$$I = \tan^{-1}\left[\sqrt{h_1^2+h_2^2} \ / \ h_3\right] \tag{A-9}$$

where h_1, h_2, h_3 are the components of $\bar{h}$.

$$\bar{p} = [S]\bar{r} \tag{A-10}$$

where the entries to the S matrix are:

$$\left.\begin{aligned} s_{11} &= \cos \Omega \\ s_{12} &= \sin \Omega \\ s_{13} &= 0 \\ s_{21} &= -\sin \Omega \cos I \\ s_{22} &= \cos \Omega \cos I \\ s_{23} &= \sin I \\ s_{31} &= \sin \Omega \sin I \\ s_{32} &= -\sin I \cos \Omega \\ s_{33} &= \cos I \end{aligned}\right\} \tag{A-11}$$

then:

$$\omega + f = \tan^{-1}\left(p_2 / p_1\right) \tag{A-12}$$

$$\dot{r} = \left[v^2 - h^2 / r^2\right]^{1/2} \tag{A-13}$$

$$a = \frac{r \mu_{\oplus}}{(2\mu_{\oplus} - rv^2)} \tag{A-14}$$

$$e = \sqrt{1 - h^2 / \mu_{\oplus} a} \tag{A-15}$$

$$\cos E = \frac{(a - r)}{ae} \tag{A-16}$$

$$\sin E = \frac{r\dot{r}}{e\sqrt{\mu_{\oplus} a}} \tag{A-17}$$

$$f = \tan^{-1}\left[\frac{\sqrt{1 - e}\sin E}{\cos E - e}\right] \tag{A-18}$$

$$M = E - e \sin E \tag{A-19}$$

APPENDIX B

DOPPLER MODEL EQUATIONS

The Doppler frequency shift data is modeled using the range difference method.[39] The estimated Doppler observable, $\dot{\rho}$, can be computed over some counting interval (typically sixty seconds) τ, using the following set of range equations (see Figure B-1).

$$\bar{\rho}_4 = \bar{r}^* \left(t_r - \frac{\rho_4}{c}\right) - \bar{r}_{sr}\,(t_r) \tag{B-1}$$

$$\bar{\rho}_3 = \bar{r}^* \left(t_r - \frac{\rho_4}{c}\right) - \bar{r}_{st}\left[t_r - \left(\frac{\rho_3 + \rho_4}{c}\right)\right] \tag{B-2}$$

$$\bar{\rho}_2 = \bar{r}^* \left(t_r - \frac{\rho_2}{c} - \tau\right) - \bar{r}_{sr}\,(t_r - \tau) \tag{B-3}$$

$$\bar{\rho}_1 = \bar{r}^* \left(t_r - \frac{\rho_2}{c} - \tau\right) - \bar{r}_{sr}\left[t_r - \tau - \left(\frac{\rho_1 + \rho_2}{c}\right)\right] \tag{B-4}$$

and

$$\bar{r}^* = \bar{r} + \bar{r}_{em} \tag{B-5}$$

where $\bar{r}_{em}$ is the earth-moon distance. $\bar{\rho}_1$, $\bar{\rho}_2$, $\bar{\rho}_3$, $\bar{\rho}_4$ are the topocentric ranges of the satellite, $\bar{r}_{sr}$ and $\bar{r}_{st}$ are the

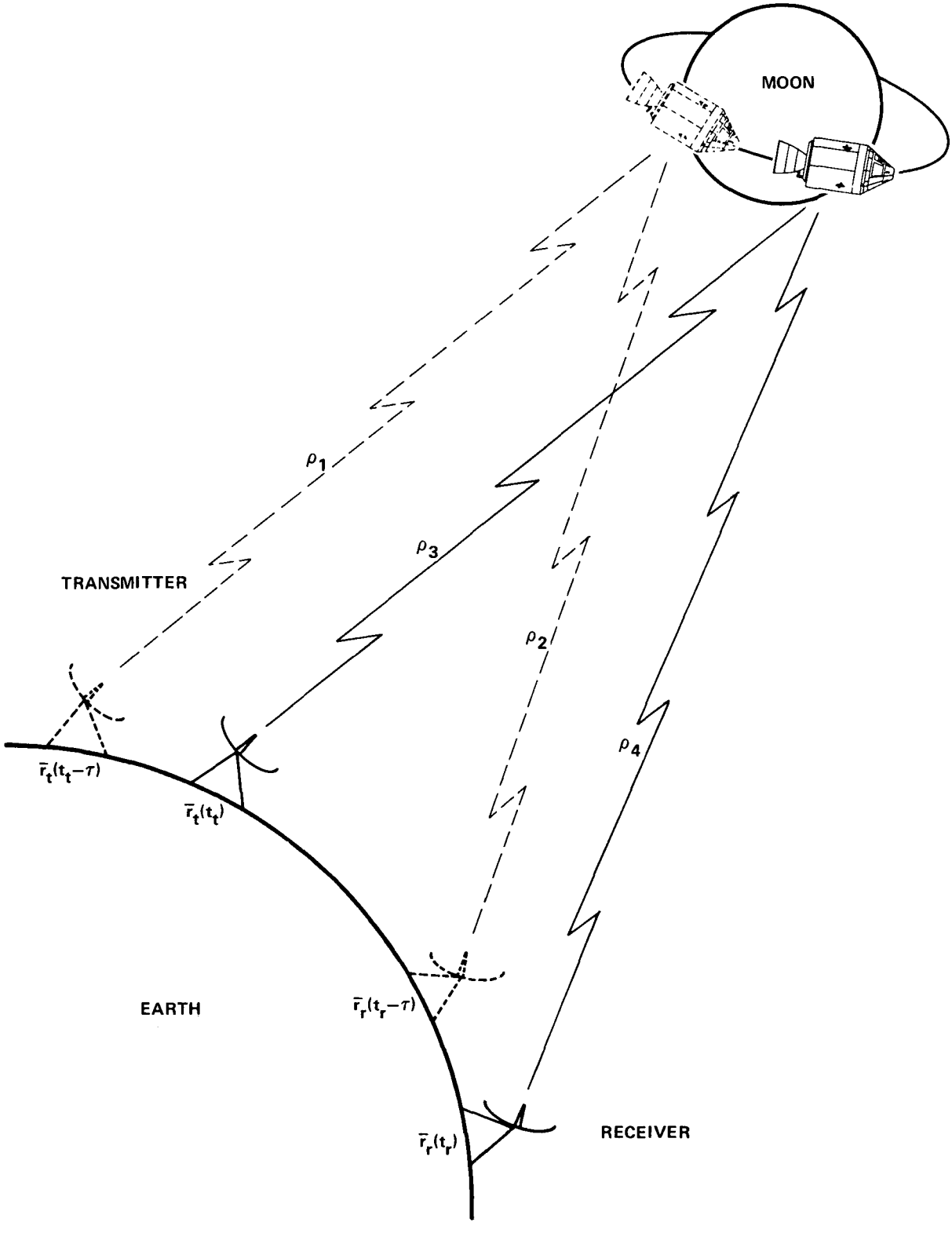

FIGURE B-1 - TRACKING CONFIGURATION

receiving and transmitting station positions in earth centered inertial coordinates, t_r is the Doppler time (at the end of the counting interval) and is the time the signal is acquired by the receiving station, c is the speed of light, and τ is the length of the counting interval.

The equations for these four ranges are solved iteratively. The estimated observable is found as follows:

$$\dot{\rho} = \frac{1}{2\tau} \left[\left(\rho_3 + \rho_4\right) - \left(\rho_1 + \rho_2\right) \right] \qquad \text{(B-6)}$$

where $\dot{\rho}$ is expressed in units of length per time. This value of $\dot{\rho}$ is considered valid at the time $t = t_r - \frac{\tau}{2} - \frac{\rho_4}{c}$.

APPENDIX C

PARTIAL DERIVATIVES

I. PARTIAL DERIVATIVES OF DOPPLER WITH RESPECT TO STATE

The partial derivatives of the Doppler data with respect to satellite position and velocity are:[40]

$$\frac{\partial \dot{\rho}}{\partial \bar{r}} = \frac{1}{2}\left[\frac{\dot{\bar{\rho}}_3}{\rho_3} - \frac{\dot{\rho}_3\,\bar{\rho}_3}{\rho_3^2} + \frac{\dot{\bar{\rho}}_4}{\rho_4} - \frac{\dot{\rho}_4\,\bar{\rho}_4}{\rho_4^2}\right] \tag{C-1}$$

$$\frac{\partial \dot{\rho}}{\partial \bar{v}} = \frac{1}{2}\left[\frac{\bar{\rho}_3}{\rho_3} + \frac{\bar{\rho}_4}{\rho_4}\right] \tag{C-2}$$

In these equations:

$$\bar{\rho}_4 = \bar{r}^*\left(t_r - \frac{\tau}{2} - \frac{\rho_4}{c}\right) - \bar{r}_{sr}\left(t_r - \frac{\tau}{2}\right) \tag{C-3}$$

$$\dot{\bar{\rho}}_4 = \dot{\bar{r}}^*\left(t_r - \frac{\tau}{2} - \frac{\rho_4}{c}\right) - \dot{\bar{r}}_{sr}\left(t_r - \frac{\tau}{2}\right) \tag{C-4}$$

$$\bar{\rho}_3 = \bar{r}^*\left(t_r - \frac{\tau}{2} - \frac{\rho_4}{c}\right) - \bar{r}_{st}\left(t_r - \frac{\tau}{2} - \frac{[\rho_3 + \rho_4]}{2}\right) \tag{C-5}$$

$$\dot{\bar{\rho}}_3 = \dot{\bar{r}}^*\left(t_r - \frac{\tau}{2} - \frac{\rho_4}{c}\right) - \dot{\bar{r}}_{st}\left(t_r - \frac{\tau}{2} - \frac{[\rho_3 + \rho_4]}{2}\right) \tag{C-6}$$

and $\rho_i = |\bar{\rho}_i|$, $\dfrac{d\rho_i}{dt} = \dfrac{\bar{\rho}_i \cdot \dot{\bar{\rho}}_i}{\rho_i}$

II. PARTIAL DERIVATIVES OF STATE WITH RESPECT TO KEPLER ELEMENTS

The partial derivatives of the satellite state $(\bar{r},\bar{v})$ with respect to the Kepler elements (a,e,I,Ω,ω,M) are:

$$\frac{\partial \bar{r}}{\partial a} = \frac{\bar{r}}{a} \tag{C-7}$$

$$\frac{\partial \bar{r}}{\partial e} = [R]\ \frac{\partial \bar{q}}{\partial e} \tag{C-8}$$

where:

$$\frac{\partial \bar{q}}{\partial e} = \begin{bmatrix} -a - \dfrac{q_2^{\,2}}{r(1-e^2)} \\ \dfrac{q_1 q_2}{r(1-e^2)} \\ 0 \end{bmatrix} \tag{C-9}$$

$$\frac{\partial \bar{r}}{\partial I} = \begin{bmatrix} z \sin \Omega \\ -z \cos \Omega \\ y \cos \Omega - x \sin \Omega \end{bmatrix} \tag{C-10}$$

$$\frac{\partial \bar{r}}{\partial \Omega} = \begin{bmatrix} -y \\ x \\ 0 \end{bmatrix} \tag{C-11}$$

$$\frac{\partial \bar{r}}{\partial \omega} = [T]\ \bar{q} \tag{C-12}$$

where:

$$\left.\begin{aligned} t_{11} &= -\cos\Omega\sin\omega - \sin\Omega\cos I\cos\omega \\ t_{12} &= -\cos\Omega\cos\omega + \sin\Omega\cos I\sin\omega \\ t_{13} &= t_{23} = t_{33} = 0 \\ t_{21} &= -\sin\Omega\sin\omega + \cos\Omega\cos I\cos\omega \\ t_{22} &= -\sin\Omega\cos\omega - \cos\Omega\cos I\sin\omega \\ t_{31} &= \sin I\cos\omega \\ t_{32} &= -\sin I\sin\omega \end{aligned}\right\} \quad \text{(C-13)}$$

$$\frac{\partial \bar{r}}{\partial M} = [R]\,\frac{\partial \bar{q}}{\partial M} \quad \text{(C-14)}$$

where:

$$\frac{\partial \bar{q}}{\partial M} = \begin{bmatrix} \dfrac{-aq_2}{r\sqrt{1-e^2}} \\ \dfrac{a}{r}\sqrt{1-e^2}\,(q_1 + ae) \\ 0 \end{bmatrix} \quad \text{(C-15)}$$

$$\frac{\partial \bar{v}}{\partial a} = -\frac{\bar{v}}{2a} \quad \text{(C-16)}$$

$$\frac{\partial \bar{v}}{\partial e} = [R]\,\frac{\partial \dot{\bar{q}}}{\partial e} \quad \text{(C-17)}$$

$$\frac{\partial \dot{\bar{q}}}{\partial e} = \begin{bmatrix} \dot{q}_1\left(\dfrac{a}{r}\right)^2\left[2\left(\dfrac{q_1}{a}\right) + \dfrac{e}{1-e^2}\left(\dfrac{q_2}{a}\right)^2\right] \\ \dfrac{\sqrt{\mu_\oplus a}}{r^2\sqrt{1-e^2}}\left[\dfrac{q_1^2}{r} - \dfrac{1}{a(1-e^2)}\,q_2^2\right] \\ 0 \end{bmatrix} \quad \text{(C-18)}$$

$$\frac{\partial \bar{v}}{\partial I} \quad \begin{bmatrix} \dot{z} \sin \Omega \\ -\dot{z} \cos \Omega \\ \dot{y} \cos \Omega - \dot{x} \sin \Omega \end{bmatrix} \tag{C-19}$$

$$\frac{\partial \bar{v}}{\partial \Omega} = \begin{bmatrix} -\dot{y} \\ \dot{x} \\ 0 \end{bmatrix} \tag{C-20}$$

$$\frac{\partial \bar{v}}{\partial \omega} = [T] \dot{\bar{q}} \tag{C-21}$$

$$\frac{\partial \bar{v}}{\partial M} = -n \left(\frac{a}{r}\right)^3 \bar{r} \tag{C-22}$$

where $$n = \sqrt{\frac{\mu_{\oplus}}{a^3}}$$

III. PARTIAL DERIVATIVES OF THE ORBITAL ELEMENTS WITH RESPECT TO THE KEPLERIAN PARAMETERS

A typical orbital element, eccentricity for example, is represented in the following way:

$$e(t) = e_o + e_1 t + e_2 t^2 + \delta e_{\oplus} + \delta e_{\odot} + \Delta e_{SR} \tag{C-23}$$

Although the variations arising from the earth, sun, and solar radiation are functions of the Kepler state variables,

analysis has shown this dependence to be extremely weak. As a result the partial derivatives of the Kepler elements with respect to the solution parameters do not include the third body and solar radiation effects. It should be noted that the omission of these small parts (on the order of one ten thousandth the smallest existing term) does not affect convergence. Hence the necessary partial derivatives are:

$$\left.\begin{aligned} \frac{\partial e}{\partial e_o} &= 1 \\ \frac{\partial e}{\partial e_1} &= t \\ \frac{\partial e}{\partial e_2} &= t^2 \end{aligned}\right\} \qquad \text{(C-24)}$$

APPENDIX D

MEAN VALUE SEMI-MAJOR AXIS EQUATION FOR EARTH PERTURBATIONS

The mean value calculation for the semi-major axis of a lunar satellite under earth perturbations is carried out using a procedure following Danby's[41] for the sun perturbations on the moon's orbit about the earth. Essentially this method finds an equivalent mass for the three body system and using this mass value and the Kepler motion equation, deduces an adjusted semi-major axis value (mean value). The accuracy to which this derivation is valid is of order e. Hence all terms that are eccentricity dependent are assumed zero. This assumption introduces only small errors for the purposes of this investigation since all orbits used have an eccentricity of e = .3 or less.

The radial perturbing force experienced by the satellite, averaged over the satellite and earth periods is given as follows:

$$\bar{F}_r = \frac{n_\oplus^2 a}{2} [1 - 3/2 \sin^2 I] \qquad (D\text{-}1)$$

The total averaged radial force exerted on the lunar satellite is as follows:

$$\frac{\mu_{\leftmoon}}{a^2} - \bar{F}_r \qquad \text{(D-2)}$$

If an equivalent mass, $\tilde{\mu}$, is defined this radial force can then be obtained from an equivalent central force law. Hence

$$\frac{\tilde{\mu}}{a^2} \equiv \frac{\mu_{\leftmoon}}{a^2} - \bar{F}_r \qquad \text{(D-3)}$$

or

$$\tilde{\mu} = \mu_{\leftmoon} \left[1 + \frac{n_{\oplus}^2}{2n^2} (3/2 \sin^2 I - 1) \right] \qquad \text{(D-4)}$$

The mean value of the mean motion for third body perturbations is given by Anderson[42] and is as follows:

$$\bar{n} = n_o \left[1 - \frac{7}{4} \frac{n_{\oplus}^2}{n^2} (1 - 3/2 \sin^2 I) \right] \qquad \text{(D-5)}$$

where $n_o = \sqrt{\frac{\mu_{\leftmoon}}{a_o^3}}$ and a_o is the average value (constant in this case) of the semi-major axis. Using equations D-4 and D-5 an equivalent Kepler motion law can be written for the perturbed motion.

$$\bar{a}^3 \bar{n}^2 = \tilde{\mu} \qquad \text{(D-6)}$$

where $\bar{a}$ is the desired mean value of the semi-major axis. Solving this equation using the expressions for $\bar{n}$ and $\tilde{\mu}$, the mean value expression for the semi-major axis is as follows:

$$\bar{a} = a_o \left[1 + \frac{n_\oplus^2}{n^2} (1 - 3/2 \sin^2 I) \right] \qquad \text{(D-7)}$$

APPENDIX E

WEIGHTED LEAST-SQUARES DATA REDUCTION

The covariance matrix for the Doppler data weighted least-squares process, assuming zero mean errors in the estimates, is found by forming the expected value of $\left\langle \overline{\hat{\Delta K}}\ \overline{\hat{\Delta K}}^T \right\rangle$ using equation (3.31);

$$\text{Exp}\left\langle \overline{\hat{\Delta K}}\ \overline{\hat{\Delta K}}^T \right\rangle = [H^T W H]^{-1}\ H^T W\ \text{Exp}\left\langle \overline{\Delta\dot{\rho}}\ \overline{\Delta\dot{\rho}}^T \right\rangle WH[H^T WH]^{-1} \qquad \text{(E-1)}$$

If it is now assumed that the residuals are serially uncorrelated and are normally distributed random variables such that

$$\text{Exp}\left\langle \overline{\Delta\dot{\rho}}\ \overline{\Delta\dot{\rho}}^T \right\rangle = \sigma^2 \underset{\sim}{I} \qquad \text{(E-2)}$$

(where σ^2 is the variance of the Doppler measurements and $\underset{\sim}{I}$ is the identity matrix) and the weight used in the least-squares processing is the inverse variance of the Doppler,

$$W = [\sigma^2 \underset{\sim}{I}]^{-1} \qquad \text{(E-3)}$$

then

$$\text{Exp}\left\langle \overline{\hat{\Delta K}}\ \overline{\hat{\Delta K}}^T \right\rangle = [H^T WH]^{-1} \qquad \text{(E-4)}$$

It is only under these conditions that the $[H^TWH]^{-1}$ matrix is the true covariance matrix of the process.

If conditions (E-2) and (E-3) are not satisfied, the $[H^TWH]^{-1}$ matrix is not the covariance matrix. For the case of the empirical orbit determination processor neither of these conditions can be met since the residuals are systematic and are also serially correlated. Hence no interpretation of variance is made of the diagonal terms in the $[H^TWH]^{-1}$ matrix.

BIBLIOGRAPHY

1. Lorell, J., "Lunar Orbiter Gravity Analysis," The Moon, Vol. 1, 190-231, 1970.

2. Michael, W. H., "Physical Properties of the Moon as Determined From Lunar Orbiter Data," Presented at the Fourteenth General Assembly of the International Union of Geodesy and Geophysics Meeting, Lucerne, Switzerland, Sept. 1967.

3. Tolson, R. H. and Gapcynski, J. P., "An Analysis of the Lunar Gravitational Field as Obtained from Lunar Orbiter Tracking Data," Presented at the IQSY/COSPAR Assemblies, London, England, July, 1967.

4. Gapcynski, J. P., Blackshear, T. W. and Compton, H. R., "The Lunar Gravitational Field as Determined from the Tracking Data of the Lunar Orbiter Series of Spacecraft," Presented at the AIAA-AAS Astrodynamics Specialists Conference, Grand Teton National Park, Wyoming, Sept. 1968.

5. Blackshear, T. W., Compton, H. R., and Schiess, J. R., "Preliminary Results on the Lunar Gravitational Field from Analysis of Long-period and Secular Effects of Lunar Orbiter I," Presented at NASA Seminar on Guidance Theory and Trajectory Analysis, Electronics Research Center, Cambridge, Mass., May 1967.

6. Lorell, J. and Sjogren, W. L., "Lunar Gravity: Preliminary Estimates from Lunar Orbiter," Science, Vol. 159, 3815, 1968.

7. Risdal, R. E., "Development of a Simple Lunar Model for Apollo," Contract Report D2-100819-1, The Boeing Company, Seattle, Washington, 1968.

8. McCuskey, S. W., Introduction to Celestial Mechanics, Addison-Wesley Publishing Company, Inc., Reading, Mass., 1963.

9. Caputo, M., The Gravity Field of the Earth from Classical and Modern Methods, Academic Press, New York, 1967.

10. "Transactions of the International Astronautical Union," Vol. XIB, Proceedings of the 11th General Assembly, Berkeley, 1961, D. H. Sadler ed., Academic Press, New York, 1962.

11. Kaula, W. M., Theory of Satellite Geodesy, Blaisdell Publishing Co., Waltham, Mass., 1966.

12. Pollard, H., Mathematical Introduction to Celestial Mechanics, Prentice-Hall, Inc., Englewood Cliffs, New Jersey, 1966.

13. Bullock, M. V. and Ferrari, A. J., "Orbit Determination For Lunar Parking Orbits Using Time-Varying Orbital Elements," NASA Contractor Report 110008, May 1970.

14. Kozai, Y., " The Motion of a Close Earth Satellite," Astro.J., Vol. 64, 378-397, 1959.

15. Kozai, Y., "Second Order Solution of Artificial Satellite Theory Without Drag." Astro. J., Vol. 67, 446-61, 1962.

16. Brouwer, D. and Clemence, G. M., Methods of Celestial Mechanics, Academic Press, New York, 1961.

17. Lorell, J. and Liu, A., "Method of Averages Expansion for Artificial Satellite Application," Jet Propulsion Lab. Report 32-1513, April 1971.

18. Ferrari, A. J. and Heffron, W. G.,"Effects of Physical Librations of the Moon on the Orbital Elements of a Lunar Satellite," Presented at AIAA-AAS Astrodynamics Conference, Ft. Lauderdale, Fla., August 1971.

19. Kozai, Y., "Effects of Solar Radiation Pressure on the Motion of an Artificial Satellite," Smithsonian Institution, Special Report No. 56, January 1961.

20. Gaposchkin, E. M., "Differential Orbit Improvement," Smithsonian Institution, Special Report No. 161, 1964.

21. de Vezin, H. G., "Doppler Observable Modeling for Apollo Real-Time Orbit Determination Program," Presented at Astrodynamics Conference, Manned Spacecraft Center, Houston, Texas, Dec. 1967.

22. Sage, A. P., Optimum Systems Control, Prentice-Hall, Inc., Englewood Cliffs, New Jersey, 1968.

23. Izsak, I. G., "Differential Orbit Improvement with the Use of Rotated Residuals," Smithsonian Institution, Special Report No. 73, 1961.

24. Wollenhaupt, W. R., "Apollo Orbit Determination and Navigation," Presented at AIAA 8th Aerospace Sciences Meeting, New York, N. Y., January 1970.

25. Kozai, Y., op. cit., 1959.

26. Kozai, Y., Smithsonian Astrophysical Observatory, Private Communication, February 1971.

27. Anderson, J. D., "Long Term Perturbations of a Moon Satellite by the Earth and Sun," Jet Propulsion Laboratory Technical Memorandum 312-162, February 1962.

28. Durbin, J., "The Fitting of Time - Series Models," Revue Inst. Int. De Stat., 233-243, 1960.

29. Battin, R. H., Astronautical Guidance, McGraw-Hill Book Co., New York, 1964.

30. Melbourne, W. G. et al, "Constants and Related Information for Astrodynamic Calculations, 1968," Jet Propulsion Lab. Technical Report 32-1306, July 1968.

31. "Natural Environment and Physical Standards for the Apollo Program and the Apollo Applications Program," NASA M-DE-8020.00C, SE -15-001-1B, July 1969.

32. Peabody, P. R., Scott, J. F., and Orozco, E. G.,"Users Description of JPL Ephemeris Tapes," Jet Propulsion Laboratory Report No. 32-580, March, 1964.

33. Muller, P. M., and Sjogren, W. L., "Lunar Mass Concentrations," Science, Vol. 161, 3842, 1968.

34. Kaula, W. M., op. cit., 1966.

35. Koziel, K., "The Constants of the Moon's Physical Libration Derived on the Basis of Four Series of Heliometric Observations from the Years 1877 to 1915," Icarus, Vol. 7, 1-28, 1967.

36. Michael, W. M., et al, "Results on the Mass and Gravitational Field of the Moon as Determined from Dynamics of Lunar Satellites," Dynamics of Satellites 1969, Bruno Morando ed., Springer-Verlag, Berlin, 1970.

37. Koziel, K., op. cit., 1967.

38. Liu, A. S. and Laing, P. A., "Lunar Gravity Field as Determined by Orbiters," Presented at 14th Plenary Meeting of COSPAR, Seattle, Washington, June 1971.

39. de Vezin, H. G., op. cit., 1967.

40. de Vezin, H. G., op. cit., 1967.

41. Danby, J. M. A., Fundamentals of Celestial Mechanics, Macmillan Company, New York, 1962.

42. Anderson, J. D., op. cit., 1962.